R-08-64

Bedrock geology Forsmark Modelling stage 2.3

Implications for and verification of the deterministic geological models based on complementary data

Michael B Stephens, Geological Survey of Sweden

Assen Simeonov, Svensk Kärnbränslehantering AB

Hans Isaksson, GeoVista AB

December 2008

Svensk Kärnbränslehantering AB
Swedish Nuclear Fuel
and Waste Management Co
Box 250, SE-101 24 Stockholm
Tel +46 8 459 84 00

ISSN 1402-3091
SKB Rapport R-08-64

Bedrock geology Forsmark Modelling stage 2.3

Implications for and verification of the deterministic geological models based on complementary data

Michael B Stephens, Geological Survey of Sweden

Assen Simeonov, Svensk Kärnbränslehantering AB

Hans Isaksson, GeoVista AB

December 2008

Abstract

The Swedish Nuclear Fuel and Waste Management Company is in the process of completing site descriptive modelling at two locations in Sweden, with the objective to site a deep geological repository for spent nuclear fuel. At Forsmark, the results of the stage 2.2 geological modelling formed the input for downstream users. Since complementary ground and borehole geological and geophysical data, acquired after model stage 2.2, were not planned to be included in the deterministic rock domain, fracture domain and deformation zone models supplied to the users, it was deemed necessary to evaluate the implications of these stage 2.3 data for the stage 2.2 deterministic geological models and, if possible, to make use of these data to verify the models. This report presents the results of the analysis of the complementary stage 2.3 geological and geophysical data. Model verification from borehole data has been implemented in the form of a prediction-outcome test.

The stage 2.3 geological and geophysical data at Forsmark mostly provide information on the bedrock outside the target volume. Additional high-resolution ground magnetic data and the data from the boreholes KFM02B, KFM11A, KFM12A and HFM33 to HFM37 can be included in this category. Other data complement older information of identical character, both inside and outside this volume. These include the character and kinematics of deformation zones and fracture mineralogy. In general terms, it can be stated that all these new data either confirm the geological modelling work completed during stage 2.2 or are in good agreement with the data that were used in this work. In particular, although the new high-resolution ground magnetic data modify slightly the position and trace length of some stage 2.2 deformation zones at the ground surface, no new or modified deformation zones with a trace length longer than 3,000 m at the ground surface have emerged. It is also apparent that the revision of fracture orientation data, which was carried out after the completion of the geological models during stage 2.2, has had little affect on the orientation parameters for the fractures along some important deformation zones that intersect the local model volume.

By contrast, the cored borehole KFM08D intersects the central part of the target volume and the data from this borehole provide a stringent test of the stage 2.2 deterministic geological models inside this critical volume. Furthermore, since gravity measurements at the site have never been used in the development of the geological models, the modelling of gravity and petrophysical data also provides an independent test of the validity of the regional rock domain model for the site. The predictions provided by local model stage 2.2 for the position and character of the intersections of rock domains, fracture domains and deformation zones along borehole KFM08D have been verified highly satisfactorily by the outcome of the single-hole interpretation of this borehole during stage 2.3. In addition, gravity modelling work provides a good support to the regional rock domain model for the site, at least where it concerns the critical rock domain RFM029.

In summary, it can be stated that the analysis presented in this report provides a basis for confidence in the deterministic geological models. However, if Forsmark is selected as a site for the deep geological repository, then it will be necessary to complete minor modifications to the deterministic geological models prior to construction work that take account of the stage 2.3 data.

Contents

1 Introduction

1.1 Background

Since 2002, the Swedish Nuclear Fuel and Waste Management Company (SKB) has carried out investigations at two different locations, the Forsmark and Laxemar-Simpevarp areas, with the objective of siting a geological repository for spent nuclear fuel. The investigations have been conducted in campaigns punctuated by data freezes. After each data freeze, the site data have been analysed and modelling work has been completed. Following the data freeze referred to as stage 2.2, the geological models for the Forsmark site, together with complementary geophysical and geological studies, were presented in /Stephens et al. 2007/ and /Stephens and Skagius (edits.) 2007/, respectively. These models have been used in the subsequent modelling work carried out by other disciplines in the modelling team as well as for an updated design of the potential repository layout. These models are also used in the assessment of safety and environmental impact.

At the time of the stage 2.2 data freeze, some geological and geophysical data, including the data from four cored boreholes and five percussion boreholes, were not available for analysis and were not utilized in the generation of the stage 2.2 geological models. Furthermore, gravity data acquired at an early stage during the site investigation had not been used at any time during the modelling work. With these points in mind, all these data have been analysed during stage 2.3 and evaluated in the context of the already established, stage 2.2 deterministic geological models.

During the stage 2.2 modelling work, the sources of error for the orientation data from cored boreholes were evaluated and quantitative estimates of uncertainty in these data were derived /Munier and Stigsson 2007/. A recalculation of all orientation data for geological features in the cored boreholes was carried out during the summer 2007, after completion of the stage 2.2 modelling work. In order to evaluate the significance of the latest changes in the data, a selection of the revised fracture orientation data along some deformation zones have been compared with the similar data used in model stage 2.2. In this context, it is important to keep in mind that such orientation data are of little significance in the geometric modelling work since the orientation of rock domains or deformation zones is not based on the local orientation of rock contacts or fractures, respectively, in boreholes /see Stephens et al. 2007/. However, these data are important for the establishment of the orientation of, for example, fractures along zones, i.e. as a part of the property assignment.

1.2 Scope and objectives

The present report addresses solely the new geological and geophysical data assembled between the data freezes 2.2 and 2.3. Since geological information from percussion boreholes is more uncertain in character relative to that from cored boreholes, the data from the percussion boreholes are only addressed briefly in this report. The prime objective of the report was to evaluate the implications of these complementary stage 2.3 data for the deterministic geological models that were presented and provided to downstream users during model stage 2.2.

One of the cored boreholes (KFM08D) is sited inside the central part of the potential repository volume and is spatially isolated from other boreholes, particularly at 400 to 500 m depth. For this reason, it was judged to be an excellent candidate for a verification test for the deterministic geological models in this volume. This test, as well as the evaluation of the data in the three other cored boreholes, has been carried out on a prediction-outcome basis. Furthermore, since gravity data had not been used earlier in the modelling of rock domains, these data were also judged to be feasible for a verification test for the deterministic, regional rock domain model.

Thus, a second important objective of the report concerned a verification of the stage 2.2 deterministic geological models for the Forsmark site. A verification of the Forsmark stage 2.2 geological discrete fracture network models was carried out in /Fox et al. 2007/.

Finally, the report assesses the implications of the revision in borehole orientation data, which was completed during the summer 2007, for the mean and κ values of fracture orientation sets in the stage 2.2 property tables for deformation zones. In particular, a comparative study has been completed for the steeply dipping zones ZFMENE0060A and ZFMWNW0123, and the gently dipping zones ZFMA2, ZFMA8 and ZFMF1, all of which are situated in the north-western part of the candidate volume, i.e. inside and along the margins of the potential repository volume.

1.3 Overview of complementary data acquired after model stage 2.2

The following geological and geophysical data have been acquired at Forsmark between the data freeze for model stage 2.2 and the final stage 2.3 data freeze on 2007-03-30. As pointed out above, none of these data have been used in the development of the stage 2.2 geological models for the site /Stephens et al. 2007/ that have been adopted by downstream users:

- Complementary, high-resolution ground magnetic data to the south-east and west of Bolundsfjärden, and mostly in the sea area around SFR, the repository for low and medium level radioactive waste (Figure 1-1).
- Geological and geophysical data from four cored boreholes (KFM02B, KFM08D, KFM11A and KFM12A) and five percussion boreholes (HFM33, HFM34, HFM35, HFM36 and HFM37) close to drill sites 11 and 12 (Figure 1-2 and Figure 1-3). Only borehole KFM8D penetrates the bedrock inside the north-western part of the candidate volume (Figure 1-2), i.e. inside the target volume. The following data were acquired in connection with the standard site investigation work carried out by SKB along boreholes:
  1. Borehole TV-logging with BIPS.
  2. Standard geophysical logging and interpretation.
  3. Borehole radar logging with interpretation.
  4. Geological mapping of the crystalline bedrock, alteration phenomena and both ductile and brittle structures (Boremap).
  5. Integrated geological and geophysical single-hole geological interpretation (SHI) of each borehole (stage 1 SHI work, see /Stephens et al. 2007/).
- Complementary stage 2 SHI work (see /Stephens et al. 2007/) for the possible deformation zones that have been recognised with high confidence along the cored boreholes KFM01C, KFM01D, KFM02B, KFM06C, KFM07B, KFM07C, KFM08C, KFM08D, KFM09A, KFM09B, KFM10A, KFM11A and KFM12A. This work addresses in more detail, relative to the stage 1 work, the character of these zones, in particular the character of fault core, if present, and the kinematics. A large part of the cored borehole KFM11A is situated within a deformation zone (Singö and adjacent zones, see chapter 5) and complementary stage 2 SHI data have only been acquired from the borehole interval 489 to 630 m.
- Complementary fracture mineralogy data from the nine cored boreholes KFM01C, KFM01D, KFM02B, KFM08C, KFM08D, KFM09A, KFM09B, KFM10A, KFM11A.

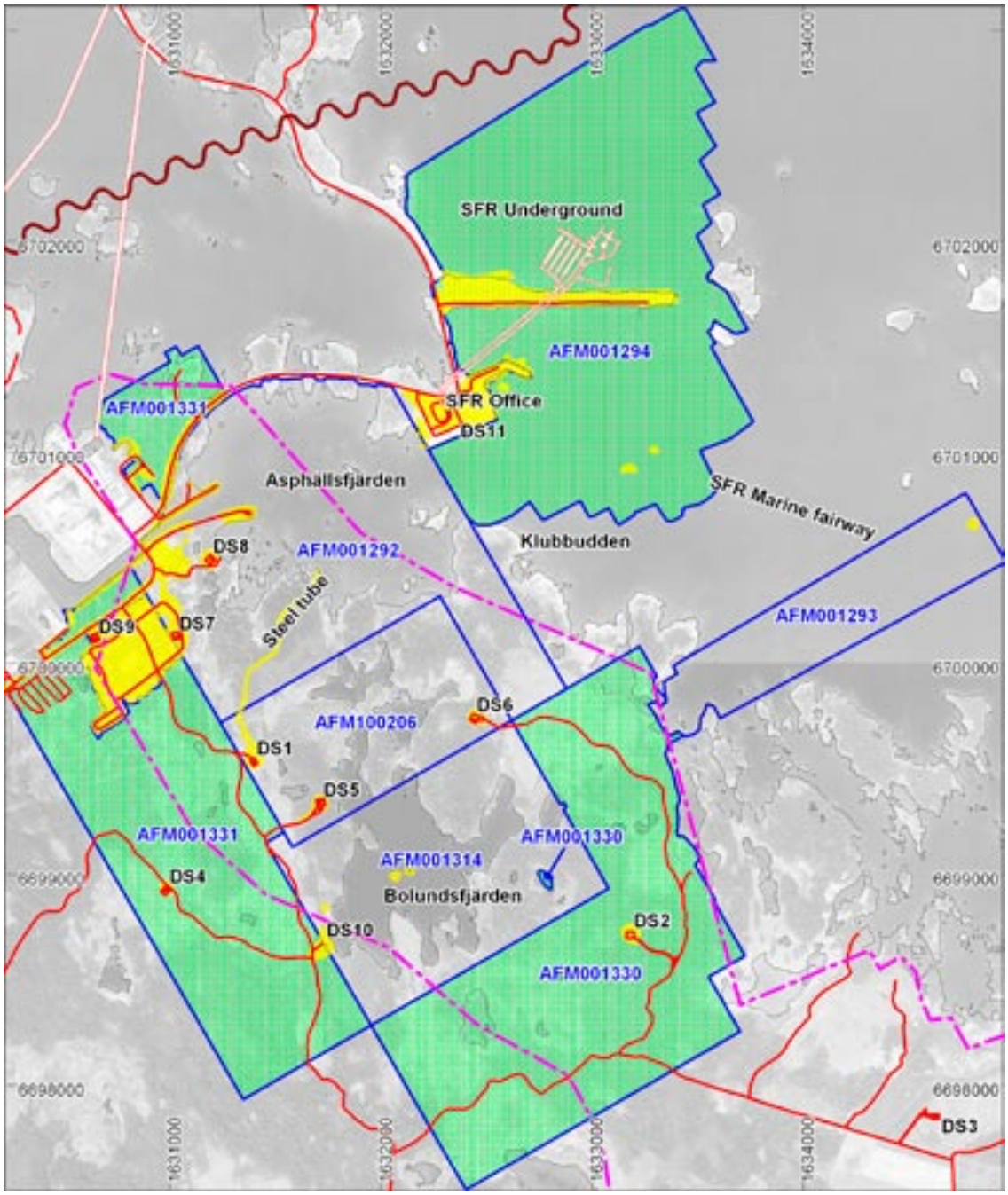

Figure 1-1. *Location and extension of all the high-resolution, ground magnetic surveys at Forsmark. The areas where complementary data were acquired between data freezes 2.2 and 2.3 are shown in green (activity codes AFM001294, AFM001330 and AFM001331). Disturbed areas are shown in yellow. The Fenno-Scan HVDC cable between Sweden and Finland is displayed as a brown wavy line, whereas the SFR underground facilities and the cooling water tunnels from reactors Forsmark 1–2 and Forsmark 3 are shown with red lines and white filling. The Forsmark candidate area is delimited with a thick, dot-dashed magenta line, whereas roads and drill sites are marked with red colour.* *Modified slightly after /Isaksson et al. 2007/.*

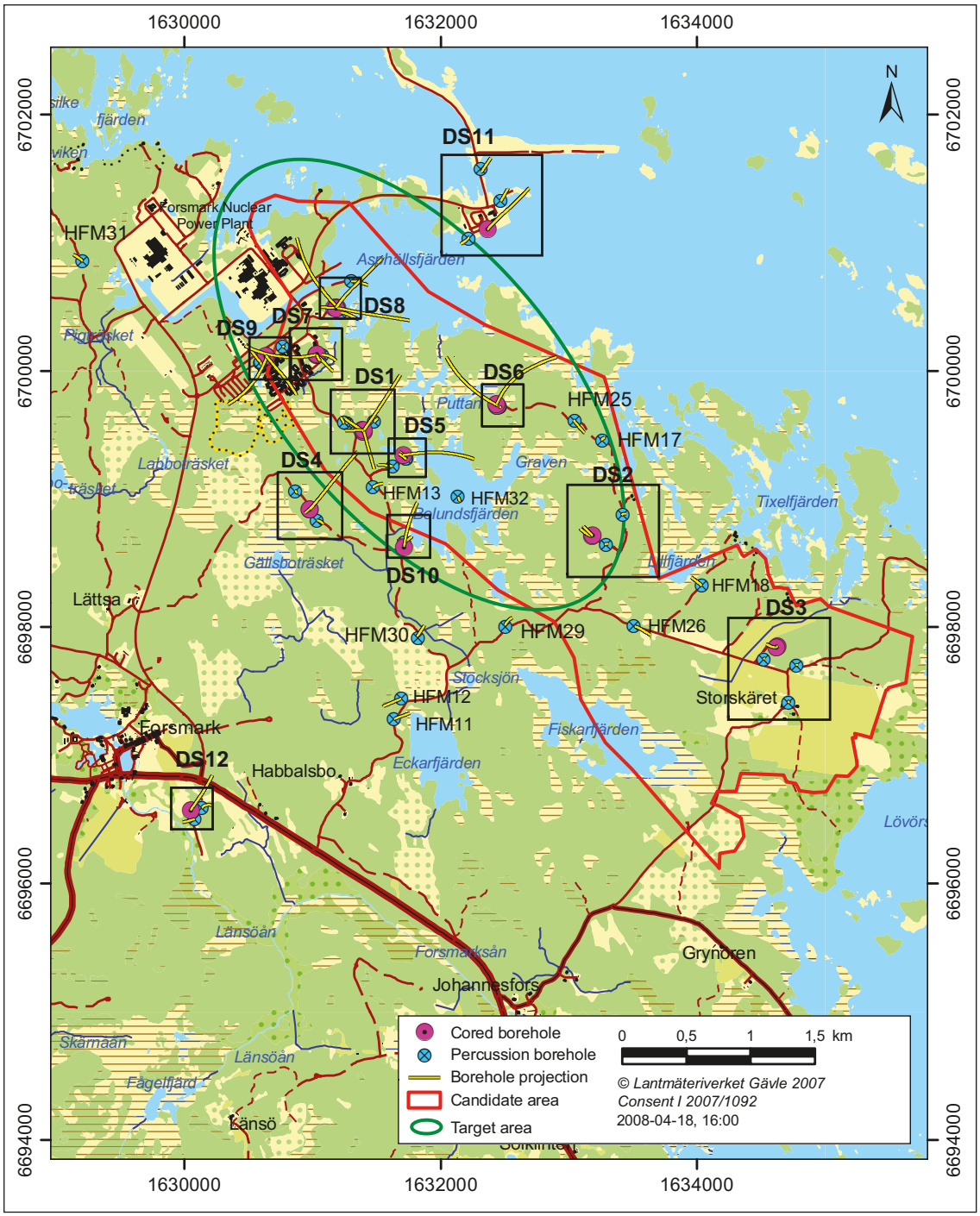

Figure 1-2. *Location of drill sites and projection of boreholes on the ground surface at the Forsmark site. Only the geological and geophysical data from the cored boreholes KFM02B, KFM08D, KFM11A and KFM12A, and the percussion boreholes HFM33, HFM34, HFM35, HFM36 and HFM37 were acquired after model stage 2.2. Coordinates are provided using the RT90 (RAK) system.*

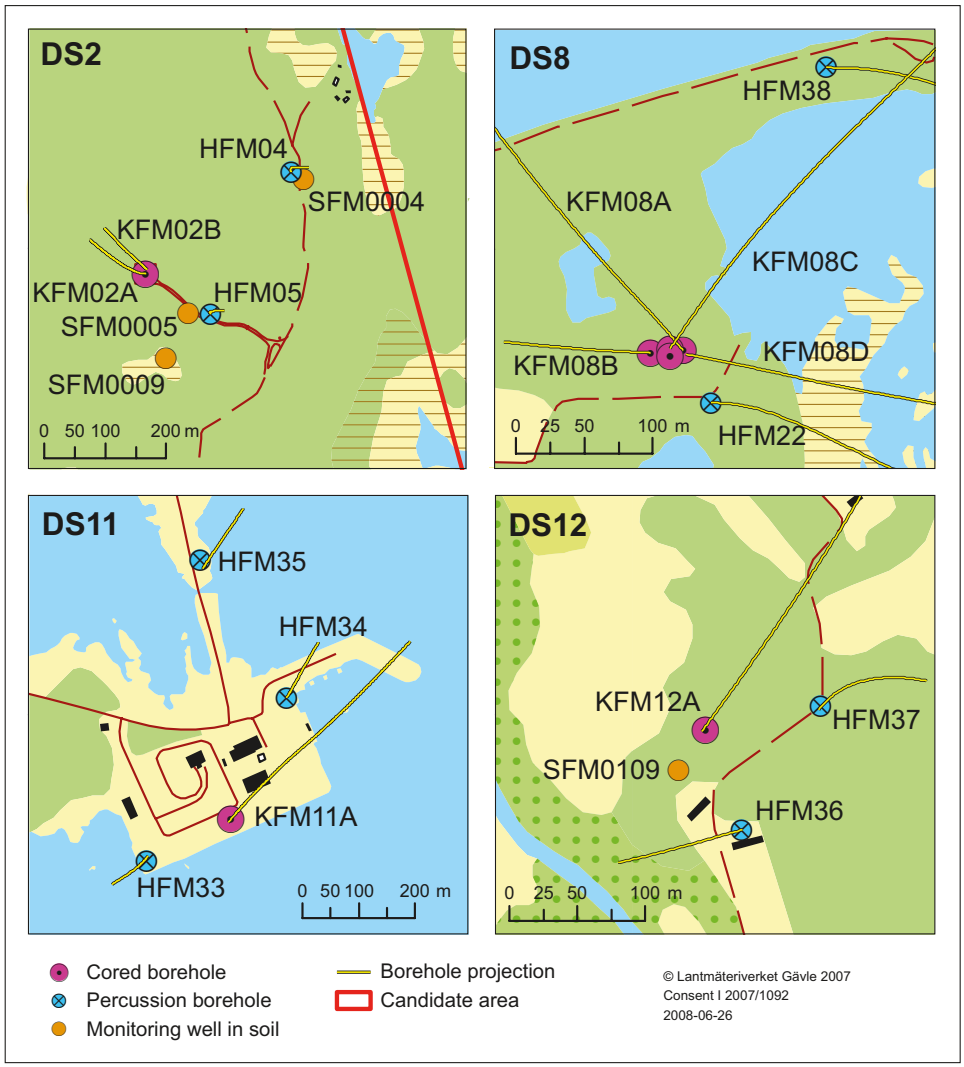

Figure 1-3. *Detailed view of the location and projection of boreholes on the ground surface at drill sites 2, 8, 11 and 12 (DS2, DS8, DS11 and DS12).*

1.4 Structure of this report

The implications of the complementary, high-resolution ground magnetic data for the interpretation of low magnetic lineaments and deformation zones in the stage 2.2 geological models are addressed in chapter 2. The new borehole data, arranged according to drill site (2, 8, 11 and 12), are evaluated in chapters 3 to 6, respectively. The new data from each site have been analysed in the same manner as in previous modelling stages and the predicted intersection of various geological entities along each borehole are compared with the results of the respective single-hole interpretation. On this basis, the implications for the deterministic geological models (stage 2.2) can be addressed and in, one example (KFM08D), the analysis provides a verification test for the models. An assessment of the validity of the regional rock domain model, based on the modelling of gravity and petrophysical data, is also completed in chapter 7.

Chapters 8 and 9 evaluate the complementary data that bear on the character and kinematics of possible deformation zones, and fracture mineralogy. The consequences of the revision in fracture orientation data, after stage 2.2, for the deterministic models for deformation zones (stage 2.2) are discussed in chapter 10. Finally, a concluding statement that provides an overall assessment of the validity of the stage 2.2 deterministic geological models based on the analysis of the complementary stage 2.3 data is presented in chapter 11.

2 Complementary high-resolution ground magnetic data

2.1 Opening remarks

During and after the work with geological model stage 2.2, new high-resolution ground magnetic data were acquired in three areas that surround the previous survey area (Figure 1-1 and Figure 2-1). The interpretation of these new data and an integration with previous interpretations of magnetic lineaments at Forsmark /Isaksson et al. 2006ab/ were subsequently presented (/Isaksson et al. 2007/ and Figure 2-2). The objective of the present study is to evaluate the implications of the new lineament interpretation for the stage 2.2 geological modelling work, by comparing the deterministic deformation zones in stage 2.2 /Stephens et al. 2007/ with the updated version of magnetic lineaments presented in /Isaksson et al. 2007/.

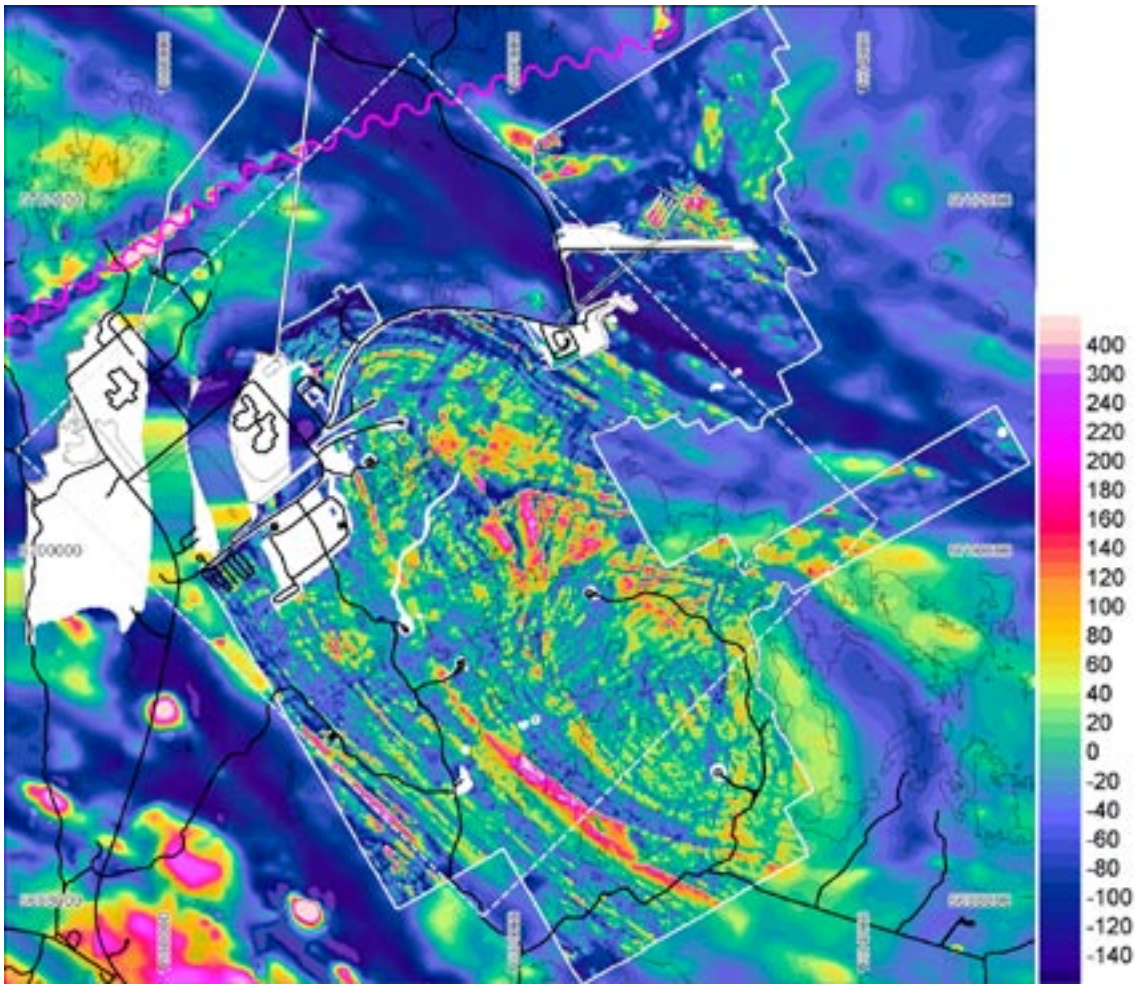

Figure 2-1. *Combined magnetic map composed of the NS-directed helicopter survey and the high-resolution ground magnetic survey. Units in nanoTesla [nT]. Base level for the helicopter borne survey is 51,230 nT and for the ground survey 51,407 nT. The local model area is outlined by a dashed white line and the detailed ground survey areas by a solid white line. White areas represent areas with poor coverage or poor quality due to disturbances. The magenta wavy line represents the location of the Fenno-Scan HVDC (high voltage, direct current) cable. Buildings, roads and drill sites in black. Tunnels and underground facilities at SFR are outlined by black lines and white filling. Updated version of Figure 3-37 in /Stephens et al. 2007/. © Lantmäteriverket Gävle 2007. Consent I 2007/1092.*

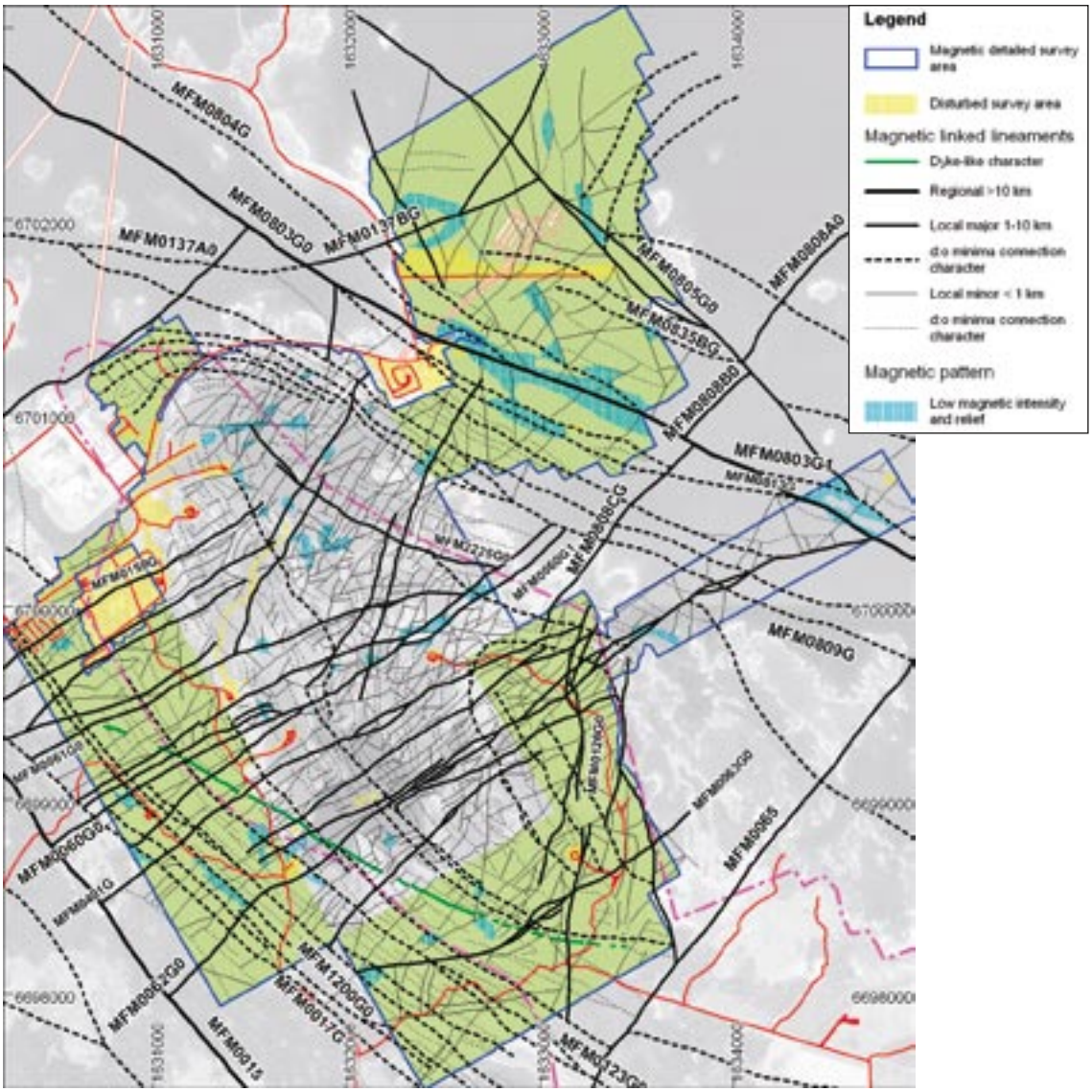

Figure 2-2. *Low-magnetic lineaments in the north-western part of the candidate area and its surroundings at Forsmark /Isaksson et al. 2007/. The lineaments have been inferred from high-resolution ground magnetic data and have been linked to lineaments inferred from the airborne helicopter survey in the areas where ground magnetic data are lacking. Magnetically disturbed areas are shown in yellow. The SFR underground facilities and the cooling water tunnels from reactors Forsmark 1–2 and Forsmark 3 are shown with red lines and white filling. The Forsmark candidate area is shown as a thick, dot-dashed, magenta line. Roads and drill sites in red. The figure is adapted from Figure 4-4 in /Isaksson et al. 2007/, with the new survey areas added in pale green. © Lantmäteriverket Gävle 2007. Consent I 2007/1092.*

The comparison is limited to a two-dimensional representation of steeply dipping deformation zones where they outcrop at the ground surface. Gently dipping deformation zones are difficult to identify in the magnetic data /Isaksson et al. 2007/ and some of these zones do not outcrop at the ground surface /Stephens et al. 2007/. Furthermore, magnetic lineaments are best represented at the ground surface. The methodology used to identify low magnetic lineaments and the geological interpretation of such lineaments are summarised in /Stephens et al. 2007, section 3.9/. Three groups of low magnetic lineaments are distinguished at the site:

- Magnetic minima that are discordant to the tectonic foliation, rock units and the banded magnetic anomaly pattern in the area. These features are inferred to be predominantly brittle deformation zones, i.e. fracture zones.

- Magnetic minima connections that are concordant with the same geological and geophysical features and are locally folded. The magnetic minima connections are inferred to be related predominantly to the earlier igneous or ductile deformational history inside the tectonic lens at Forsmark /Stephens et al. 2007/, where the candidate area is situated. Outside the tectonic lens, these lineaments are inferred to be related to both these older geological features as well as younger deformation zones.
- A third minor group consists of discordant magnetic lineaments with a dyke-like character.

2.2 Evaluation

In the evaluation work, the two-dimensional representation of model stage 2.2 deterministic deformation zones along the ground surface (data delivery GIS_Request#08_02) and linked magnetic lineaments /Isaksson et al. 2007/ were compared visually, zone by zone, using a GIS system. The results of this evaluation are documented in three tables for:

- Deformation zones longer than 1,000 m in trace length at the ground surface (Table A-1 in the appendix).
- Minor deformation zones shorter than 1,000 m in trace length at the ground surface (Table A-2 in the appendix).
- Potential local major deformation zones between 1,000 m and 3,000 m in trace length at the ground surface (Table A-3 in the appendix). These relatively short zones have not yet been included in the local deformation zone model for the site.

Differences that may have implications for the current deformation zone model for Forsmark are carefully addressed in these tables, in particular changes in the trace length at the ground surface. The lineaments based on magnetic minima are treated in three separate groups, following the division of deformation zones at the site according to size /Stephens et al. 2007, section 2.4/:

- Lineaments with a trace length longer than 3,000 m and located inside the regional model area or both the regional and local model areas. These are addressed in Table A-1 in the appendix.
- Lineaments with a trace length between 1,000 m and 3,000 m that intersect the local model area. These are addressed in Table A-1 and Table A-3 in the appendix.
- Lineaments with a trace length shorter than 1,000 m and located inside the local model area. These are addressed in Table A-2 in the appendix.

On the basis of the evaluation carried out here, the deformation zones in the stage 2.2 model have been classified into three different groups. These groups are distinguished on the basis of the degree of modification implied by the revised interpretation of low magnetic lineaments (see “Implication index” in Table A-1 and Table A-2 in the appendix):

1. Deformation zones that show no or insignificant changes for the geological model (implication index = 1). No change emerges mostly as a result of the lack of any new data in the study area.
2. Deformation zones that show no signature in the new ground magnetic data. These zones could be determined from other sources of data or the new magnetic data are disturbed or show a very low magnetic intensity or relief (implication index = 2).
3. Deformation zones that show more significant changes for the geological model, including changes in trace at the ground surface, trace length at the ground surface or a combination of these two features (implication index = 3).

2.3 Results

Only those deformation zones in model stage 2.2 that lie within the local model area and that are affected more significantly by the new ground magnetic data and its interpretation are discussed below, i.e. zones with high implication index (level 3) in Table A-1 and Table A-2 in the appendix. Zones where no signature has been detected in the new ground magnetic data (level 2) are also included. The deformation zones addressed below are also shown in Figure 2-3.

ZFMENE0061 shows a significant change in trace on the ground surface along its extension to the WSW. Based on the revised interpretation of the corresponding lineament, this zone should terminate against zone ZFMNW0017. This change has the consequence that lineament MFM2074G also needs to be considered in the local model for deformation zones.

ZFMENE0401A is significantly longer but its trace length on the ground surface remains less than 3,000 m. The south-western termination against ZFMNW0003 is the critical factor that determines its trace length.

ZFMENE2320 shows a significant change in trace on the ground surface. Due to an extension to the WSW that deviates to the south-west and a revised termination against ZFMNW0017, this zone is 620 m longer relative to that in model stage 2.2. However, there is some uncertainty due to the presence of a disturbed area.

ZFMENE2325A, a minor deformation zone, follows the same pattern as ZFMENE2320 and is now longer than 1,000 m on the ground surface.

ZFMNNE0869 (zone 3 at SFR) shows no clear signature in the new ground magnetic data. Lineament MFM3143G is coincident with the central part of the zone. However, the magnetic lineament is completely outside the local model area and is shorter than 1,000 m.

ZFMNNW0100 shows no clear signature in the new ground magnetic data to the SSE along its length and no new data are available to the NNW. However, this interpretation is uncertain since the zone is situated close to a disturbed area and in an area with a diffuse magnetic signature and partly low magnetic intensity and relief.

ZFMNNW0404. The identity code 404 is removed in the magnetic lineament database. The extension to the SSE is partly replaced by lineament MFM1196G, which is reduced in length to the north-west.

ZFMENE0060A shows no significant change in its north-eastern part but the new ground magnetic data indicate a straighter trace on the ground surface in its south-western part. Zone ZFMENE0060A corresponds to lineament MFM0060G2 for approximately 400 to 500 m along its length.

ZFMENE0060C shows a change in trace along the ground surface and is now no longer a fully attached branch of zone ZFMENE0060A. Instead, it appears to form a splay from zone ZFMENE0060A and follows lineament MFM2281G until it is terminated against zone ZFMNW0017.

ZFMENE0062A is extended towards the south-west by c. 1,000 m. It now terminates against zone ZFMNW0003 and not against zone ZFMNW0017.

ZFMWNW0001, ZFMNW0002, ZFMWNW0813 and ZFMWNW1127. The trace of the Singö deformation zone on the ground surface has been modified as a consequence of the new interpretation of magnetic lineaments. Lineament MFM1127, corresponding to zone ZFMWNW1127, has been removed and is replaced in its north-western part by MFM0804G. With these changes in mind, the south-eastern part of zone ZFMNW0002 can be redrawn to follow lineament MFM0804G. The deformation zone area in the vicinity of the Singö deformation zone is now represented by lineaments MFM0803, MFM0813 and MFM0804 with interstitial areas of low magnetic intensity and relief. The reader is also referred to the comments on zones ZFMWNW0813 and ZFMWNW1127 in Table A-1 in the appendix. Although lineament

MFM0803 has a slightly different trace at the ground surface compared with ZFMWNW0001, there is no significant change in the length of this deformation zone.

ZFMWNW0123. Lineament MFM0123G in its north-western part is not terminated against ZFMENE0060A. It continues an additional 480 m towards the north-west.

Other deformation zones with an implication index of 2 or 3 include: ZFMENE0103, ZFMENE0169, ZFMENE1192, ZFMENE2332, ZFMNNE0725, ZFMNNW0101, ZFMWNW1056, ZFMNE0808C, ZFMNW1200, ZFMWNW0809A, ZFMWNW0809B, ZFMWNW0835B, ZFMNW0805, ZFMWNW0044, ZFMNNE0130, ZFMNE0870, ZFMENE1057, ZFMNE1188, ZFMNE2282, ZFMNE2374 and ZFMENE2403. The reader is referred to Table A-1 and Table A-2 in the appendix for details concerning observations and changes.

Revised low magnetic lineaments with a trace length at the ground surface between 1,000 m and 3,000 m, which intersect the local model area and are currently not included as a deformation zone in the geological model, have some implications for the deterministic modelling work.

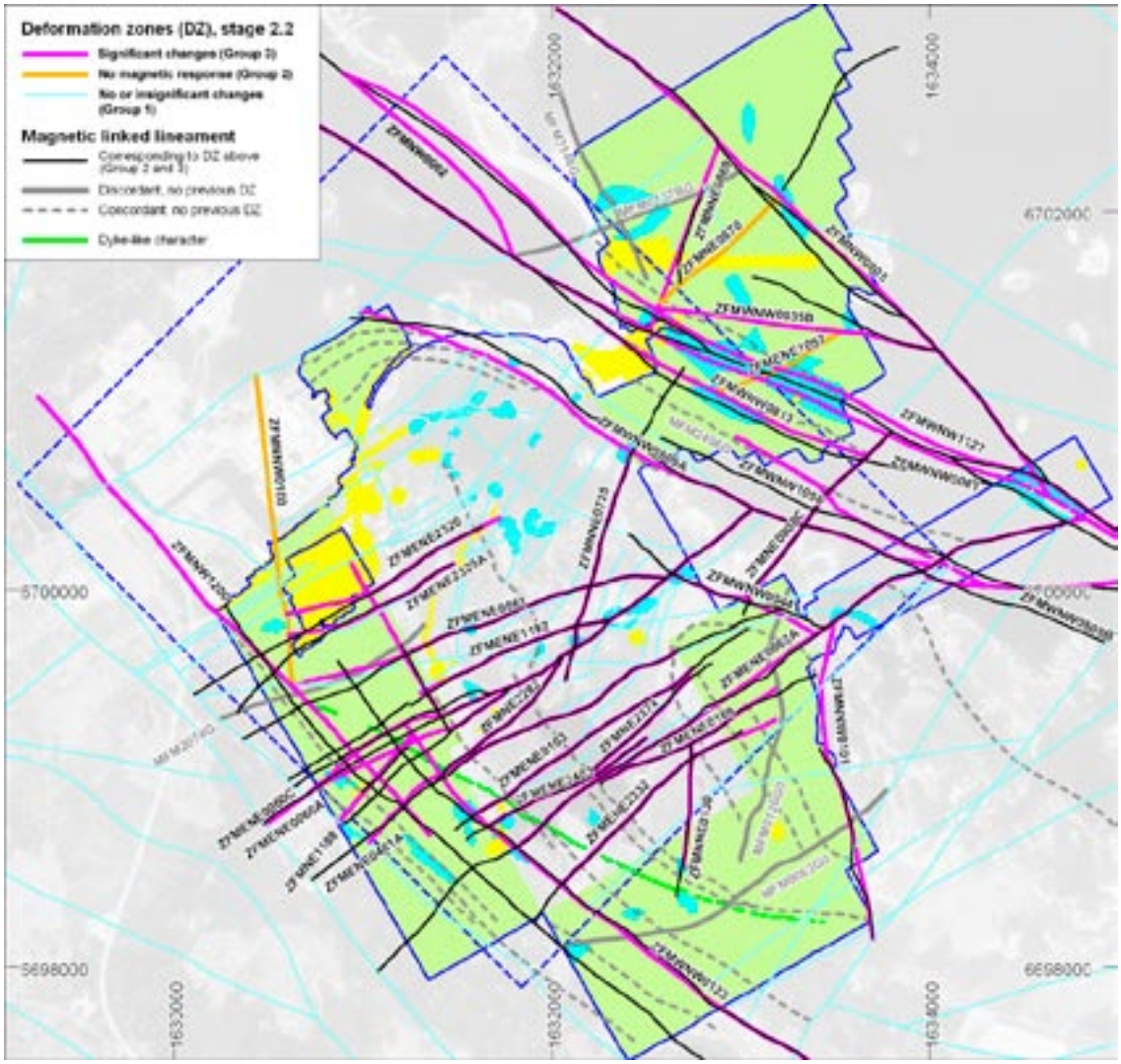

Figure 2-3. *Deterministic deformation zones according to the stage 2.2 geological model at Forsmark /Stephens et al. 2007/ compared with linked magnetic lineaments inferred from new high-resolution ground magnetic data (light green areas) and previous lineaments /Isaksson et al. 2007/. Local model area is marked with blue, dashed line. Magnetically disturbed areas are marked with yellow.*

These lineaments are referred to as MFM2074G, MFM0063G0, MFM0126G0, MFM0137BG, MFM3148G and MFM2496G (see Table A-3 in the appendix). MFM2074G is the most important with a central position in the local model area close to and possibly parallel to zone ZFMENE0061. However, it is ranked with high uncertainty.

Finally, there are anomalies of dyke-like character in the south-western part of the ground magnetic survey area. These lineaments are discordant features and are often narrow, high-magnetic linear anomalies. These were identified in the Forsmark area during the previous interpretation of ground magnetic data /Isaksson et al. 2006ab/. The dyke-like anomaly pattern in the south-western part of Bolundsfjärden extends both to the north-west and to the south-east (Figure 2-2) in the new survey /Isaksson et al. 2007/. The lineaments are characterised by combined, narrow and parallel magnetic minima and maxima in the north-western part. To the south-east, the character changes to be only magnetic maxima connections, slightly discordant to the general magnetic banding. The whole structure is totally c. 3,000 m in length and is situated outside the target area at Forsmark (Figure 2-3). The geological characteristics of these magnetic lineaments are not fully resolved.

3 Borehole KFM02B

3.1 Background

Drilling of borehole KFM02B was primarily carried out to provide rock stress measurements in the bedrock above and below the gently dipping deformation zone ZFMA2 and to complete groundwater flow measurements and tracer tests between boreholes KFM02A and KFM02B (Figure 1-3). The decision statement and motivation for borehole KFM02B are provided in document ID 1048010. The position, inclination, bearing and borehole length are summarised in Table 3-1.

3.2 Prediction of intersections of geological features along borehole KFM02B based on model stage 2.2

With the help of a software system developed by SKB for three-dimensional modelling and visualisation of geometric models (RVS), a prediction of the intersections with borehole KFM02B of rock domain boundaries, fracture domain boundaries and deterministically modelled deformation zones, which were included in model stage 2.2 /Stephens et al. 2007/, has been carried out.

No intersection of rock domain boundaries was predicted in KFM02B (Table 3-2), since the entire borehole is drilled within rock domain 29 (RFM029) that is dominated by medium grained metagranite-granodiorite. Two different fracture domains are predicted to be present in the borehole (Table 3-2). Fracture domain FFM03 is predicted to be present down to c. 407 m borehole length (c. 393 m depth, RHB 70) and FFM01 between c. 430 m (c. 417 m depth, RHB 70) and the remainder of the borehole. The boundary between these two fracture domains corresponds to the gently dipping deformation zone ZFMA2 (Table 3-3). The strongly altered vuggy rock in the upper part of borehole KFM02A /Stephens et al. 2007/ is predicted by the model not to intersect borehole KFM02B. This observation is consistent with the geological model for this feature, i.e. a steeply plunging alteration pipe between zones ZFMA2 and ZFMA3 with restricted, horizontal spatial extension /Stephens et al. 2007/.

According to the geological model stage 2.2, there are no intersections of steeply dipping deformation zones along borehole KFM02B. However, the model predicts the intersection along this borehole of four gently dipping deformation zones (ZFM866, ZFMA3, ZFMA2 and ZFMF1) that have been recognised in other boreholes with a high degree of confidence, in particular the adjacent borehole KFM02A. The predicted upper and lower borehole intersections of these four gently dipping deformation zones are shown in Table 3-3. The properties of these zones, based on intersections in boreholes other than KFM02B, are presented in /Appendix 15 in Stephens et al. 2007/ and addressed in the text below. A selection of these properties, including confidence of existence, orientation and inferred trace length at the ground surface, are also shown in Table 3-3.

Table 3-1. Position, inclination, bearing and length of borehole KFM02B. Data extracted from Sicada database: Sicada_08_109 (2008-05-09).

Borehole	Drill site	Easting RT 90, 2.5 gon W (m)	Northing RT 90, 2.5 gon W (m)	Inclination (°)	Bearing (°)	Length (m)
KFM02B	2	1633186	6698719	–80	313	573

Table 3-2. Predicted intersections of deterministically modelled rock and fracture domains in model stage 2.2 with borehole KFM02B. Borehole intersections have been extracted with the assistance of RVS, using data on the bearing and inclination of the trace of borehole KFM02B and the geometry of rock domains in the regional model, stage 2.2 /Stephens et al. 2007/. The boundaries between fracture domains along this borehole are based on /Olofsson et al. 2007/.

Modelled rock domain (RFM)	Modelled fracture domain (FFM)	Cored borehole length (m)	
		Upper intersection	Lower intersection
RFM029	FFM03	Start of the borehole	407
RFM029	FFM01	430	Beneath cored borehole length

Table 3-3. Predicted intersections of deformation zones modelled deterministically in model stage 2.2 with borehole KFM02B. All these zones belong to the gently dipping set. Borehole intersections have been extracted with the assistance of RVS, using data on the bearing and inclination of the trace of borehole KFM02B and the geometry of deformation zones in regional model, stage 2.2. Zone confidence, orientation and trace length at the ground surface are extracted from /Appendix 15 in Stephens et al. 2007/. UI = Upper intercept, LI = Lower intercept. All borehole lengths are adjusted values. All orientations are provided as strike/dip using the right-hand-rule-method.

Modelled deformation zone (ZFM)	Seismic reflector	Confidence of existence	Orientation. Strike/dip (°)	Inferred trace length at the ground surface (m)	Borehole length (m)	
					UI	LI
ZFM866	Not present	High	080/23	1,724	104	115
ZFMA3	A3	High	046/22	3,234	153	176
ZFMA2	A2	High	080/24	3,987	407	430
ZFMF1	F1	High	070/10	No intersection with the ground surface	472	515

The confidence of existence of the four gently dipping fracture zones ZFM866, ZFMA2, ZFMA3 and ZFMF1 is high (Table 3-3). Three of these zones have been modelled by linking one or more borehole intersections with a corresponding seismic reflector (Table 3-3). The intersection trace of zones ZFMA2 and ZFMA3 at the ground surface is greater than 3,000 m (Table 3-3), which has been adopted as the critical zone length in the consideration of respect distance /Munier and Hökmark 2004/. By contrast, the intersection trace of zone ZFM866 is considerately less than 3,000 m in length (Table 3-3) and zone ZFMF1 fails to intersect the ground surface (Table 3-3).

Sections with red-stained bedrock that contain fine-grained hematite dissemination are present along the four gently dipping deformation zones inferred to intersect borehole KFM02B. This type of alteration has been mapped and is referred to in the Sicada database as oxidation. Sealed fractures dominate in zones ZFMA2, ZFMA3 and ZFMF1, and open fractures dominate in zone ZFM866. The mean pole of the dominant set of fractures along the four zones is consistent with the inferred orientation of the zones (Figure 3-1).

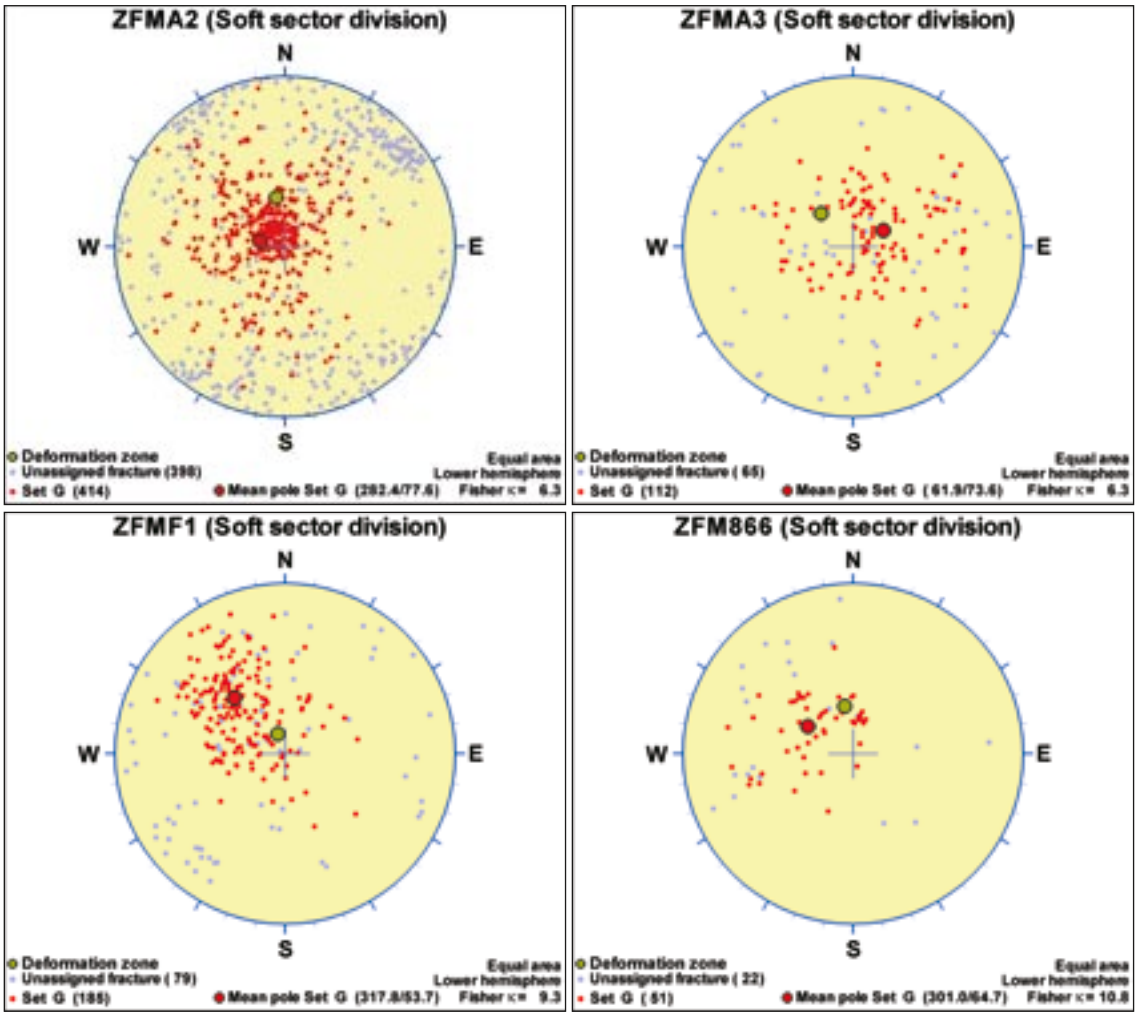

Figure 3-1. *Mean poles to fracture sets inside the deterministically modelled deformation zones ZFMA2, ZFMA3, ZFMF1 and ZFM866, model stage 2.2 /Appendix 15 in Stephens et al. 2007/. The data have been acquired from boreholes other than KFM02B. The methodology used to identify fracture sets is also described in /Appendix 15 in Stephens et al. 2007/.*

The dominant minerals that fill and coat fractures along the four gently dipping zones predicted to intersect KFM02B are calcite and chlorite. Epidote, which belongs to the oldest generation of fracture minerals at the site /Sandström et al. 2008a/, occurs in zones ZFMA2 and ZFMF1 (Figure 3-2a, c). Adularia/hematite and prehnite, which belong to a younger generation than epidote /Sandström et al. 2008a/, are present along all the zones but not to the same extent as in the steeply dipping ENE to NNE set of deformation zones in the candidate area. The even younger generation of fracture minerals /Sandström et al. 2008a/, including clay minerals and pyrite, as well as no mineral filling are common along open fractures (Figure 3-2).

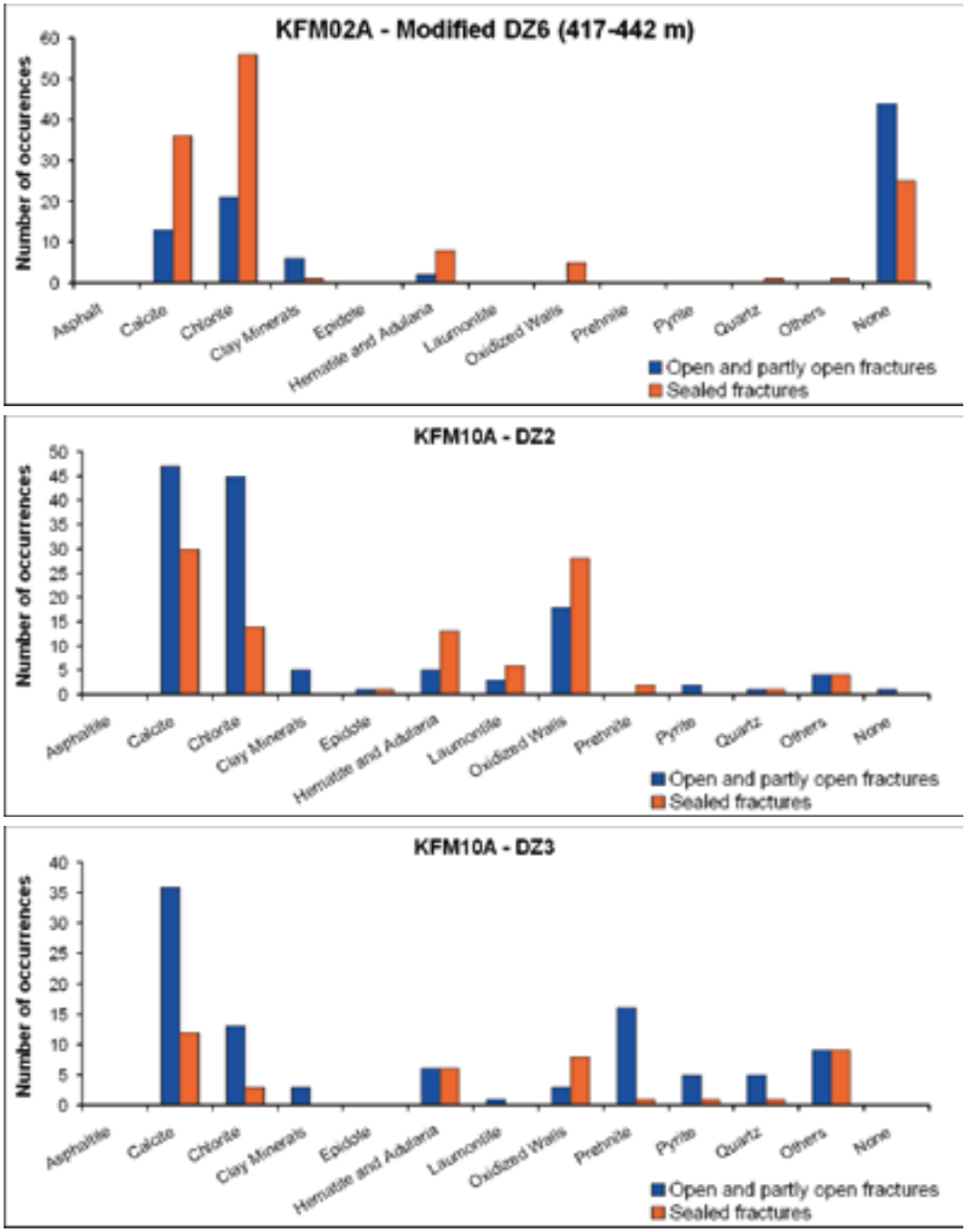
KFM02A - Modified DZ6 (417-442 m)
Number of occurences
Asphalt
Calcite
Chlorite
Clay Minerals
Epidote
Hematite and Adularia
Limonite
Oxidized Walls
Prehnite
Pyrite
Quartz
Others
None
Open and partly open fractures
Sealed fractures
KFM10A - DZ2
Number of occurrences
Asphaltite
Calcite
Chlorite
Clay Minerals
Epidote
Hematite and Adularia
Limonite
Oxidized Walls
Prehnite
Pyrite
Quartz
Others
None
Open and partly open fractures
Sealed fractures
KFM10A - DZ3
Number of occurrences
Asphaltite
Calcite
Chlorite
Clay Minerals
Epidote
Hematite and Adularia
Limonite
Oxidized Walls
Prehnite
Pyrite
Quartz
Others
None
Open and partly open fractures
Sealed fractures

a) ZFMA2

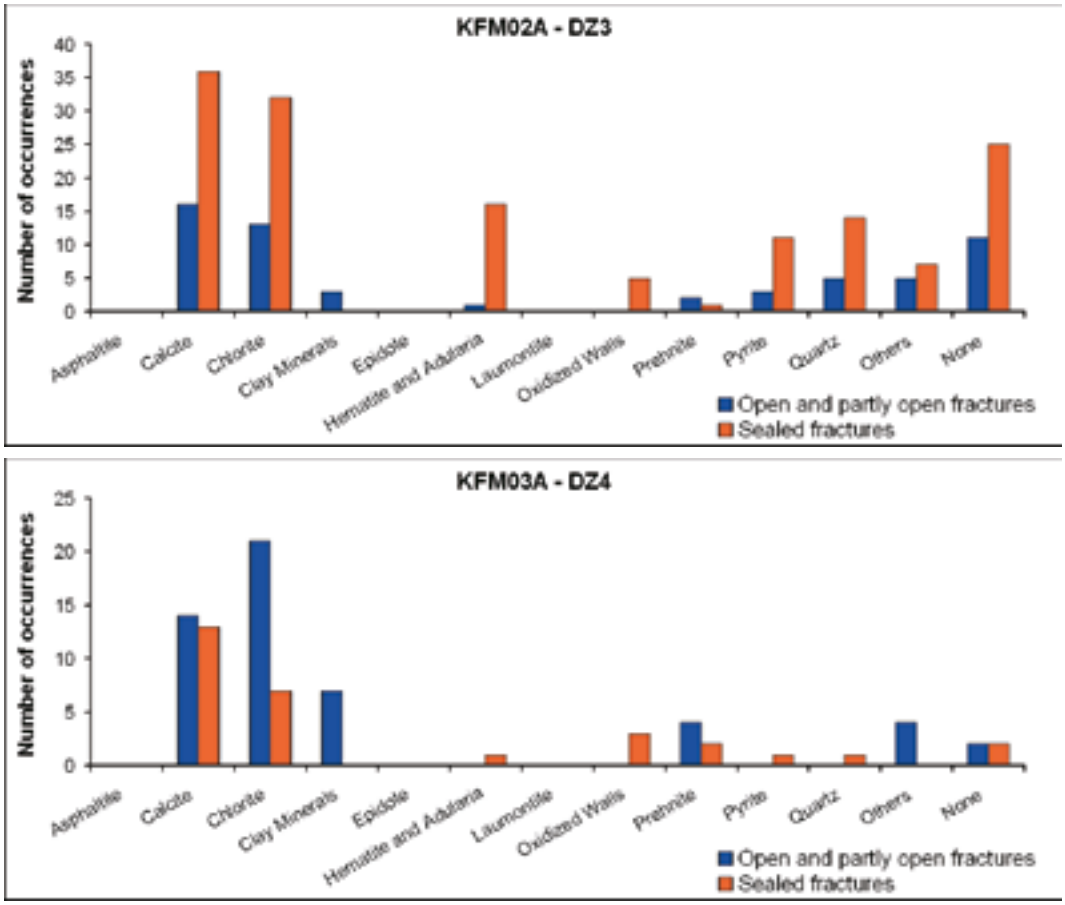

b) ZFMA3

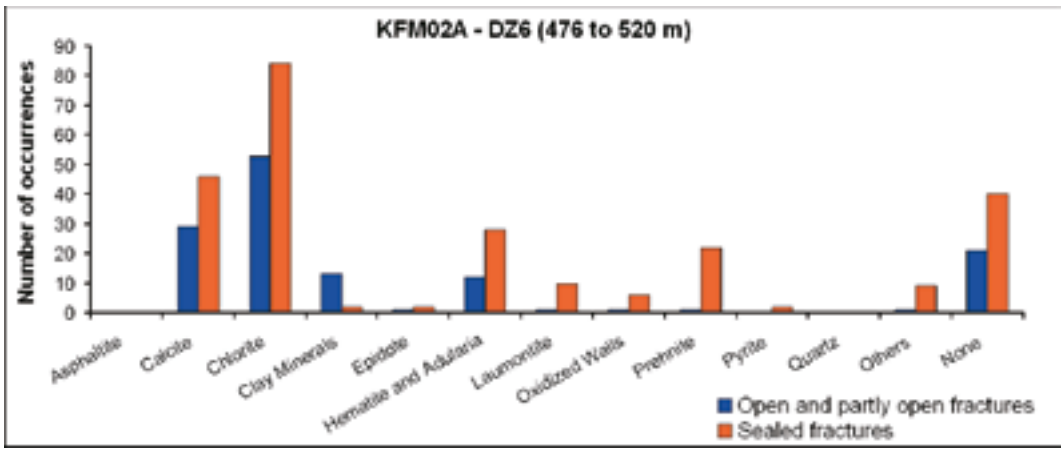

c) ZFMF1

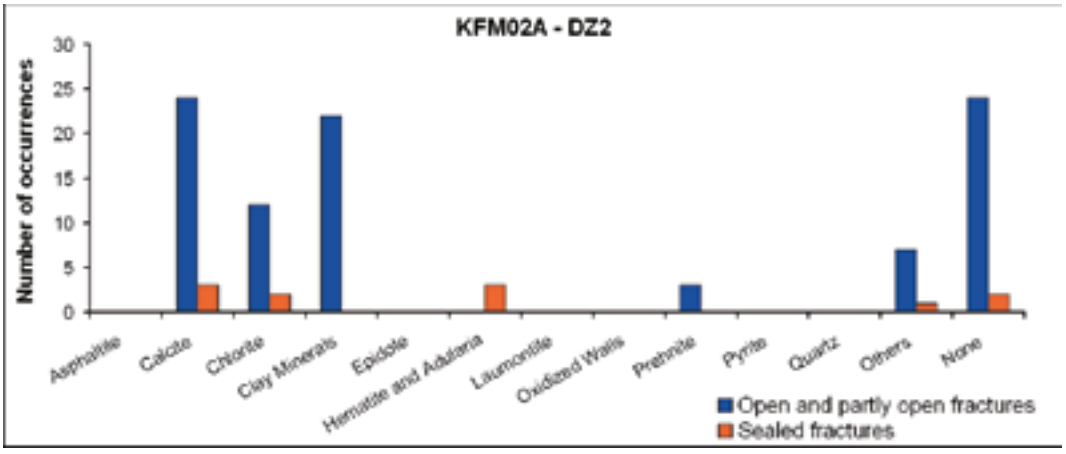

d) ZFM866

Figure 3-2. *Occurrence of different minerals as fillings and coatings along the fractures in deformation zones (a) ZFMA2, (b) ZFMA3, (c) ZFMF1 and (d) ZFM866 /Appendix 15 in Stephens et al. 2007/. The data have been acquired from boreholes other than KFM02B.*

3.3 Single-hole interpretation of borehole KFM02B − outcome

In the first stage of the geological single-hole interpretation (SHI), rock units as well as the possible deformation zones that are intersected by the borehole KFM02B were identified. Key geological and geophysical data in this borehole that have been used in this stage of the work, including rock alteration, the frequency of different types of fractures and focused resistivity, are shown in Figure 3-3 together with the results of the single-hole interpretation /Carlsten et al. 2007a/. The second stage of the SHI, providing the character and kinematics of the possible deformation zones, is documented in /Nordgulen and Saintot 2008/ and evaluated in chapter 8 in this report. A review of the methodology used in the SHI work can be found in /Stephens et al. 2007, p. 35–37/.

Two rock units (RU1 and RU2) in three separate sections have been identified in KFM02B (/Carlsten et al. 2007a/ and Figure 3-3). RU1a in the upper part of the borehole between c. 89 and 323 m borehole length is dominated by medium-grained metagranite-granodiorite (101057) and subordinate occurrences of amphibolite (102017), pegmatitic granite (101061) and fine- to medium-grained metagranitoid (101051). This rock unit is repeated in the lower part of the borehole (RU1b) from c. 428 to the end of the borehole. The intermediate rock unit (RU2) is more inhomogeneous in composition. It is dominated by fine- to medium granite (111058) above c. 393 m and pegmatitic granite (101061) between c. 393 and 428 m. The geophysical logs along the borehole KFM02B show that both the natural gamma radiation and the density decrease in the borehole section between c. 393 and 428 m /Carlsten et al. 2007a/. This can be correlated with the conspicuous occurrence of pegmatitic granite along this borehole interval.

A moving average plot for the frequency of fractures along borehole KFM02B (Figure 3-4) shows several borehole intervals with an anomalous frequency of both open and sealed fractures. The most distinctive anomalies have been interpreted as possible deformation zones (DZ). They are described in /Carlsten et al. 2007a/ and their locations are shown in Figure 3-3. These anomalies occur in the upper part of the borehole between c. 98–115 m (DZ1) and c. 145–204 m (DZ2), and in the lower part of the borehole between c. 411–431 m (DZ3), c. 447–451 m (DZ4), c. 462–473 m (DZ5) and c. 485 and 512 m (DZ6).

All six possible deformation zones only show brittle deformation and are possible fracture zones. They are characterised by an increased frequency of open and sealed fractures (Figure 3-4), and minor occurrences of incohesive crush rock, particularly in the zones in the lower part of the borehole. The geophysical signature of these six possible zones is apparent in the form of low

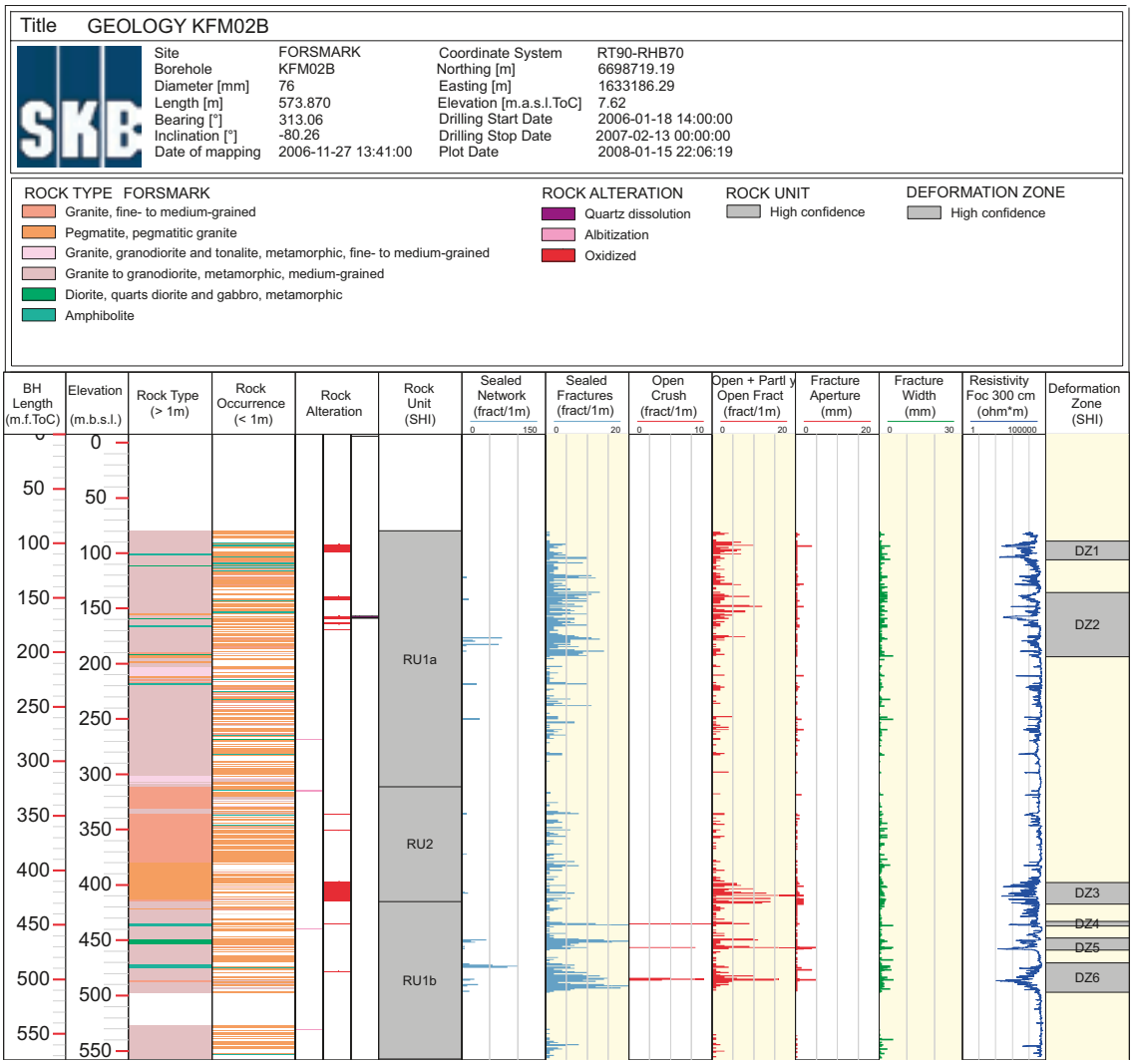

Figure 3-3. *WellCad diagram for the cored borehole KFM02B, showing a selected suite of base geological and geophysical data that have been used to identify rock units and possible deformation zones in the single-hole interpretation of this borehole. The letter after a rock unit helps to distinguish the occurrence of the same rock unit at different intervals along the borehole.*

resistivity anomalies (Figure 3-5), low P-wave velocity and a decrease in magnetic susceptibility. The low resistivity anomalies generally reflect borehole sections with open fractures and incohesive crush rock. They correspond to the anomalies with an increased frequency of especially open fractures in borehole KFM02B (compare Figure 3-4 and Figure 3-5).

Both open and sealed fractures that dip gently form a conspicuous component of fractures along all the possible zones with the exception of DZ4 (Figure 3-6) and a faint to medium oxidation is present along all these structures. Vuggy rock with quartz dissolution is locally present along DZ2. The fracture filling and coating minerals calcite and chlorite are present in all of the possible zones. The older mineral epidote as well as prehnite are conspicuous along fractures in DZ2, DZ4, DZ5 and DZ6 (Figure 3-6b, d, e and f) and adularia/hematite is conspicuous in DZ1, DZ2 and DZ6 (Figure 3-6a, b and f). By contrast, the fracture mineral laumontite is uncommon (Figure 3-6). Clay minerals are present along open fractures in DZ3, DZ5 and DZ6 (Figure 3-6c, e and f). The orientation and mineralogy of the fractures along each possible deformation zone are summarised, together with the confidence level assigned for each possible zone, in Table 3-4.

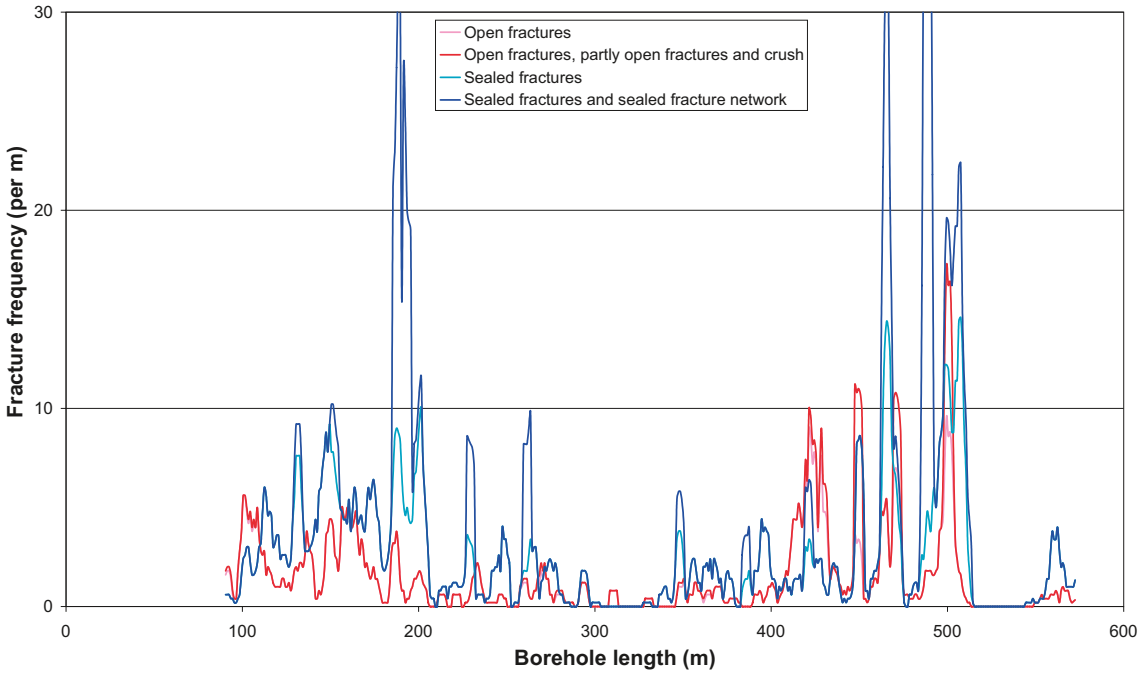

Figure 3-4. *Fracture frequency along borehole KFM02B. Separate moving average plots for open fractures, combined open fractures, partly open fractures and crush zones, sealed fractures, and combined sealed fractures and sealed fracture networks are shown in the diagram. A 5 m window and 1 m steps have been used in the calculation procedure for each plot.*

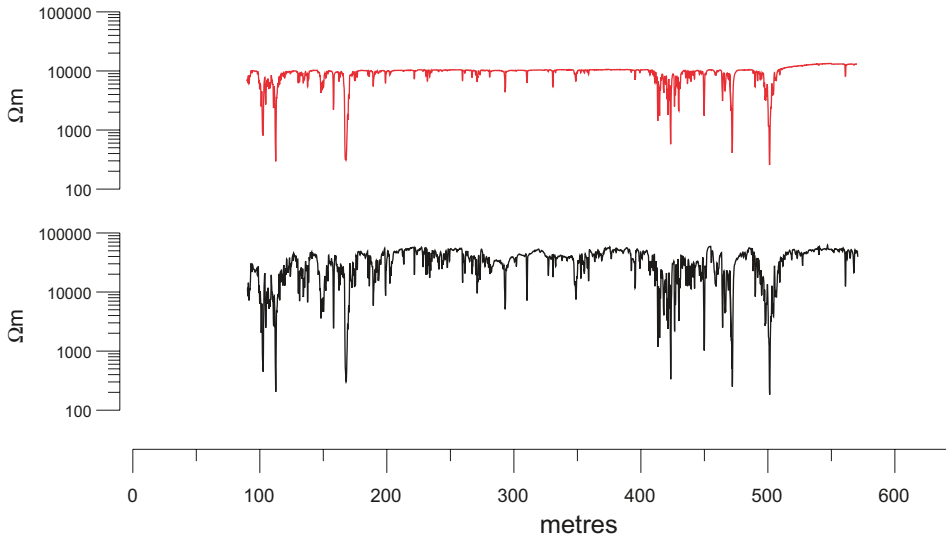

Figure 3-5. *Focused resistivity values along borehole KFM02B. Note the generally good correspondence with the fracture frequency anomalies in Figure 3-4.*

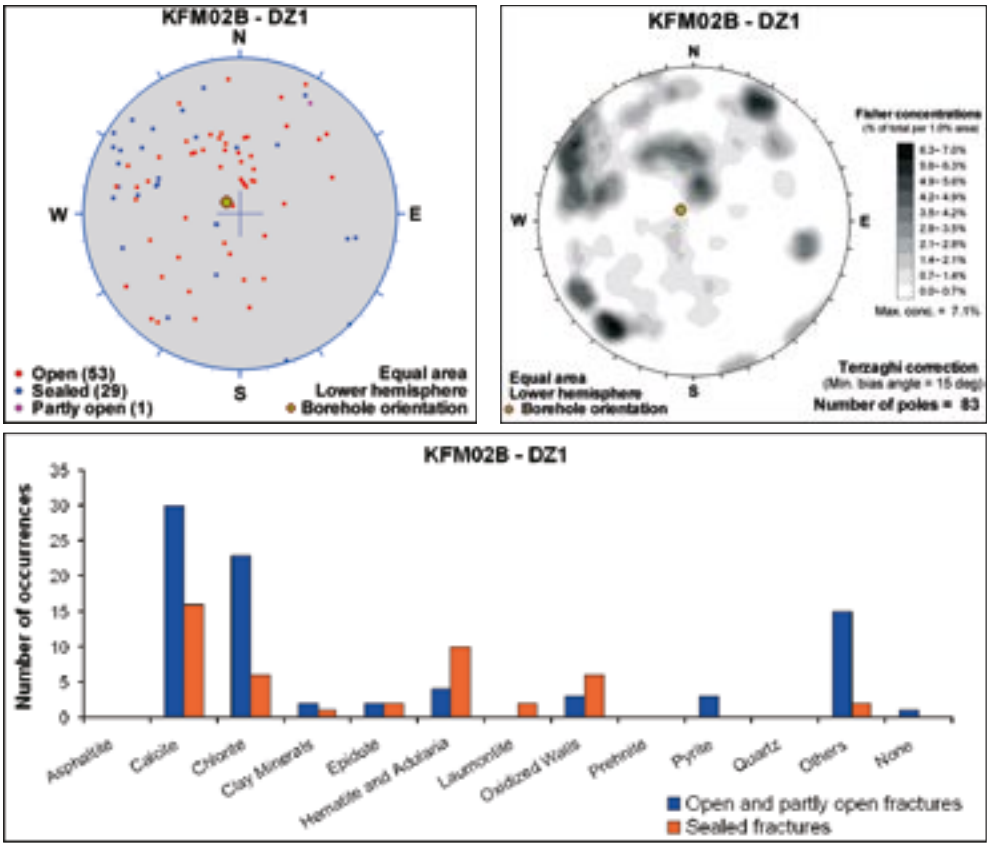
KFM02B - DZ1
N
W
E
S
Open (53)
Sealed (29)
Partly open (1)
Equal area
Lower hemisphere
Borehole orientation
KFM02B - DZ1
Fisher concentrations
Terzaghi correction
Number of poles = 83
KFM02B - DZ1
Number of occurrences
Asphaltite
Calcite
Chlorite
Clay Minerals
Epidote
Hematite and Adularia
Laumontite
Oxidized Wallr
Prehnite
Pyrite
Quartz
Others
None
Open and partly open fractures
Sealed fractures

a)

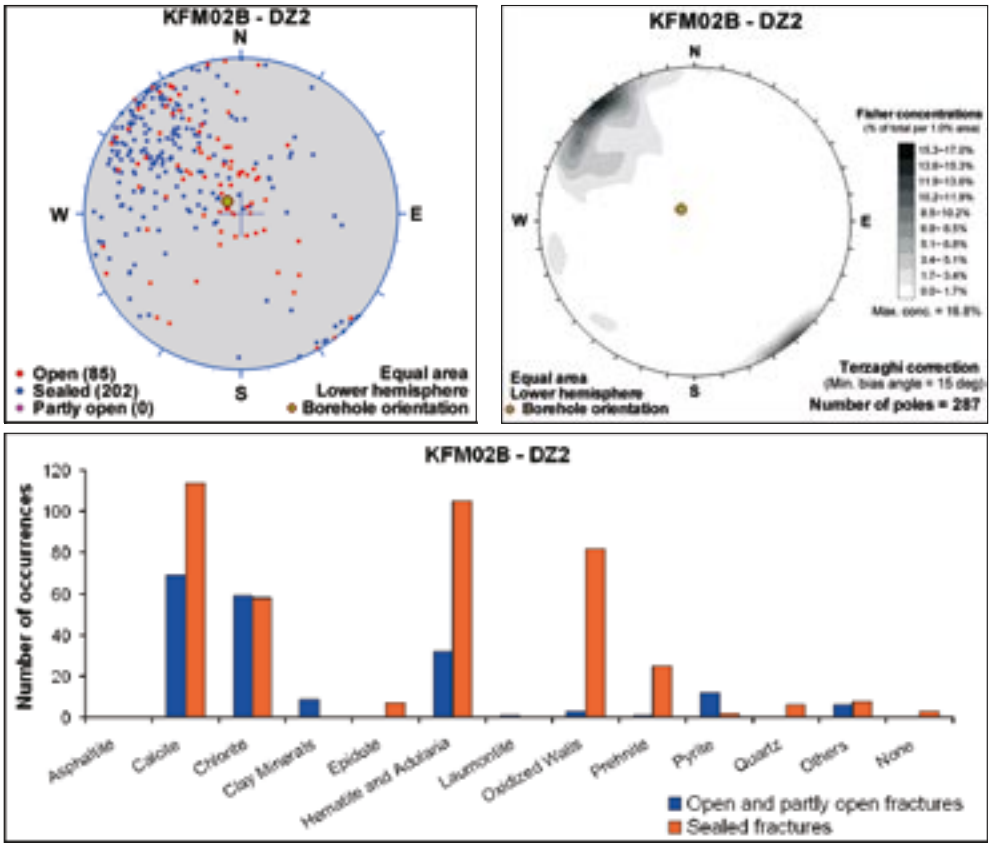
KFM02B - DZ2
N
W
E
S
Open (85)
Sealed (202)
Partly open (0)
Equal area
Lower hemisphere
Borehole orientation
KFM02B - DZ2
Fisher concentrations
Terzaghi correction
Number of poles = 287
KFM02B - DZ2
Number of occurrences
Asphaltite
Calcite
Chlorite
Clay Minerals
Epidote
Hematite and Adularia
Laumontite
Oxidized Wallr
Prehnite
Pyrite
Quartz
Others
None
Open and partly open fractures
Sealed fractures

b)

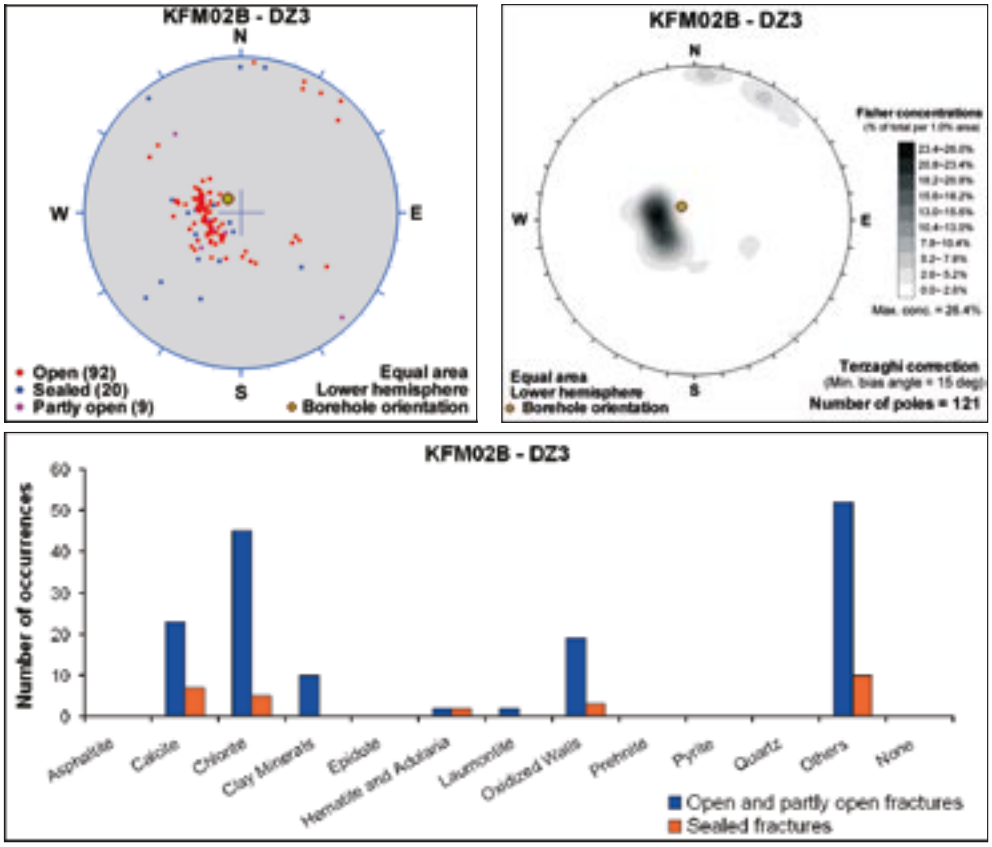
KFM02B - DZ3
N
W
E
S
Open (92)
Sealed (20)
Partly open (9)
Equal area
Lower hemisphere
Borehole orientation
KFM02B - DZ3
Fisher concentrations
Max. conc. = 26.4%
Terzaghi correction
Number of poles = 121
KFM02B - DZ3
Number of occurrences
Asphaltite
Calcite
Chlorite
Clay Minerals
Epidote
Hematite and Adularia
Laumontite
Oxidized Walls
Prehnite
Pyrite
Quartz
Others
None
Open and partly open fractures
Sealed fractures

c)

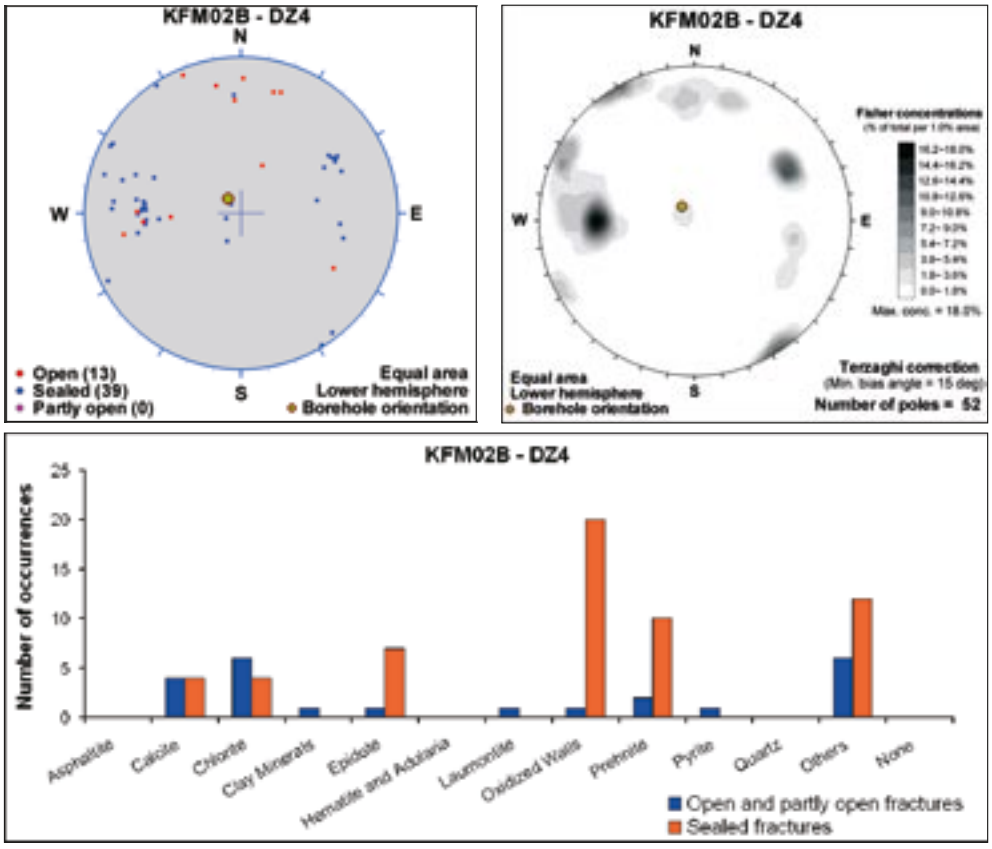
KFM02B - DZ4
N
W
E
S
Open (13)
Sealed (39)
Partly open (0)
Equal area
Lower hemisphere
Borehole orientation
KFM02B - DZ4
Fisher concentrations
Max. conc. = 18.0%
Terzaghi correction
Number of poles = 52
KFM02B - DZ4
Number of occurrences
Asphaltite
Calcite
Chlorite
Clay Minerals
Epidote
Hematite and Adularia
Laumontite
Oxidized Walls
Prehnite
Pyrite
Quartz
Others
None
Open and partly open fractures
Sealed fractures

d)

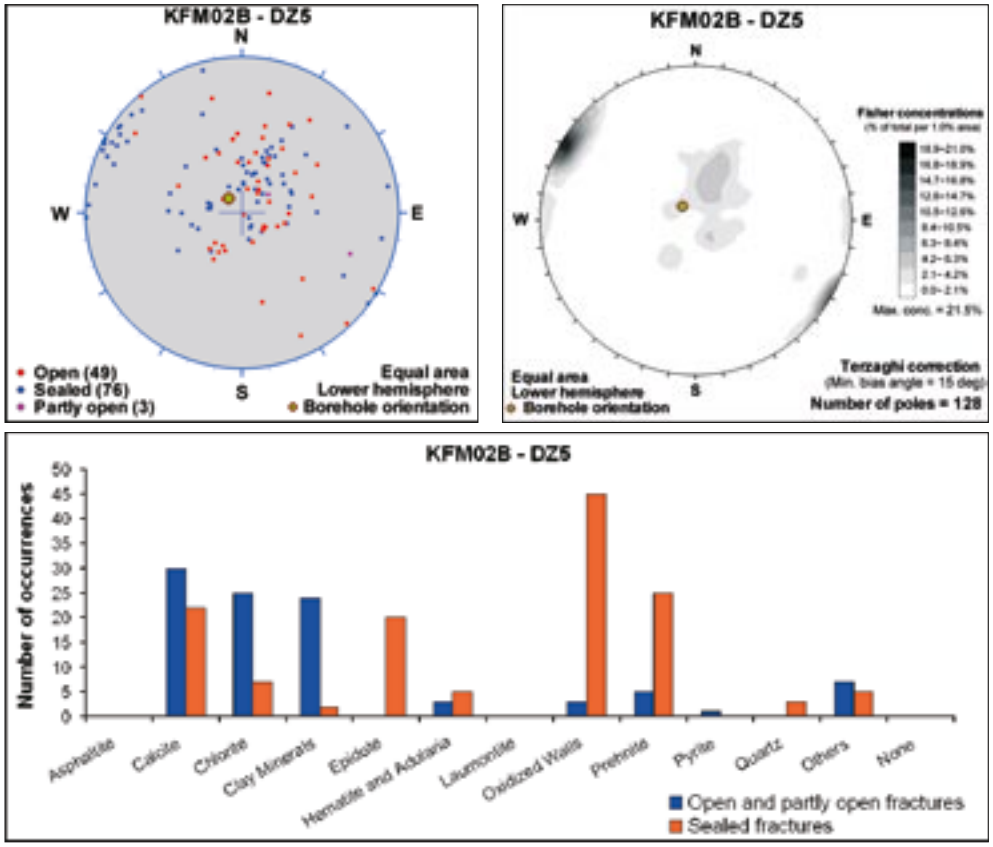

e)

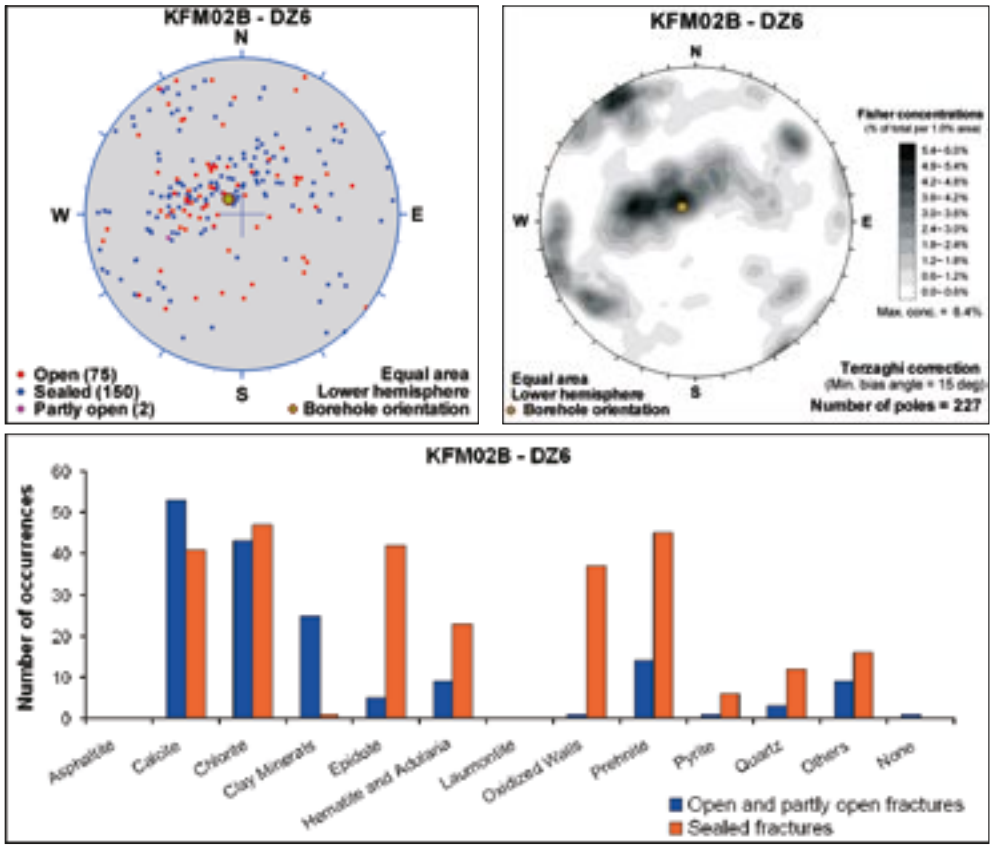

f)

Figure 3-6. *Mean poles to fracture sets and occurrence of different minerals as fillings and coatings along the fractures from six borehole intervals inside the possible deformation zones DZ1 (a), DZ2 (b), DZ3 (c), DZ4 (d), DZ5 (e) and DZ6 (f) in borehole KFM02B.*

Table 3-4. Confidence level, fracture orientation and fracture mineralogy of the possible deformation zones in borehole KFM02B. All borehole lengths are adjusted values. Data extracted from Sicada database: SICADA_07_395 (2007-10-26).

Possible deformation zone	Borehole length (m)		Confidence level	Fracture orientation (strike/dip)	Fracture mineralogy
	UI	LI			
DZ1	98	115	High	Variable orientation	calcite, chlorite, adularia/ hematite, ±clay minerals, ±epidote
DZ2	145	204	High	NE-SW/variable dip mostly to SE including especially gently dipping open fractures	calcite, chlorite, adularia/ hematite, prehnite, quartz, ±clay minerals, ±epidote
DZ3	411	431	High	Gentle	chlorite, calcite, clay minerals, ±adularia/ hematite, ±laumontite
DZ4	447	451	High	Variable orientation	prehnite, chlorite, calcite, epidote,
DZ5	462	473	High	1. Gentle 2. NNE-SSW/steep dip	chlorite, calcite, prehnite, clay minerals, epidote, ±adularia/hematite, ±quartz
DZ6	485	512	High	Gentle	chlorite, calcite, prehnite, epidote, adularia/hematite, clay minerals, ±quartz, ±pyrite

3.4 Prediction − outcome: A comparison

A visualisation of the prediction-outcome test for deformation zones is shown in Figure 3-7. A more detailed comparison between the boundaries of rock domains, fracture domains and deformation zones along borehole KFM02B, as predicted from the deterministic modelling work during stage 2.2 /Stephens et al. 2007/, and the results of the single-hole interpretation of this borehole /Carlsten et al. 2007a/ are presented in Table 3-5, Table 3-6 and Table 3-7, respectively. A statement is made beneath each geological object in these tables, which specifies the changes that need to be made to the corresponding deterministic model, so that the results from the single-hole interpretation of borehole KFM02B are accounted for.

Table 3-5. Correlation between rock domains (RFM) modelled deterministically in regional model stage 2.2 /Stephens et al. 2007/ and rock units (RU) in the single-hole interpretation (SHI) of borehole KFM02B /Carlsten et al. 2007a/. The implications for the regional rock domain model, stage 2.2, are summarised in the text beneath the geological object. UI = Upper intercept, LI = Lower intercept. The borehole lengths are adjusted values.

RFM in local model stage 2.2	Confidence level for RFM in local model stage 2.2	Prediction, borehole length (m)		RU in SHI	Confidence level for RU in SHI	Outcome, borehole length (m)	
		UI	LI			UI	LI
RFM029	High	Start of the borehole	Beneath cored borehole length	RU1a, RU2, RU1b	High	88.56 (top of cored borehole length)	573.54 (base of cored borehole length)
No changes are required.							

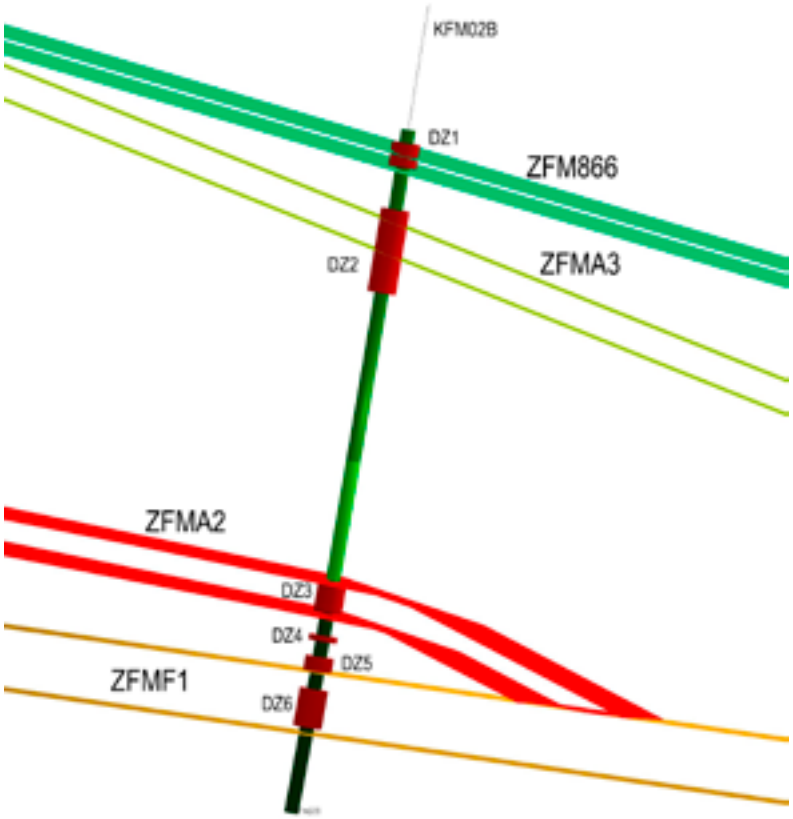

Figure 3-7. *Prediction-outcome verification test for deformation zones along borehole KFM02B. Modelled deformation zones stage 2.2 (ZFM) compared with the six possible deformation zones in the single-hole interpretation (red cylinders). The orientation of the fractures along DZ4 and the geometric relationships shown in the figure argue against a correlation between this possible zone and the zones included in model stage 2.2. The length of borehole KFM02B is c. 573 m. See text for further discussion.*

Table 3-6. Correlation between fracture domains modelled deterministically in stage 2.2 /Olofsson et al. 2007/ and rock units (RU) in the single-hole interpretation (SHI) of borehole KFM02B /Carlsten et al. 2007a/. The implications for the fracture domain model, stage 2.2, are summarised in the text beneath each geological object. UI = Upper intercept, LI = Lower intercept. All borehole lengths are adjusted values.

FFM in local model stage 2.2	Prediction, borehole length (m)		RU in SHI	Outcome, borehole length (m)	
	UI	LI		UI	LI
FFM03	Start of the borehole	407	Bedrock outside deformation zones and inside RU1a and RU2	88.56 (top of cored borehole length)	411
Very minor adjustment is required due to thickness of zone ZFMA2 along the borehole.					
FFM01	430	Beneath cored borehole length	Bedrock outside deformation zones and inside RU1b and	431	573.54 (base of cored borehole length)
Very minor adjustment is required due to thickness of zone ZFMA2 along the borehole.					

Table 3-7. Correlation between deformation zones modelled deterministically in model stage 2.2 (ZFM) and possible deformation zones (DZ) in the single-hole interpretation (SHI) of borehole KFM02B. The changes in properties that are required, so to be consistent with the stage 2.3 data, are listed here. The possible deformation zone referred to as DZ4 in the SHI, which was recognised with a high degree of confidence, cannot be linked to any modelled zone. UI = Upper intercept, LI = Lower intercept. All borehole lengths are adjusted values.

ZFM in model stage 2.2	Confidence level for ZFM in model stage 2.2	Prediction, borehole length (m)		DZ in SHI	Confidence level for DZ in SHI	Outcome, borehole length (m)	
		UI	LI			UI	LI
ZFM866	High	104	115	DZ1	High	98	115
No changes are required for an intersection along KFM02B. Thickness along KFM02B is 16 m.							
ZFMA3	High	153	176	DZ2	High	145	204
Thickness needs to be modified. Thickness along KFM02B is 58 m.							
ZFMA2	High	407	430	DZ3	High	411	431
No changes are required for an intersection along KFM02B. Thickness along KFM02B is 20 m.							
				DZ4	Medium	447	451
Possibly not a deformation zone. High fracture frequency of steeply dipping fractures related to rock type (amphibolite).							
ZFMF1	High	472	515	DZ5	High	462	473
				DZ6		485	512
Thickness needs to be modified. ZFMF1 intersects both DZ6 and the lower part of DZ5 in KFM02B. Probably two segments of same gently dipping zone (ZFMF1). Thickness along KFM02B is 50 m (includes less deformed segment between DZ5 and DZ6).							

The entire borehole KFM02B is drilled within a bedrock that can be assigned to rock domain RFM029. Thus, as predicted, no rock domain boundaries are intersected along the borehole. The boundary between fracture domains FFM03 and FFM01 corresponds to the gently dipping deformation zone ZFMA2. The predicted position of the boundary, i.e. the upper and the lower boundary of ZFMA2, occurs only 4 m and 1 m, respectively, deeper than that predicted in the stage 2.2 deterministic modelling work (Table 3-6).

The fracture orientation, fracture mineralogy, alteration and style of deformation of the six possible deformation zones identified in the single-hole interpretation /Carlsten et al. 2007a/ support the correlation of five of these possible zones with the gently dipping fracture zones ZFM866, ZFMA3, ZFMA2 and ZFMF1 already modelled deterministically in stage 2.2 (Figure 3-7 and Table 3-7). It is inferred that both DZ5 and DZ6 represent two separate segments of zone ZFMF1. These four fracture zones intersect the possible deformation zones along KFM02B directly, without any need for modification (ZFM866 and ZFMA2) or after a modification of the thickness (ZFMA3 and ZFMF1). One possible deformation zone (DZ4), which was identified in the SHI with a high degree of confidence, cannot be matched to a deterministically modelled zone in stage 2.2. Bearing in mind the high frequency of steeply dipping fractures along this structure, its short length and its spatial association with a minor amphibolite body, it is tentatively inferred that this feature is not a deformation zone but a local cluster of fractures related to a lithology (Table 3-7).

It is concluded that the results from the drilling of KFM02B are in good agreement with all the deterministic geological models in the vicinity of this borehole. However, since borehole KFM02A is located close to borehole KFM02B and the data from the former borehole has been used in model stage 2.2, the prediction-outcome test for borehole KFM02B, presented above, does not bear too much weight as a model verification tool.

4 Borehole KFM08D

4.1 Background

A strategic decision was taken in connection with the deterministic modelling of steeply dipping deformation zones, stage 2.1, to focus attention on low magnetic lineaments in the identification of such zones at the Forsmark site /SKB 2006/. As a consequence of this decision, high-resolution ground magnetic surveys were undertaken during 2006 and 2007 (/Isaksson et al. 2006ab, 2007/ and Figure 2-1). These data complement the earlier airborne (helicopter) geophysical measurements. The ground surveys aimed to identify and constrain more precisely the position of predominantly brittle deformation zones (fracture zones) that occur inside the target area, in the north-western part of the candidate area. These new data firstly provided an excellent image of the major fold structure (synform) inside the tectonic lens at Forsmark (Figure 2-1). They also indicated two sub-sets of low magnetic lineaments that trend ENE and NNE inside this area (Figure 2-2). The improved resolution provided, for the first time, a clear indication of lineaments with a NNE trend in the target area.

The NNE sub-set of lineaments is prominent under Asphällsfjärden, south-west of the start of the tunnel system to the SFR facility (Figure 2-2), and it was soon realised that there are insufficient data – both along the ground surface and at depth along cored boreholes – that permit a characterisation of this sub-set. Data analysis and modelling work during the autumn 2006, in connection with model stage 2.2, as well as a special study instigated by the modelling team that involved excavation of two of these lineaments /Petersson et al. 2007/, confirmed that at least some of them are fracture zones in the bedrock. Furthermore, the possible zone DZ7 in KFM06A, which is modelled deterministically as zone ZFMNNE0725 /Stephens et al. 2007/, contains groundwater along fractures that strike NNE-SSW and dip steeply /Follin et al. 2007/.

In order to obtain further data that can reduce uncertainties in both the geological and, not least, the hydrogeological character of possible fracture zones related to these lineaments, a new telescope borehole, KFM08D, was planned (Figure 1-2). This borehole also served to provide geological, hydrogeological and hydrogeochemical information at the depth for a potential repository, in a part of the target volume where such data were absent (Figure 1-2). The decision statement and motivation for borehole KFM08D are provided in document ID 1062642. The position, inclination, bearing and borehole length are summarised in Table 4-1. Since borehole KFM08D is situated inside the target volume and lies some considerable distance away from other boreholes at potential repository depth, it provides an excellent opportunity to test the validity of the stage 2.2 geological models inside the potential repository volume, using a prediction-outcome working mode. This section provides the results of this analysis and documents the implications for the stage 2.2 geological models.

Table 4-1. Position, inclination, bearing and length of borehole KFM08D. Data extracted from Sicada database: SICADA_07_292 (2007-08-14).

Borehole	Drill site	Easting RT 90, 2.5 gon W (m)	Northing RT 90, 2.5 gon W (m)	Inclination (°)	Bearing (°)	Length (m)
KFM08D	8	1631199	6700492	–55	100	942

4.2 Prediction of intersections of geological features along borehole KFM08D based on model stage 2.2

With the help of the RVS software, a prediction of the intersections with borehole KFM08D of the boundaries of rock domains, fracture domains and deterministic deformation zones, which are included in model stage 2.2 /Olofssson et al. 2007, Stephens et al. 2007/, can be carried out.

The boundary in the local model between the rock domain dominated by medium-grained metagranite-granodiorite (RFM029) and that dominated by altered (albitized) metagranite (RFM045) is predicted to intersect the borehole at a length of 362 m (Table 4-2). This rock domain boundary also corresponds to the boundary between fracture domains FFM01 and FFM06 (Table 4-2). According to model stage 2.2, rock domain RFM045 and fracture domain FFM06 occupy the remainder of borehole KFM08D. The boundary between fracture domains FFM02 and FFM01 has been modelled to be relatively shallow close to drill site 8, and the boundary between these two domains is predicted to intersect borehole KFM08D at 60 m, i.e. FFM02 is not present in the cored part of the borehole (Table 4-2).

Table 4-3 shows the predicted upper and lower borehole intersections of the deformation zones modelled deterministically in model stage 2.2 along borehole KFM08D. The properties of these local major and minor deformation zones are provided in /Appendices 15 and 16 in Stephens et al. 2007/, respectively, and selected aspects (confidence of existence, orientation, orientation class, trace length at the ground surface and size class) are also shown in Table 4-3. The properties of an addional two minor zones (ZFMENE0168, ZFMNNE2300), which are situated near to the base of borehole KFM08D but are not predicted to intersect this borehole in model stage 2.2, are also presented in /Appendix 16 in Stephens et al. 2007/. All the terminology used here that refers to deformation zones is in accordance with that provided in /Stephens et al. 2007, section 2.4/.

The modelling work during stage 2.2 predicts that seven, steeply dipping fracture zones that occur in the orientation sub-sets referred to as ENE and NNE /Stephens et al. 2007, chapter 5/ intersect borehole KFM08D and two more minor zones, with the same orientation (ZFMENE0168, ZFMNNE2300) are also present close to the base of the borehole. At the base of the borehole, a steeply dipping zone classified as WNW is predicted to intersect the borehole. It is apparent that borehole KFM08D should resemble borehole KFM06A, where it concerns the frequency of occurrence of steeply dipping, ENE or NNE fracture zones.

The confidence of existence of these ten steeply dipping fracture zones varies between high and medium (Table 4-3). The four high confidence zones have been modelled by linking one or more borehole intersections with an inferred corresponding low magnetic lineament. Each of the six zones with a medium confidence of existence has been modelled by simple downward projection of a corresponding low magnetic lineament, according to the methodology and assumptions used for the modelling of deformation zones described in /Stephens et al. 2007,

Table 4-2. Predicted intersections of deterministically modelled, rock and fracture domains in model stage 2.2 with borehole KFM08D. Borehole intersections have been extracted with the assistance of RVS, using data on the bearing and inclination of the trace of borehole KFM08D and the geometry of rock and fracture domains in the local model, stage 2.2 /Stephens et al. 2007/.

Modelled rock domain (RFM)	Modelled fracture domain (FFM)	Cored borehole length (m)	
		Upper intersection	Lower intersection
RFM029	FFM02	Not present in the cored part of the borehole.	
RFM029	FFM01	Start of the cored borehole length	362
RFM045	FFM06	362	Beneath cored borehole length

Table 4-3. Predicted intersections of deformation zones modelled deterministically in model stage 2.2 with borehole KFM08D. Borehole intersections have been extracted with the assistance of RVS, using data on the bearing and inclination of the trace of borehole KFM08D and the geometry of deformation zones in local model stage 2.2 /Stephens et al. 2007/. Zone confidence, orientation and length are extracted from /Appendices 15 and 16 in Stephens et al. 2007/. UI = Upper intercept, LI = Lower intercept. All borehole lengths are adjusted values. All orientations are provided as strike/dip using the right-hand-rule-method.

Modelled deformation zone (ZFM)	Confidence of existence	Strike/dip (°) and orientation class /Stephens et al. 2007/	Inferred trace length at the ground surface (m)	Size class	Borehole length (m)	
					UI	LI
ZFMENE2120	High	237/82 Steep/ENE	239	Minor (<1 km)	193	218
ZFMENE0159A	High	239/80 Steep/ENE	1,909	Local major (<3 km)	304	345
ZFMENE0159B	Medium	238/80 Steep/ENE	673	Splay from zone ENE159A (whole zone <3 km; splay <1 km)	373	390
ZFMNNE2309	Medium	215/80 Steep/NNE	804	Minor (<1 km)	429	444
ZFMNNE2308	Medium	214/80 Steep/NNE	1,419	Local major (<3 km)	602	623
ZFMENE2320	High	244/81 Steep/ENE	1,251	Local major (<3 km)	667	740
ZFMNNE2293	Medium	208/80 Steep/NNE	996	Local major (c. 1 km)	718	739
ZFMWNW2225	High	120/75 Steep/WNW	1,613	Local major (<3 km)	906	Beneath cored borehole length

section 5.1.1/. The inferred dip in these zones has been selected by comparison with high confidence zones that show similar orientation and character. For this reason, the dips of the medium confidence zones and, consequently, their predicted intersections along the borehole have a low level of confidence /Appendices 15 and 16 in Stephens et al. 2007/. This feature needs to be taken into consideration when the prediction-outcome exercise is assessed (see below).

All the predicted zones are significantly less than 3,000 m in trace length at the surface (Table 4-3). Based on their inferred trace length, they can be described as local major (≥1,000 m) or minor (<1,000 m) zones. Three zones that are modelled with high confidence (ZFMENE0159A, ZFMENE2320 and ZFMWNW2225) are inferred to be intersected by other cored boreholes /Appendix 15 in Stephens et al. 2007/ and one of these zones (ZFMENE2120) is inferred to be intersected by a percussion borehole /Stephens et al. 2007, Appendix 16/. For this reason, data are available for some of the ENE zones and for the single WNW zone, which constrain the critical properties alteration and fracture characteristics. Kinematic data are also available for ZFMENE0159A /Appendix 15 in Stephens et al. 2007/.

Red-stained bedrock that contains fine-grained hematite dissemination is present in all the high confidence zones intersected by cored boreholes /Appendix 15 in Stephens et al. 2007/. This type of alteration has been mapped and is referred to in the Sicada database as oxidation. It is coupled with a low magnetic susceptibility in the bedrock and accounts for the correlation of these fracture zones with low magnetic lineaments. Chloritised amphibolite and vuggy rock with quartz dissolution are also locally present along one of the intersections through ZFMENE2320 /Appendix 15 in Stephens et al. 2007/.

Sealed fractures dominate in all the three high confidence zones intersected by cored boreholes /Appendix 15 in Stephens et al. 2007/. The mean pole of the dominant set of fractures along the four high confidence zones that are intersected by boreholes is consistent with the inferred orientation of the zone (Figure 4-1). Furthermore, there is more than one set of fractures along each zone. In particular, gently dipping fractures are present in all the zones.

Besides calcite and chlorite, which are present in all zones, laumontite and adularia/hematite as well as the younger generation minerals pyrite and clay minerals (see, for example, /Sandström et al. 2008a/) are present along the two ENE zones ZFNENE0159A and ZFMENE2320 (Figure 4-2a and b), while adularia/hematite, the older generation mineral epidote (see, for example, /Sandström et al. 2008a/) and younger clay minerals are present along ZFMWNW2225 (Figure 4-2c). Clay minerals are conspicuous along open fractures. It is inferred that all three zones are ancient geological structures that have been subject to reactivation and fluid movement at different times during the later geological evolution. Furthermore, the aperture observed along at least some of the open fractures is a geologically, relatively young feature.

Kinematic data from an excavation across ZFMENE0159A indicate that this zone has been affected by sinistral strike-slip displacement at some time during its tectonic evolution /Nordgulen and Saintot 2006/. Steeply dipping minor faults with NNW strike along one of the borehole intersections through this zone also show strike-slip kinematics. Strike-slip displacement is a characteristic feature of several of the steeply dipping deformation zones that are referred to as ENE, NE or NNE and that transect the target volume at Forsmark /Stephens et al. 2007/.

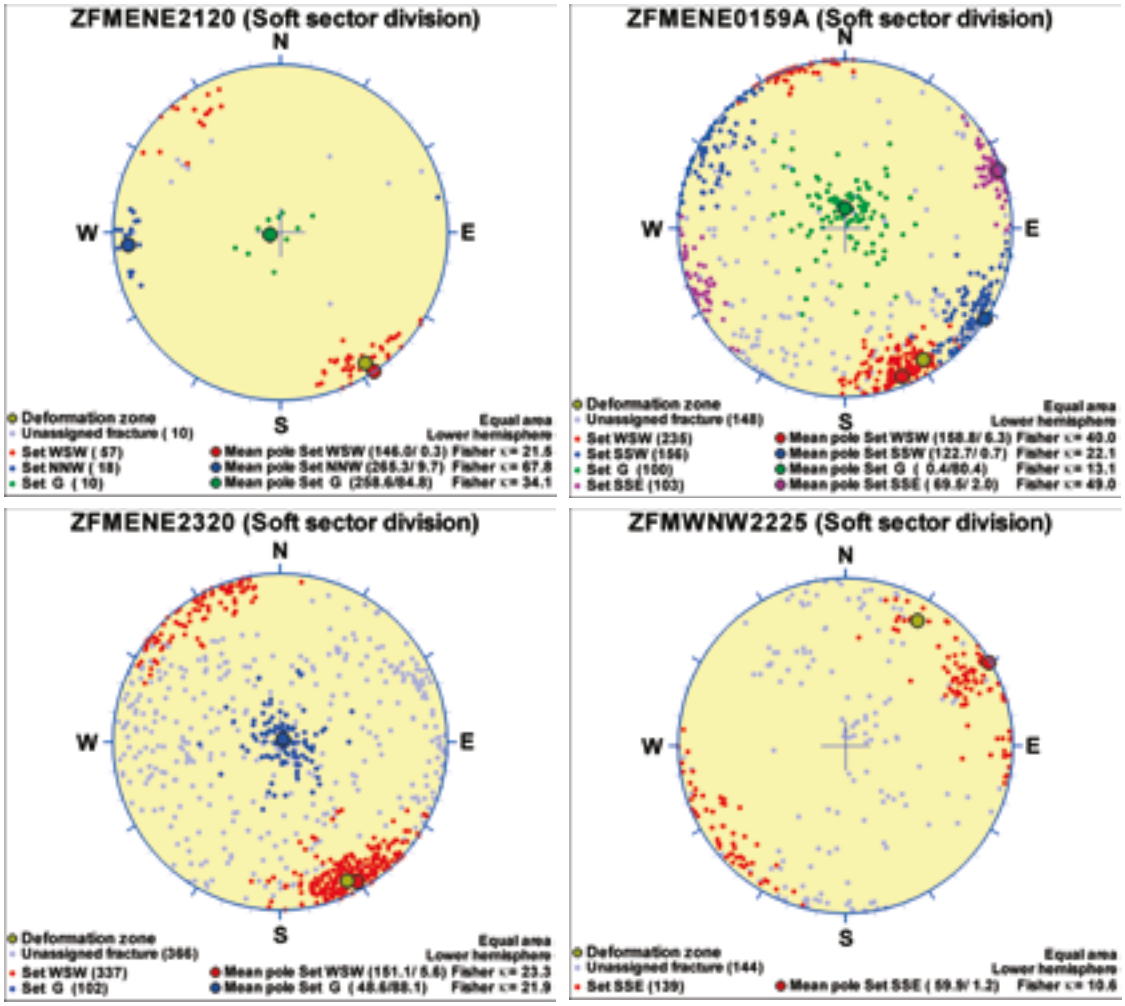

Figure 4-1. *Mean poles to fracture sets inside the deterministically modelled deformation zones ZFMENE2120, ZFMENE0159A, ZFMENE2320 and ZFMWNW2225, model stage 2.2 /Appendices 15 and 16 in Stephens et al. 2007/. The data have been acquired from boreholes other than KFM08D. The methodology used to identify fracture sets is also described in /Stephens et al. 2007/.*

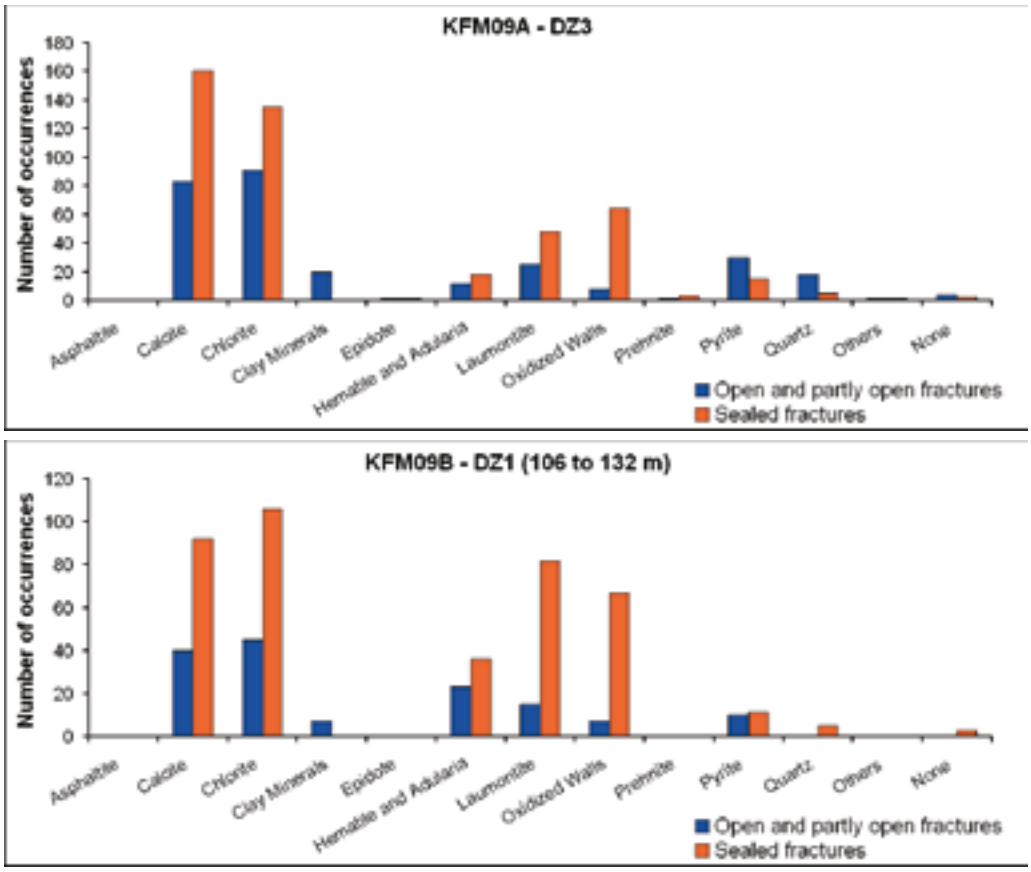

a) ZFMENE0159A

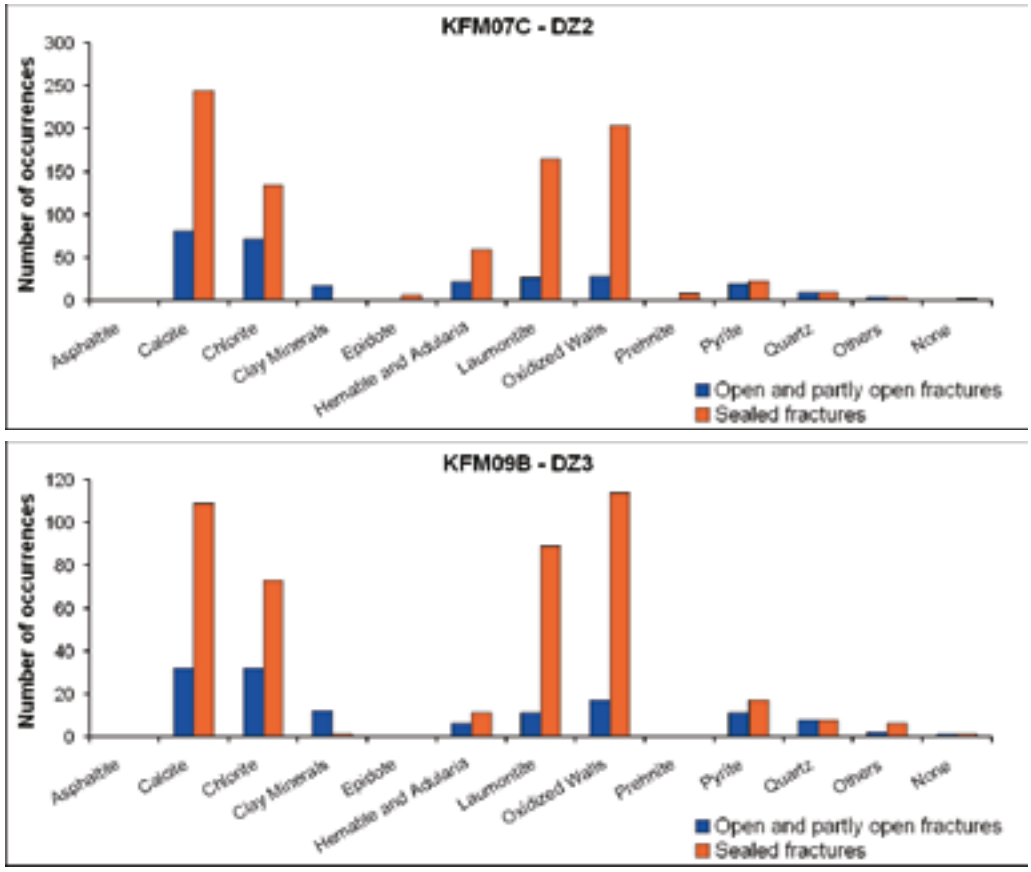

b) ZFMENE2320

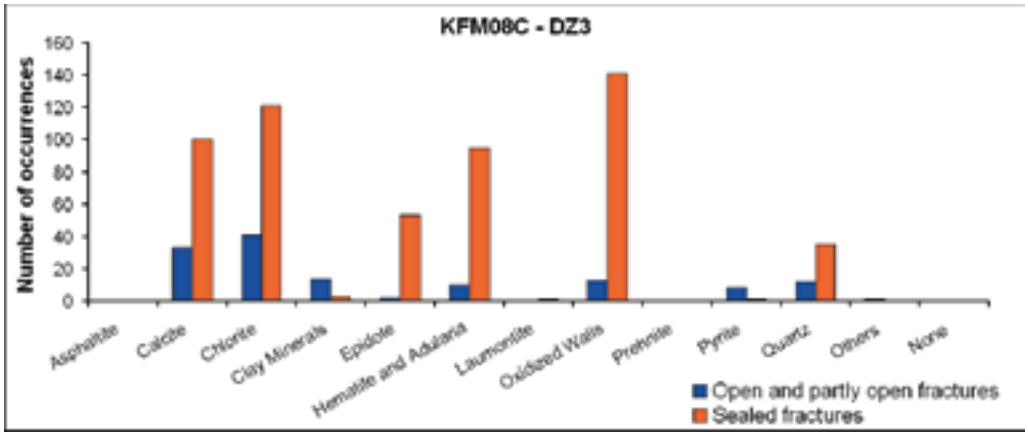

c) ZFMWNW2225

Figure 4-2. *Occurrence of different minerals as fillings and coatings along the fractures in deformation zones ZFMENE0159A (a), ZFMENE2320 (b) and ZFMWNW2225 (c), based on Appendix 15 in /Stephens et al. 2007/. The data have been acquired from boreholes other than KFM08D. There are no data for ZFMENE2120 since this zone has been modelled with the help of data from a percussion borehole.*

4.3 Single-hole interpretation of borehole KFM08D − outcome

Key geological and geophysical data in borehole KFM08D that have been used during the first stage of the single-hole interpretation (SHI) of KFM08D are shown in Figure 4-3 together with the results of the interpretation /Carlsten et al. 2007b/. The character and kinematics of the possible deformation zones, which were completed during the second stage of the SHI and are addressed in /Nordgulen and Saintot 2008/, are treated together with similar data from other complementary (stage 2.3) boreholes in chapter 8.

Geophysical logs along borehole KFM08D, which show the variation of silicate density, natural gamma radiation and a potassium depletion index based on natural gamma radiation, are presented in Figure 4-4. In general, the bedrock beneath a borehole length of c. 396 m shows a decreased natural gamma radiation. This decrease can be correlated with a depletion of potassium (Figure 4-4) and corresponds to the part of the borehole where the dominant rock type, medium-grained metagranite-granodiorite (SKB rock code 101057), shows, to variable degree, the effects of alteration referred to as albitization (SKB alteration code 104). This alteration resulted in the removal of K-feldspar and an increase in the content of quartz in granitic rocks /see p. 60–62 in Stephens et al. 2007/.

Two borehole sections, between c. 570 and 651 m and c. 842 and 929 m are more inhomogeneous and dominated by, in general, more subordinate rocks in the tectonic lens at Forsmark /Stephens et al. 2007/. Borehole sections with anomalously high silicate densities (c. 3,000 to 3,100 kg/m^3) are conspicuous between c. 570 and 597 m and between c. 897 and 929 m (Figure 4-4). They correspond to amphibolite (102017) and to metadiorite with subordinate amphibolite (101033/102017), respectively. The geological mapping indicates that these two borehole sections are also spatially associated with Group D /Stephens et al. 2003/ pegmatite and pegmatitic granite (101061) and fine- to medium-grained granite (111058), and Group C fine- to medium-grained metagranitoid (101051). The high natural gamma radiation anomalies (Figure 4-4) are present inside the Group D rocks. The Group C rocks that are present between c. 597 and 651 m and strongly dominate between c. 842 and 877 m show a moderate silicate density (c. 2,700 to 2,800 kg/m^3; Figure 4-4), which corresponds to a tonalitic or granodioritic rock composition.

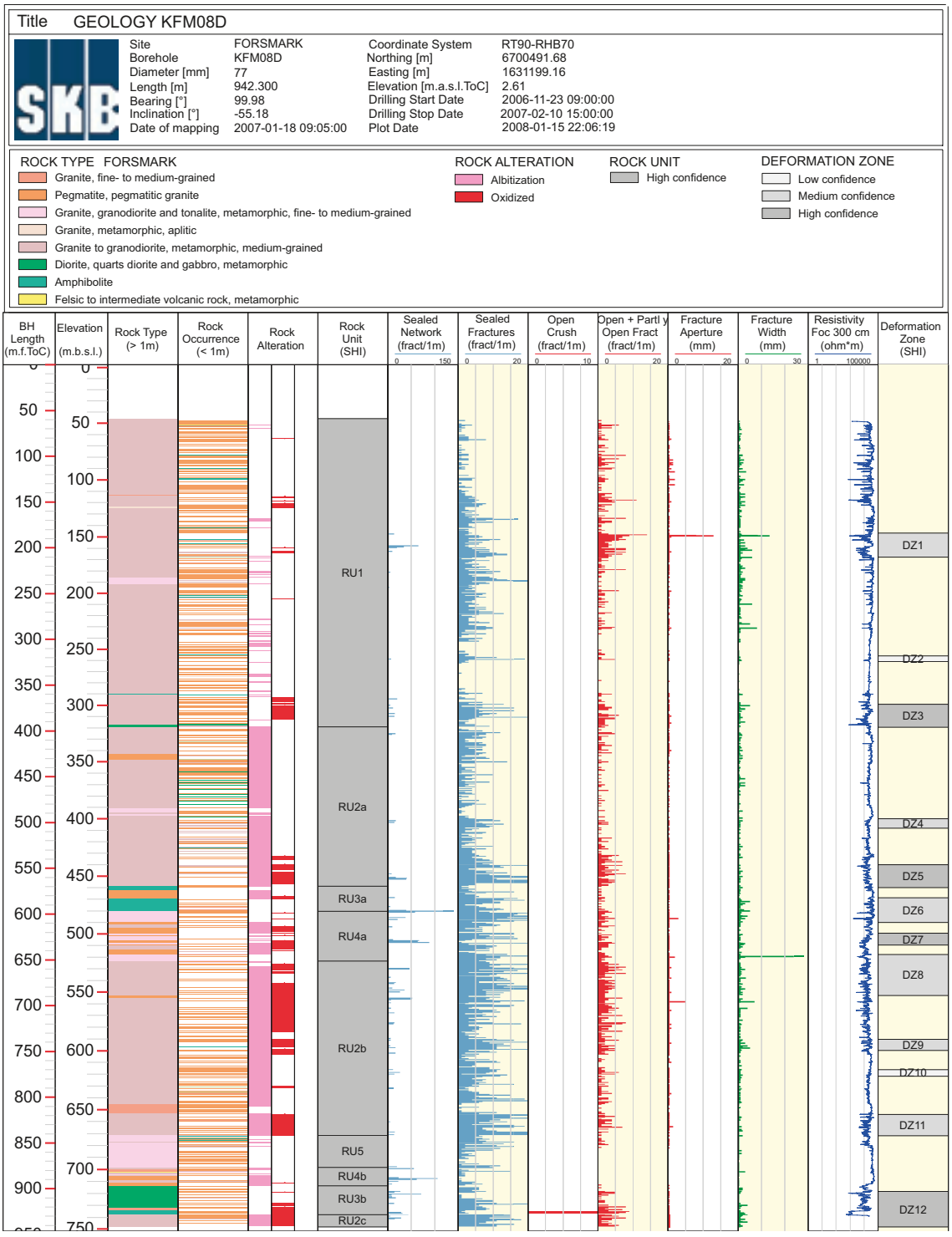

Figure 4-3. *WellCad diagram for the cored borehole KFM08D, showing a selected suite of base geological and geophysical data that have been used to identify rock units and possible deformation zones in the SHI of this borehole /Carlsten et al. 2007b/. The letter after a rock unit simply helps to distinguish the occurrence of the same rock unit at different intervals along the borehole.*

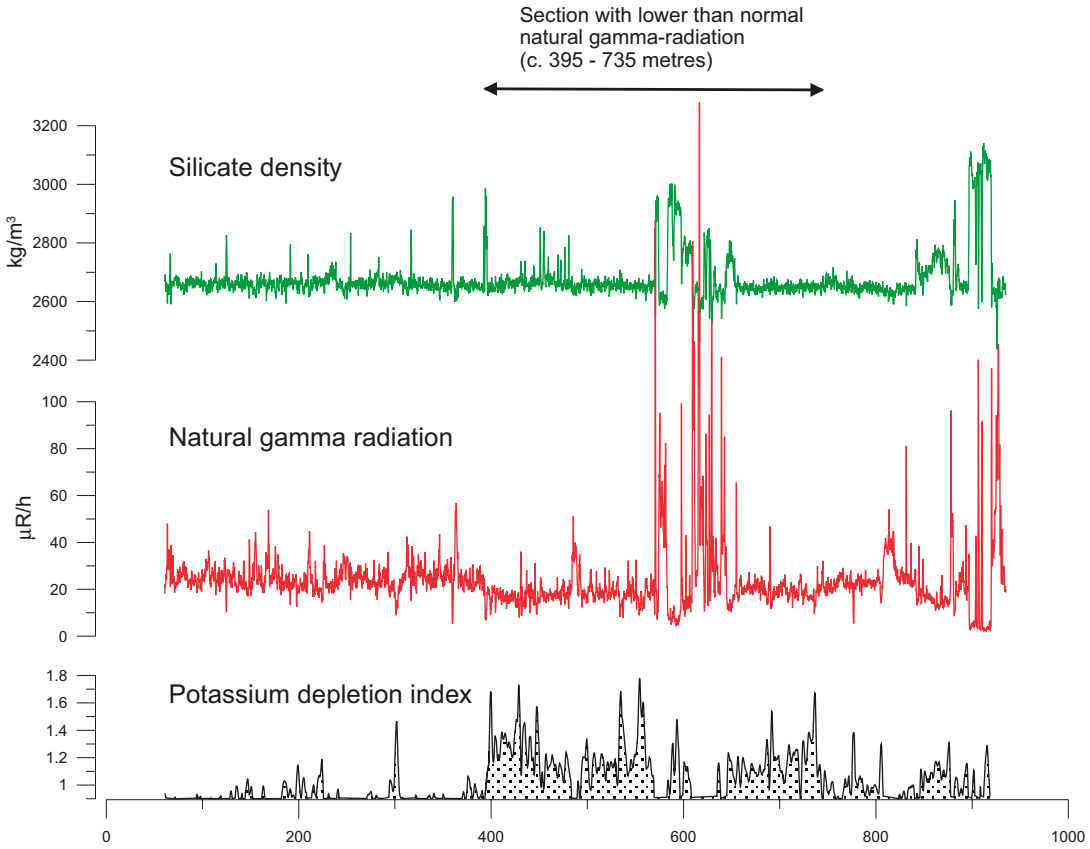

Figure 4-4. *Silicate density, natural gamma radiation and calculated potassium depletion index along borehole KFM08D. The horizontal axis shows borehole length.*

A moving average plot for the frequency of fractures along borehole KFM08D is shown in Figure 4-5. Conspicuous anomalies in all fractures, but especially in the frequency of sealed fractures and sealed fracture networks, are apparent along several borehole intervals. These anomalies are most conspicuous between c. 180 and 210 m, between c. 371 and 396 m, at several intervals between c. 500 and 775 m, between c. 820 and 840 m and close to the bottom of the borehole between c. 900 and 942 m. Furthermore, an incohesive crush rock with clay minerals is conspicuous at c. 926 m. These anomalies correspond to intervals of reduced resistivity in the bedrock (Figure 4-6). The further correlation of these anomalies with the occurrence of the type of alteration referred to as oxidation, i.e. red-staining related to hematite dissemination /see p. 60–68 in Stephens et al. 2007/, low magnetic susceptibility and low P-wave velocity has provided the basis for the identification of possible deformation zones along these intervals in the borehole. The upper part of the borehole contains a number of narrow, low resistivity anomalies (Figure 4-6) that are possibly linked to single, open fractures.

The resulting inferred rock units (five geologically distinct units along nine different borehole intervals) and possible deformation zones (twelve) are shown in Figure 4-3. The orientation and mineralogy of the fractures along each possible deformation zone are documented in Figure 4-7. These two features are summarised in Table 4-4 together with the confidence level assigned to the possible zones during the SHI work. These data indicate the frequent occurrence of possible deformation zones with steeply dipping fractures that strike ENE-WSW to NNE-SSW and that are sealed with the index minerals adularia/hematite, and to less extent laumontite and quartz. Clay mineral coatings are conspicuous along open fractures in DZ1 and, most significantly, in DZ12 at the bottom of the borehole.

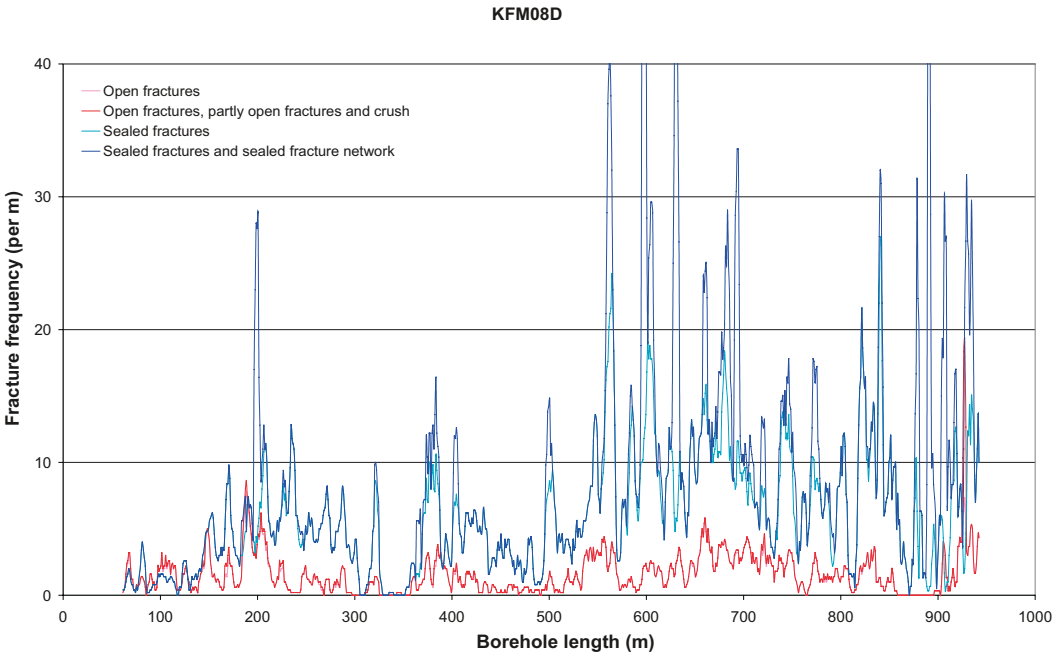

Figure 4-5. *Fracture frequency along borehole KFM08D. Separate moving average plots for open fractures, combined open fractures, partly open fractures and crush zones, sealed fractures, and combined sealed fractures and sealed fracture networks are shown in the diagram. A 5 m window and 1 m steps have been used in the calculation procedure for each plot.*

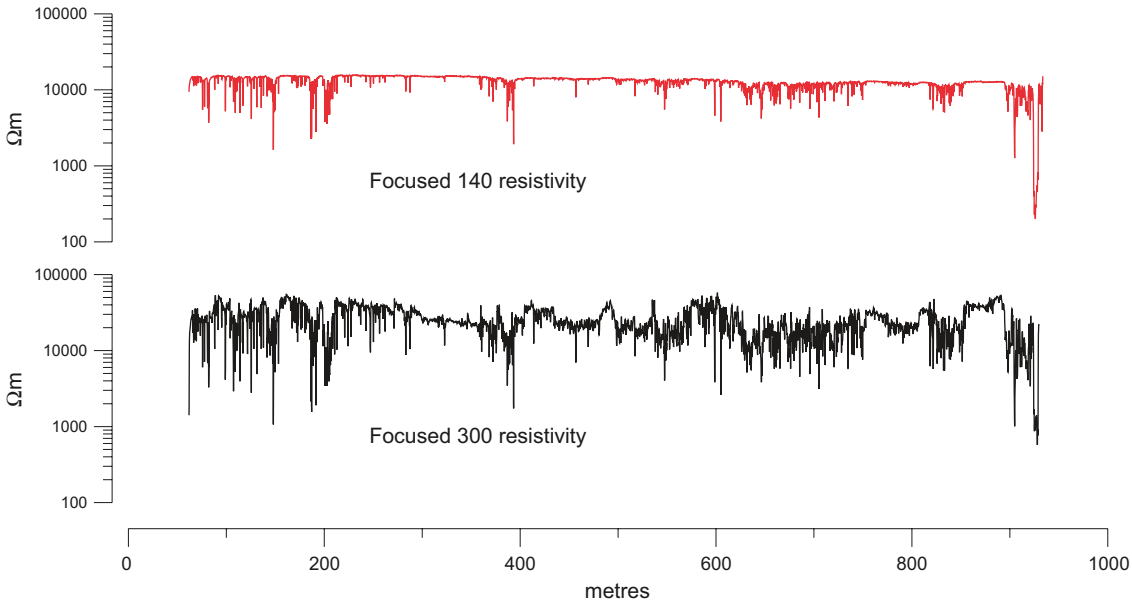

Figure 4-6. *Focused resistivity values (140 and 300 cm) along borehole KFM08D. Note the generally very good correspondence with the fracture frequency anomalies in Figure 4-5.*

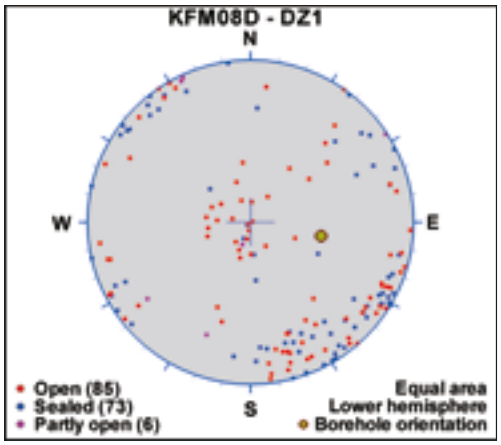
KFM08D - DZ1
N
W
E
S
Open (85)
Sealed (73)
Partly open (6)
Equal area
Lower hemisphere
Borehole orientation

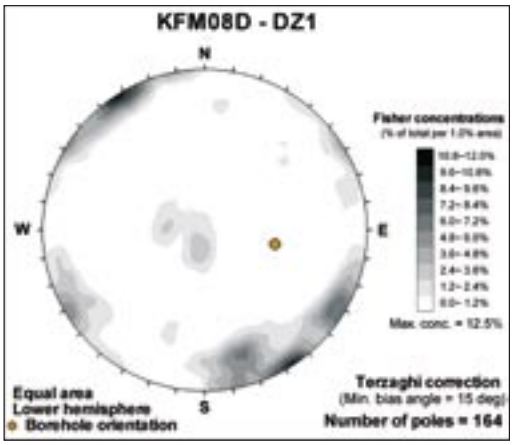
KFM08D - DZ1
N
W
E
S
Fisher concentrations
Max. conc. = 12.5%
Equal area
Lower hemisphere
Borehole orientation
Terzaghi correction
Number of poles = 164

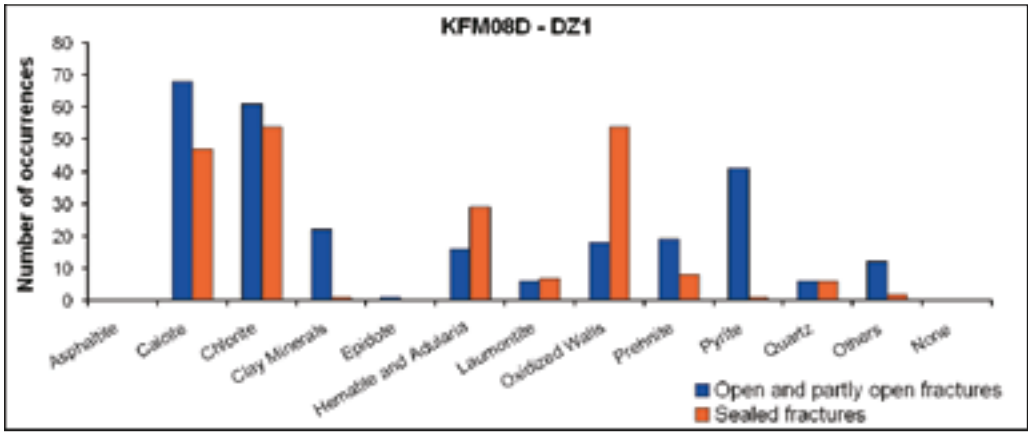
KFM08D - DZ1
Number of occurrences
0
10
20
30
40
50
60
70
80
Asphaltite
Calcite
Chlorite
Clay Minerals
Epidote
Hematite and Adularia
Laumontite
Oxidized Walls
Prehnite
Pyrite
Quartz
Others
None
Open and partly open fractures
Sealed fractures

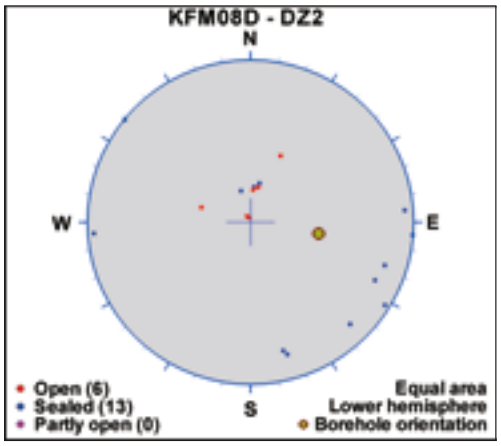
KFM08D - DZ2
N
W
E
S
Open (6)
Sealed (13)
Partly open (0)
Equal area
Lower hemisphere
Borehole orientation

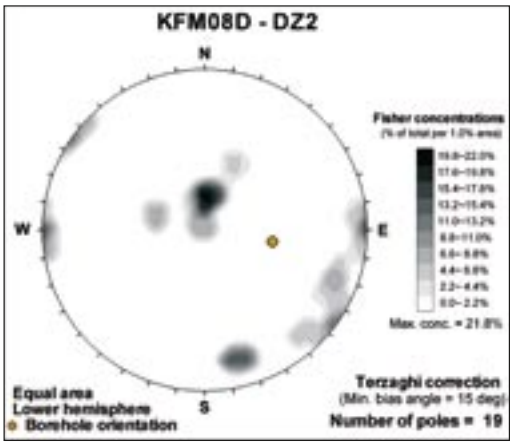
KFM08D - DZ2
N
W
E
S
Fisher concentrations
Max. conc. = 21.8%
Equal area
Lower hemisphere
Borehole orientation
Terzaghi correction
Number of poles = 19

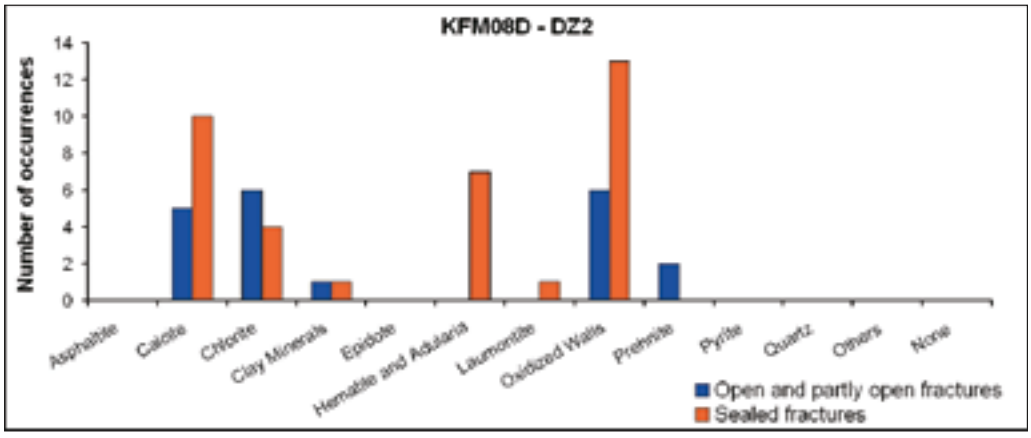
KFM08D - DZ2
Number of occurrences
0
2
4
6
8
10
12
14
Asphaltite
Calcite
Chlorite
Clay Minerals
Epidote
Hematite and Adularia
Laumontite
Oxidized Walls
Prehnite
Pyrite
Quartz
Others
None
Open and partly open fractures
Sealed fractures

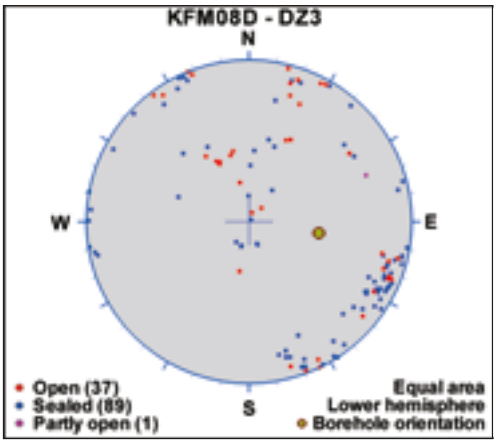
KFM08D - DZ3
N
W
E
S
Open (37)
Sealed (89)
Partly open (1)
Equal area
Lower hemisphere
Borehole orientation

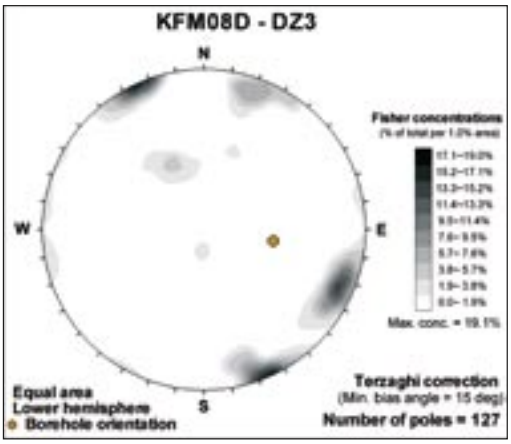
KFM08D - DZ3
N
W
E
S
Fisher concentrations
Max. conc. = 19.1%
Equal area
Lower hemisphere
Borehole orientation
Terzaghi correction
(Min. bias angle = 15 deg)
Number of poles = 127

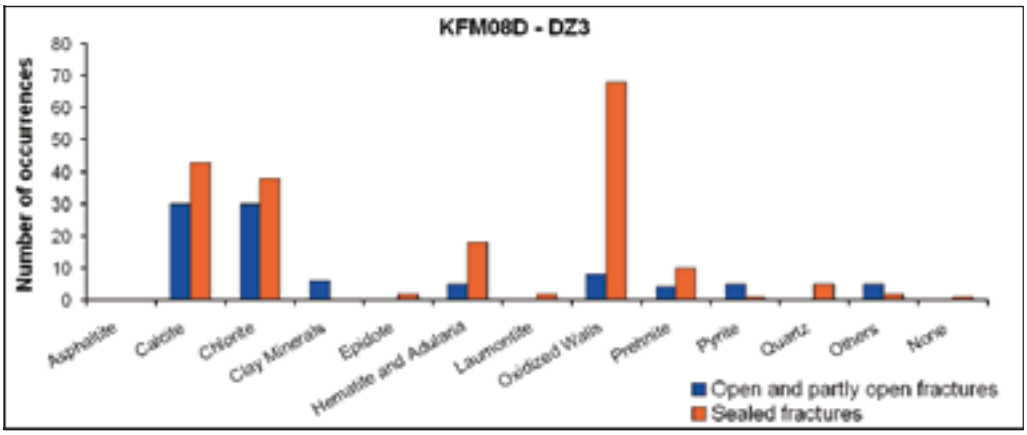
KFM08D - DZ3
Number of occurrences
0
10
20
30
40
50
60
70
80
Asphaltite
Calcite
Chlorite
Clay Minerals
Epidote
Hematite and Adularia
Laumontite
Oxidized Wallrock
Prehnite
Pyrite
Quartz
Others
None
Open and partly open fractures
Sealed fractures

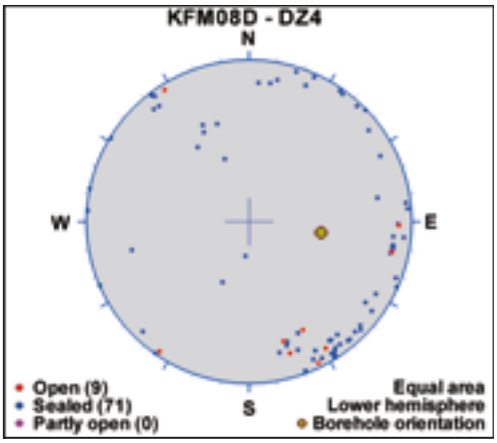
KFM08D - DZ4
N
W
E
S
Open (9)
Sealed (71)
Partly open (0)
Equal area
Lower hemisphere
Borehole orientation

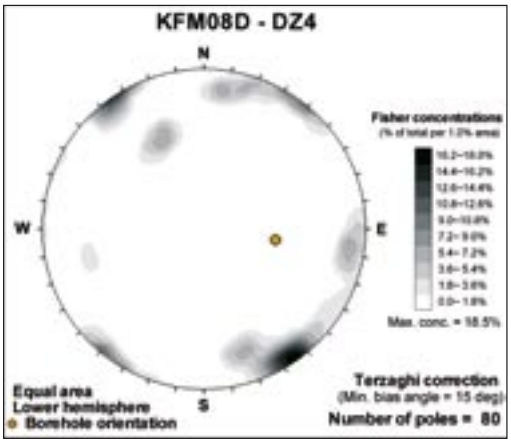
KFM08D - DZ4
N
W
E
S
Fisher concentrations
Max. conc. = 16.5%
Equal area
Lower hemisphere
Borehole orientation
Terzaghi correction
(Min. bias angle = 15 deg)
Number of poles = 80

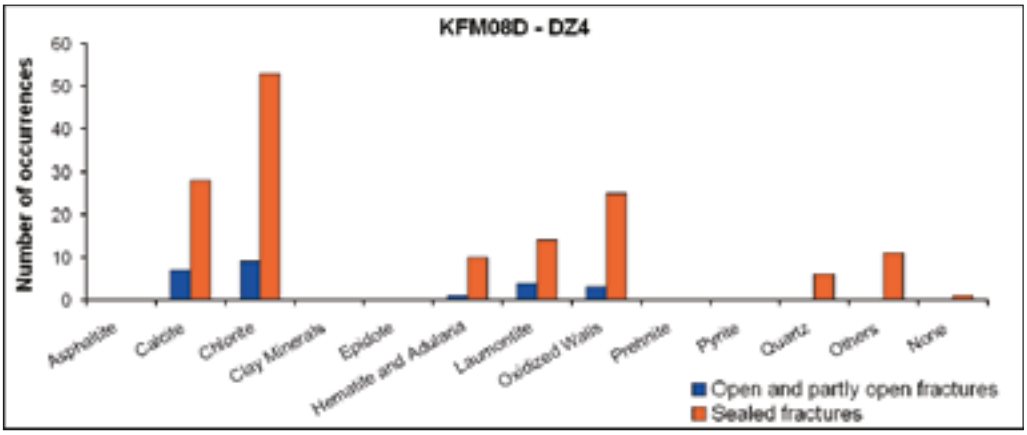
KFM08D - DZ4
Number of occurrences
0
10
20
30
40
50
60
Asphaltite
Calcite
Chlorite
Clay Minerals
Epidote
Hematite and Adularia
Laumontite
Oxidized Wallrock
Prehnite
Pyrite
Quartz
Others
None
Open and partly open fractures
Sealed fractures

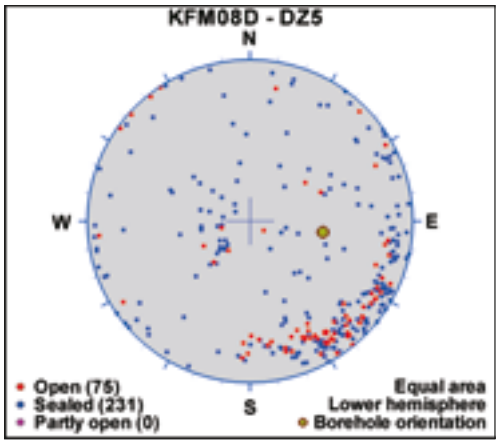
KFM08D - DZ5
N
W
E
S
Open (75)
Sealed (231)
Partly open (0)
Equal area
Lower hemisphere
Borehole orientation

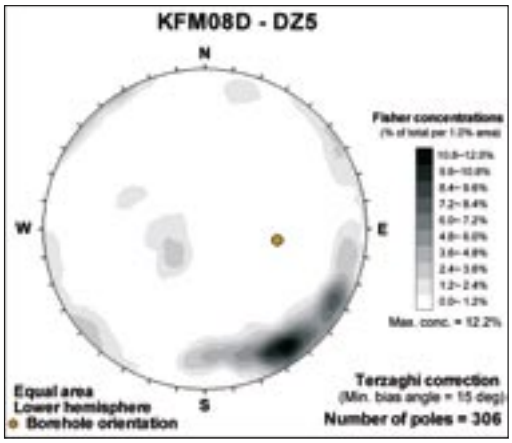
KFM08D - DZ5
N
W
E
S
Fisher concentrations
Max. conc. = 12.2%
Equal area
Lower hemisphere
Borehole orientation
Terzaghi correction
Number of poles = 306

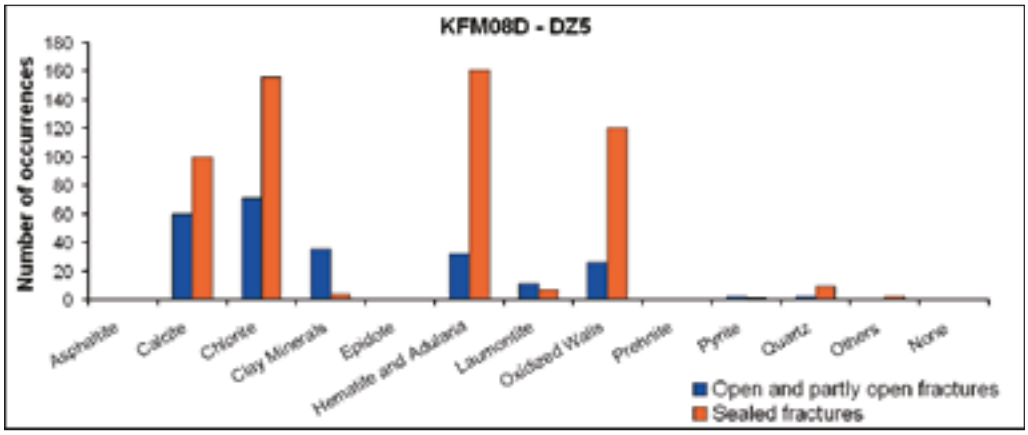
KFM08D - DZ5
Number of occurrences
180
160
140
120
100
80
60
40
20
0
Asphaltite
Calcite
Chlorite
Clay Minerals
Epidote
Hematite and Adularia
Laumontite
Oxidized Walls
Prehnite
Pyrite
Quartz
Others
None
Open and partly open fractures
Sealed fractures

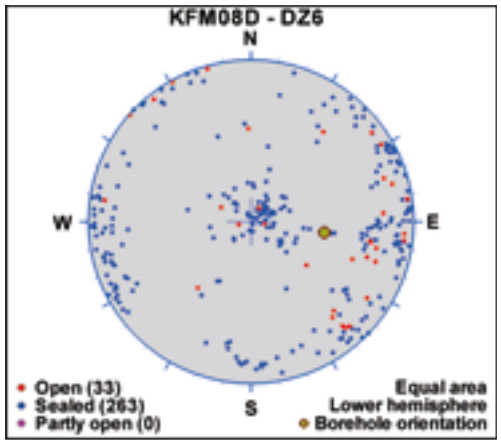
KFM08D - DZ6
N
W
E
S
Open (33)
Sealed (263)
Partly open (0)
Equal area
Lower hemisphere
Borehole orientation

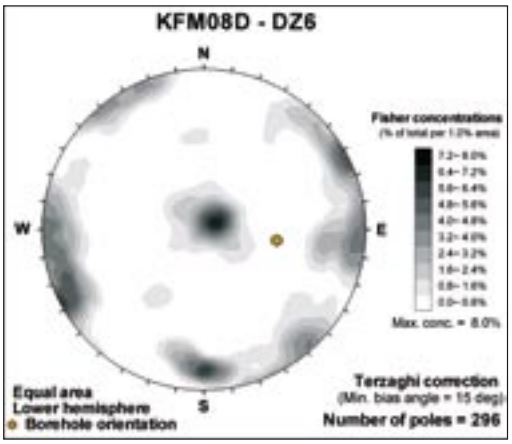
KFM08D - DZ6
N
W
E
S
Fisher concentrations
Max. conc. = 8.0%
Equal area
Lower hemisphere
Borehole orientation
Terzaghi correction
Number of poles = 296

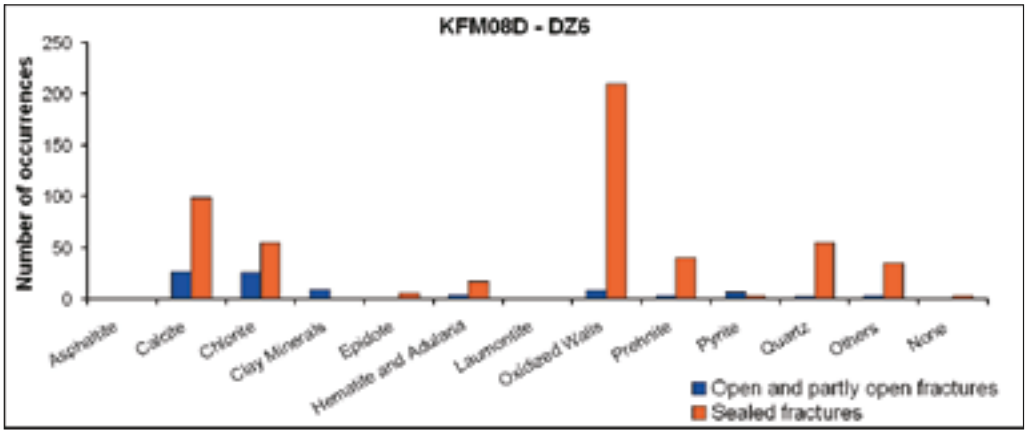
KFM08D - DZ6
Number of occurrences
250
200
150
100
50
0
Asphaltite
Calcite
Chlorite
Clay Minerals
Epidote
Hematite and Adularia
Laumontite
Oxidized Walls
Prehnite
Pyrite
Quartz
Others
None
Open and partly open fractures
Sealed fractures

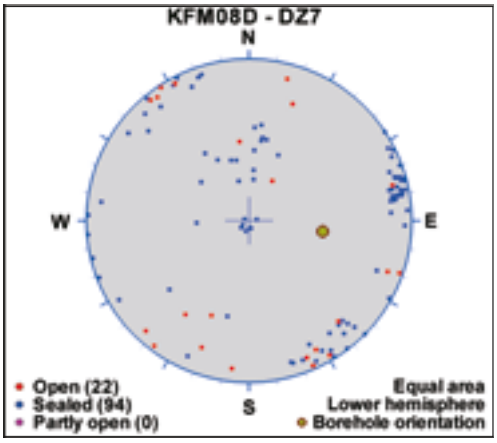
KFM08D - DZ7
N
W
E
S
Open (22)
Sealed (94)
Partly open (0)
Equal area
Lower hemisphere
Borehole orientation

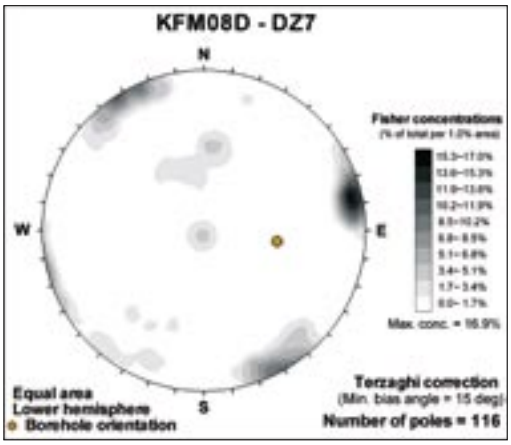
KFM08D - DZ7
N
W
E
S
Fisher concentrations
Max. conc. = 16.9%
Equal area
Lower hemisphere
Borehole orientation
Terzaghi correction
(Min. bias angle = 15 deg)
Number of poles = 116

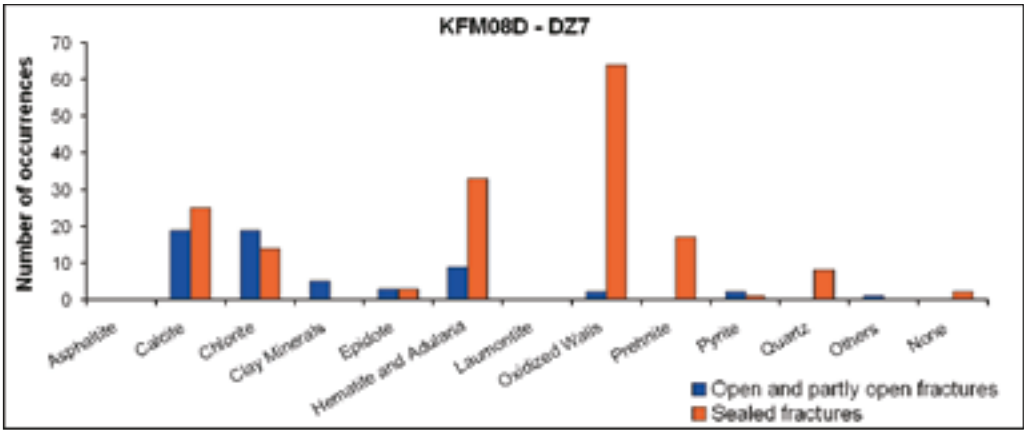
KFM08D - DZ7
Number of occurrences
0
10
20
30
40
50
60
70
Asphaltite
Calcite
Chlorite
Clay Minerals
Epidote
Hematite and Adularia
Laumontite
Oxidized Walls
Prehnite
Pyrite
Quartz
Others
None
Open and partly open fractures
Sealed fractures

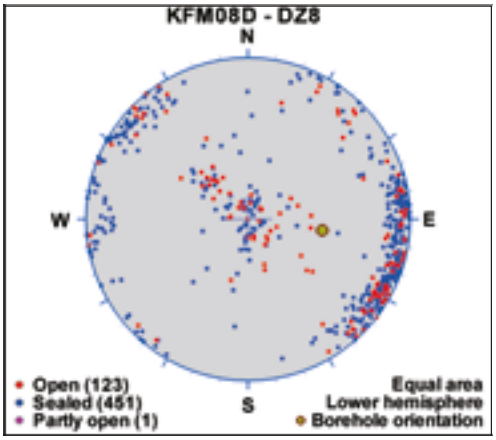
KFM08D - DZ8
N
W
E
S
Open (123)
Sealed (451)
Partly open (1)
Equal area
Lower hemisphere
Borehole orientation

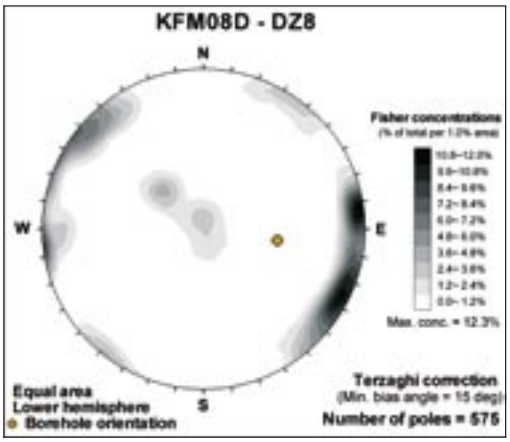
KFM08D - DZ8
N
W
E
S
Fisher concentrations
Max. conc. = 12.3%
Equal area
Lower hemisphere
Borehole orientation
Terzaghi correction
(Min. bias angle = 15 deg)
Number of poles = 575

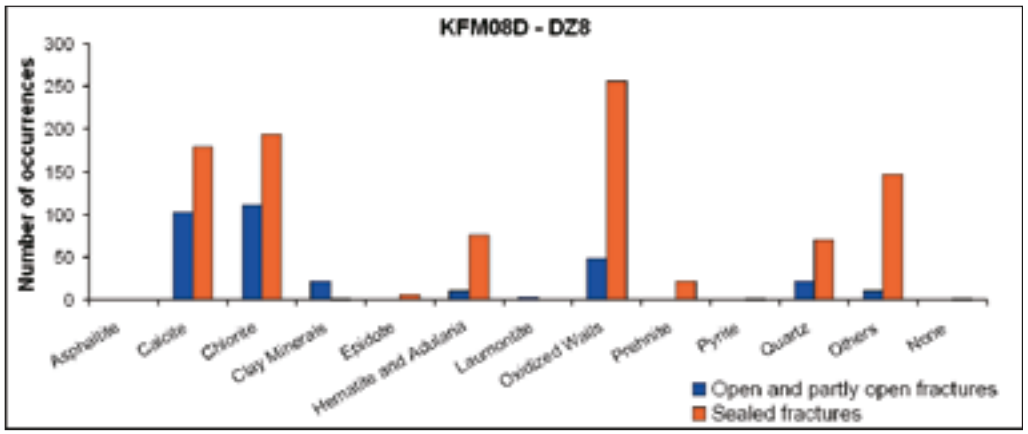
KFM08D - DZ8
Number of occurrences
0
50
100
150
200
250
300
Asphaltite
Calcite
Chlorite
Clay Minerals
Epidote
Hematite and Adularia
Laumontite
Oxidized Walls
Prehnite
Pyrite
Quartz
Others
None
Open and partly open fractures
Sealed fractures

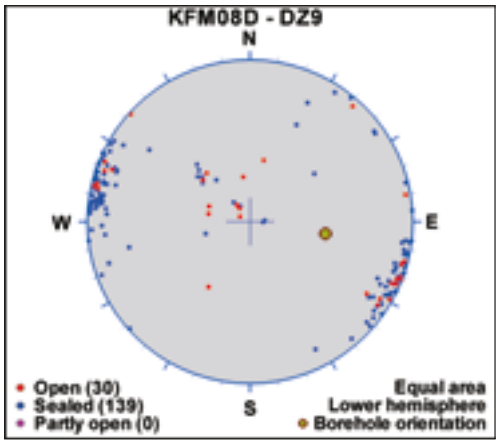
KFM08D - DZ9
N
W
E
S
Open (30)
Sealed (139)
Partly open (0)
Equal area
Lower hemisphere
Borehole orientation

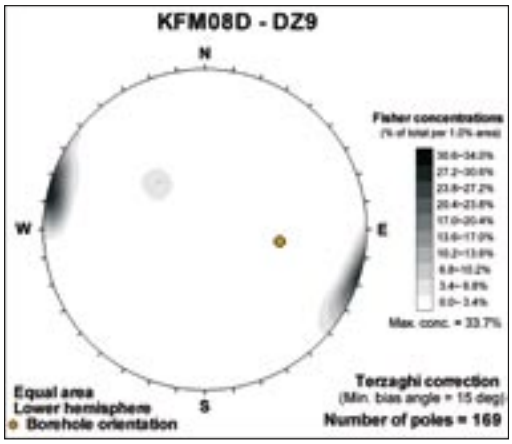
KFM08D - DZ9
N
W
E
S
Fisher concentrations
Max. conc. = 33.7%
Equal area
Lower hemisphere
Borehole orientation
Terzaghi correction
(Min. bias angle = 15 deg)
Number of poles = 169

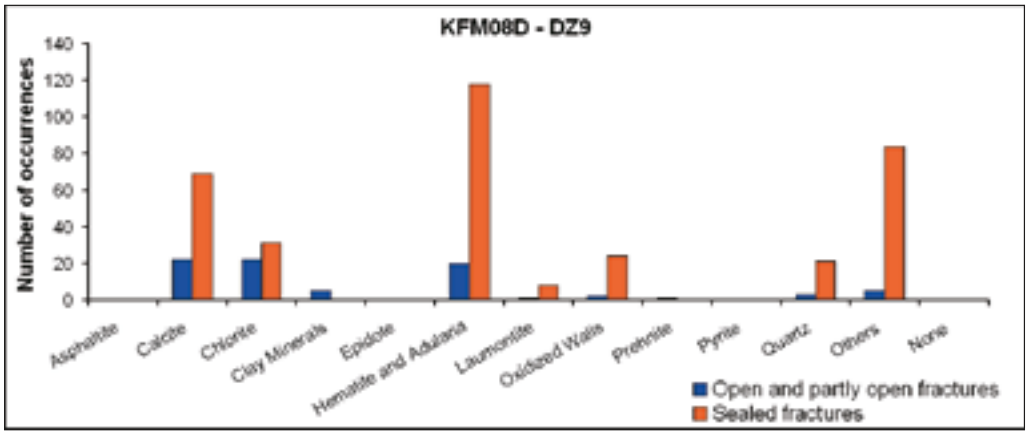
KFM08D - DZ9
Number of occurrences
0
20
40
60
80
100
120
140
Asphaltite
Calcite
Chlorite
Clay Minerals
Epidote
Hematite and Adularia
Laumontite
Oxidized Walls
Prehnite
Pyrite
Quartz
Others
None
Open and partly open fractures
Sealed fractures

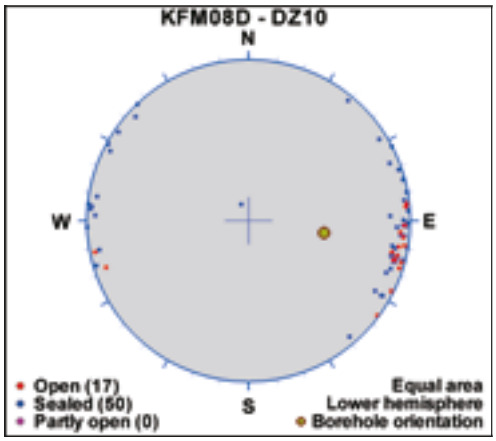
KFM08D - DZ10
N
W
E
S
Open (17)
Sealed (50)
Partly open (0)
Equal area
Lower hemisphere
Borehole orientation

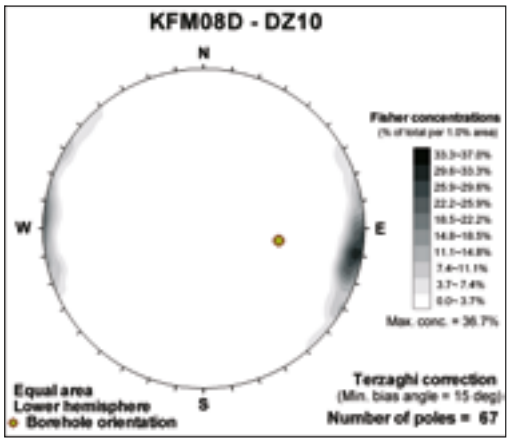
KFM08D - DZ10
N
W
E
S
Fisher concentrations
Max. conc. = 36.7%
Equal area
Lower hemisphere
Borehole orientation
Terzaghi correction
(Min. bias angle = 15 deg)
Number of poles = 67

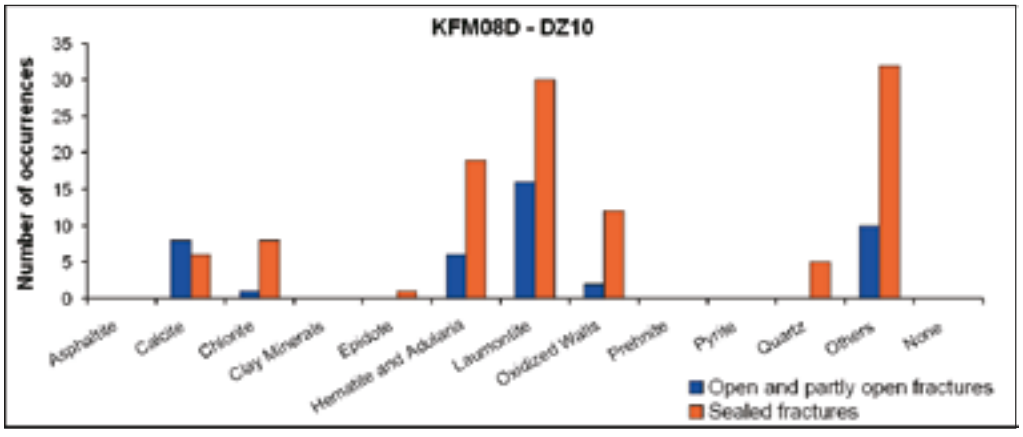
KFM08D - DZ10
Number of occurrences
0
5
10
15
20
25
30
35
Asphaltite
Calcite
Chlorite
Clay Minerals
Epidote
Hematite and Adularia
Laumontite
Oxidized Walls
Prehnite
Pyrite
Quartz
Others
None
Open and partly open fractures
Sealed fractures

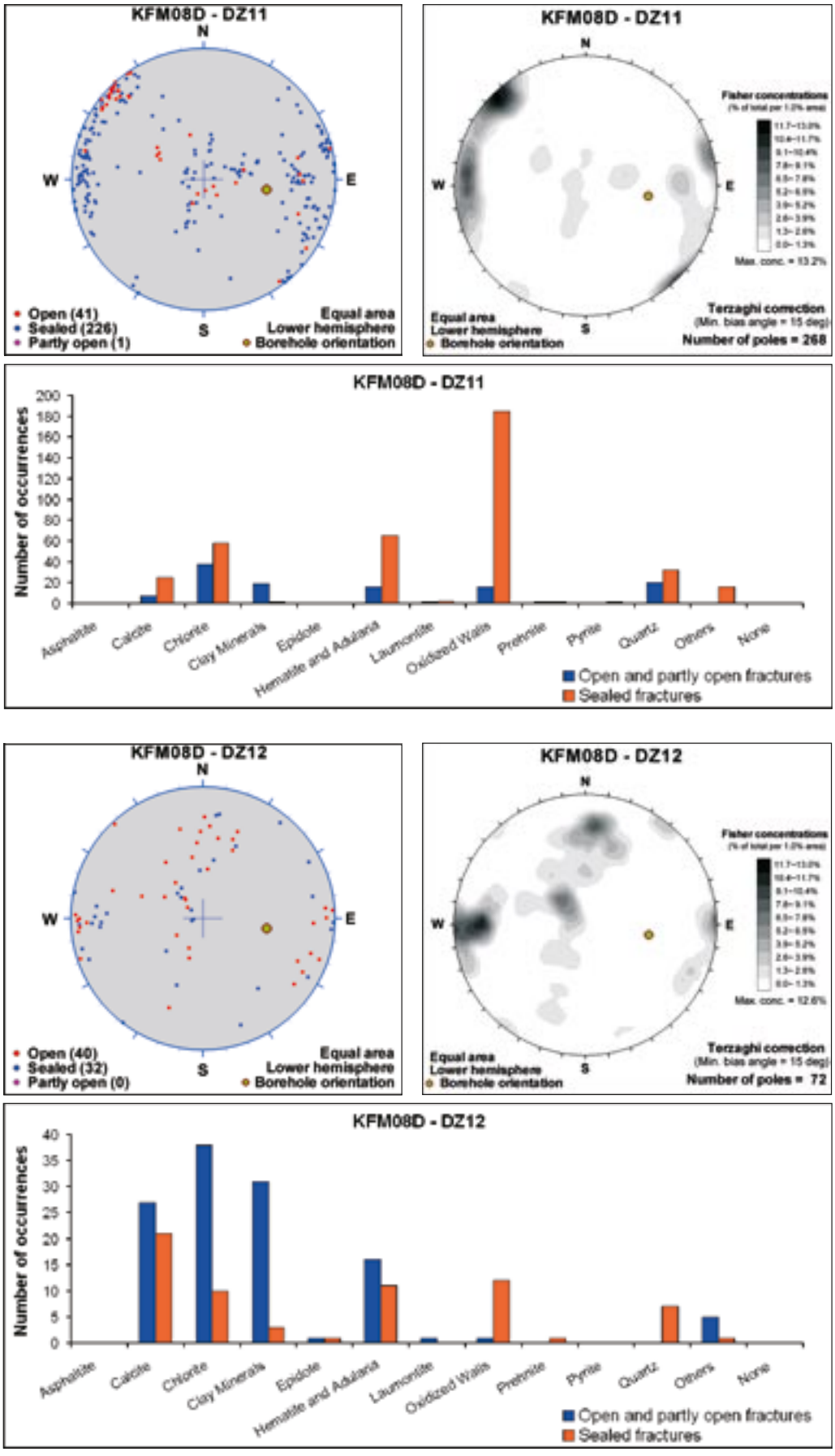

Figure 4-7. *Orientation and mineralogy of fractures inside the possible deformation zones DZ1−DZ12 along borehole KFM08D*

Table 4-4. Confidence level, fracture orientation and fracture mineralogy of the possible deformation zones in borehole KFM08D. All borehole lengths are adjusted values. Strike and dip are presented using the right-hand-rule method. Data extracted from Sicada database: SICADA_07_395 (2007-10-26).

Possible deformation zone	Borehole length (m)		Confidence level	Fracture orientation (strike dip)	Fracture mineralogy (excluding chlorite, calcite)
	Upper intersection	Lower intersection			
DZ1	184	210	Medium	1. ENE-WSW to SSW/steep dip 2. NW-SE/steep dip 3. Gentle	Adularia/hematite, pyrite, prehnite, clay minerals
DZ2	318	324	Low	1. WSW to SSW/ steep dip 2. Gentle Few data	Adularia/hematite,
DZ3	371	396	High	1. ENE-WSW and SSW/steep dip 2. WNW-ESE/steep dip 3. Gentle	Adularia/hematite, prehnite
DZ4	496	506	Medium	1. WSW to SSW/ steep dip 2. Steep/SE	Laumontite, adularia/ hematite
DZ5	546	571	High	1. WSW to SSW/ steep dip 2. Gentle	Adularia/hematite, clay minerals
DZ6	582	609	Medium	1. NNW-SSE/ steep dip 2. Gentle 3. NE-SW/steep dip	Quartz, prehnite
DZ7	621	634	High	1. ENE-WSW/steep dip 2. SSE/steep dip 3. Gentle	Adularia/hematite, prehnite
DZ8	644	689	Medium	1. NE-SW to NNE-SSW/steep dip 2. SSE/steep dip 3. Gentle	Adularia/hematite, others, quartz
DZ9	737	749	Medium	1. NNE-SSW/steep dip 2. Gentle	Adularia/hematite, others, quartz
DZ10	770	777	Low	NNE-SSW to NNW-SSE/steep dip	Laumontite, adularia/ hematite, others
DZ11	819	842	Medium	1. NE-SW to NNW-SSE/steep dip 2. Gentle	Adularia/hematite, quartz,
DZ12	903	Beneath cored borehole length	High	1. NNW-SSE/steep dip 2. Gentle 3. E-W/moderate to steep dip	Clay minerals, adularia/hematite, quartz

4.4 Prediction − outcome: A comparison

A visualisation of the prediction-outcome test for deformation zones is shown in Figure 4-8. A more detailed comparison between the boundaries of rock domains, fracture domains and deformation zones along borehole KFM08D, as predicted from the deterministic modelling work during stage 2.2 /Stephens et al. 2007/, and the results of the single-hole interpretation of this borehole /Carlsten et al. 2007b/ are presented in Table 4-5, Table 4-6 and Table 4-7, respectively. Beneath each geological object in these tables, a statement is made that specifies whether or not and which changes need to be made to the corresponding deterministic model, so that the findings along borehole KFM08D are taken into account.

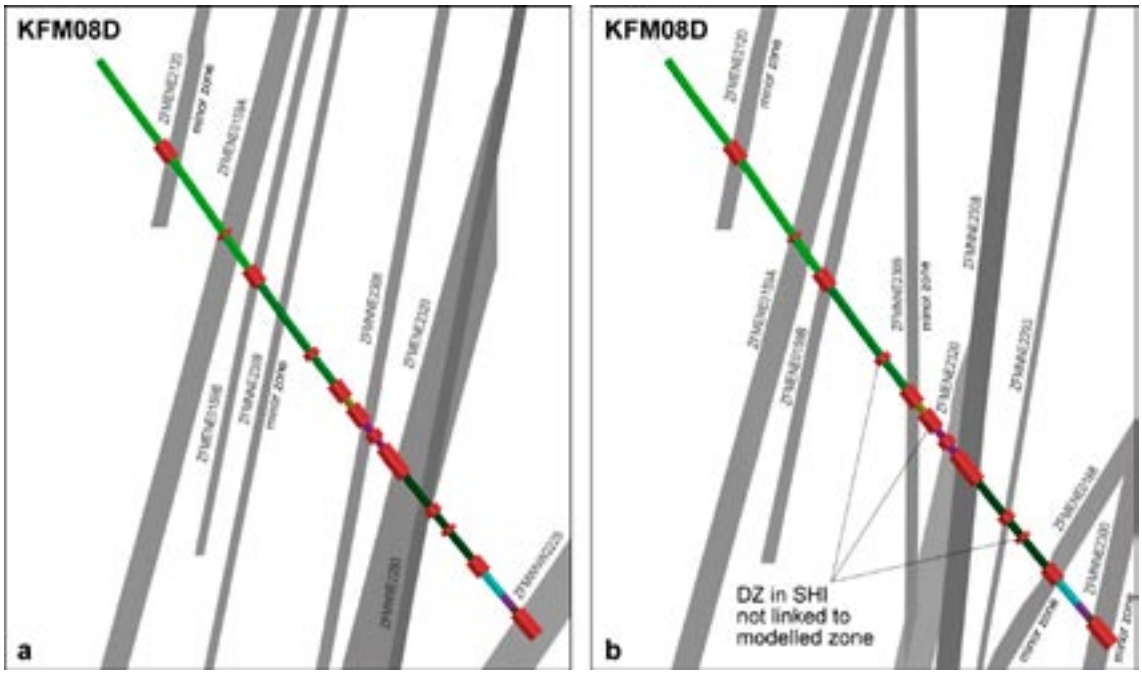

Figure 4-8. *Prediction-outcome verification test for deformation zones along borehole KFM08D. a) Modelled deformation zones stage 2.2 (ZFM) including minor zones compared with the twelve possible deformation zones in the single-hole interpretation (red ornaments). b) Modification of zones necessary to satisfactorily match the single-hole interpretation. The length of borehole KFM08D is c. 942 m. See text for further description.*

Table 4-5. Correlation between rock domains modelled deterministically in local model stage 2.2 /Stephens et al. 2007/ and rock units (RU) in the single-hole interpretation (SHI) of borehole KFM08D /Carlsten et al. 2007b/. The implications for the local rock domain model, stage 2.2, are summarised in the text beneath each geological object. UI = Upper intercept, LI = Lower intercept. All borehole lengths are adjusted values.

RFM in local model stage 2.2	Confidence level for RFM in local model stage 2.2	Borehole length (m)		RU in SHI	Confidence level for RU in SHI	Borehole length (m)	
		UI	LI			UI	LI
RFM029	High	Start of the cored borehole length	362	RU1	High	59.45 (top of cored borehole length)	395.65
The boundary between rock domains RFM029 and RFM045 needs to be modified, so that it intersects borehole KFM08D at 395.65 m instead of 362 m as in local rock domain model stage 2.2.							
RFM045	High	362	Beneath cored borehole length	RU2a, RU3a, RU4a, RU2b, RU5, RU4b, RU3b, RU2c	High	395.65	941.75 (base of cored borehole length)
Apart from the change in the boundary to RFM029 (see above), no changes are required.							

Table 4-6. Correlation between fracture domains modelled deterministically in stage 2.2 /Olofsson et al. 2007/ and rock units (RU) in the single-hole interpretation (SHI) of borehole KFM08D /Carlsten et al. 2007b/. The implications for the fracture domain model, stage 2.2, are summarised in the text beneath each geological object. UI = Upper intercept, LI = Lower intercept. All borehole lengths are adjusted values.

FFM in local model stage 2.2	Borehole length (m)		RU in SHI	Borehole length (m)	
	UI	LI		UI	LI
FFM02	Start of the borehole	60	Situated above cored borehole length	Above cored borehole length	59.45 (top of cored borehole length)
No changes are required.					
FFM01	60	362	Bedrock outside deformation zones and inside RU1	59.45 (top of cored borehole length)	395.65
The boundary between fracture domains FFM01 and FFM06 needs to be modified, so that it intersects borehole KFM08D at 395.65 m instead of 362 m as in fracture domain model stage 2.2.					
FFM06	362	Beneath cored borehole length	Bedrock outside deformation zones and inside RU2a, RU3a, RU4a, RU2b, RU5, RU4b,RU3b and RU2c	395.65	941.75 (base of cored borehole length)
Apart from the change in the boundary to FFM01 (see above), no changes are required.					

Table 4-7. Correlation between deformation zones modelled deterministically in model stage 2.2 (ZFM) and possible deformation zones (DZ) in the single-hole interpretation (SHI) of borehole KFM08D. If necessary, the changes that need to be made to the orientation of a deformation zone in the local deformation zone model, stage 2.2, in order to complete a matching with the SHI, are shown beneath the zone. The other changes in properties that are required, so to be consistent with the stage 2.3 data, are also listed here. The low and medium confidence zones referred to as DZ4, DZ6 and DZ10 in the SHI cannot be linked with previously modelled deformation zones or with low magnetic lineaments at the ground surface. They remain as possible deformation zones. UI = Upper intercept, LI = Lower intercept. All borehole lengths are adjusted values. All orientations are provided as strike/dip using the right-hand-rule-method.

ZFM in model stage 2.2	Confidence level for ZFM in model stage 2.2	Borehole length (m)		DZ in SHI	Confidence level for DZ in SHI	Borehole length (m)	
		UI	LI			UI	LI
ZFMENE2120	High	193	218	DZ1	Medium	184	210
No changes are required for an intersection with DZ1 along KFM08D. Minor zone. Thickness along KFM08D is 13 m.							
ZFMENE0159A	High	304	345	DZ2	Low	318	324
No changes are required for an intersection with DZ2 along KFM08D. Local major zone with trace length at the ground surface between 1 and 3 km. Trace length at ground surface reduced to c. 1,810 m. Thickness along KFM08D is 4 m.							
ZFMENE0159B	Medium	373	390	DZ3	High	371	396
No changes are required for an intersection with DZ3 along KFM08D. Minor splay from zone ZFMENE0159A. Thickness along KFM08D is 13 m. Confidence of existence raised to high.							
				DZ4	Medium	496	506
No modelled zone matched to this medium confidence zone in the SHI.							
ZFMNNE2309	Medium	429	444	DZ5	High	546	571
Dip needs to be modified from 80° to 90° (new orientation 215/90) for an intersection with DZ5 along KFM08D. Minor zone. Revised truncation against ZFMENE2320 and ZFMNNE2308.Thickness along KFM08D is 13 m. Confidence of existence can be raised to high.							
				DZ6	Medium	582	609
No modelled zone matched to this medium confidence zone in the SHI.							

ZFM in model stage 2.2	Confidence level for ZFM in model stage 2.2	Borehole length (m)		DZ in SHI	Confidence level for DZ in SHI	Borehole length (m)	
		UI	LI			UI	LI
ZFMENE2320	High	667	740	DZ7	High	621	634
Strike needs to be modified from 244° to 240° (new orientation 240/81) for an intersection with DZ7 along KFM08D. Local major zone with trace length at the ground surface between 1 and 3 km. Trace length at ground surface increased to c. 1,720 m. Revised truncation against ZFMNNE2308, ZFMNW0017 and 1,700 m depth. Thickness along KFM08D is 7 m.							
ZFMNNE2308	Medium	602	623	DZ8	Medium	644	689
Dip needs to be modified from 80° to 84° (new orientation 214/84) for an intersection with DZ8 along KFM08D. Local major zone with trace length at the ground surface between 1 and 3 km.Trace length at ground surface increased to c. 1,725 m. Revised truncation at 1,700 m depth. Thickness along KFM08D is 28 m. Confidence of existence can be raised to high.							
ZFMNNE2293	Medium	718	739	DZ9	Medium	737	749
Dip needs to be modified from 80° to 81° (new orientation 208/81) for an intersection with DZ9 along KFM08D. Local major zone with trace length at the ground surface c. 1 km. Thickness along KFM08D is 8 m. Confidence of existence can be raised to high.							
				DZ10	Low	770	777
No modelled zone matched to this low confidence zone in the SHI.							
ZFMENE0168	Medium	No intersection predicted		DZ11	Medium	819	842
Dip needs to be modified from 80° to 77° (new orientation 253/77) for an intersection with DZ11 along KFM08D. Local major zone with trace length at the ground surface c. 1 km. Trace length at ground surface increased to 985 m. Revised truncation at 1,000 m depth. Thickness along KFM08D is 11 m. Confidence of existence can be raised to high.							
ZFMNNE2300	Medium	906	Beneath cored borehole length	DZ12	High	903	Beneath cored borehole length
Dip needs to be modified from 80° to 79° (new orientation 208/79) for an intersection with DZ12 along KFM08D*. Minor zone. Thickness along KFM08D is 25 m. Confidence of existence can be raised to high. The correlation between DZ12 and ZFMNNE2300 is preferred over the correlation between DZ12 and ZFMWNW2225 (see text above). To avoid intersection with borehole KFM08D (see Table 4-3), the dip of zone ZFMWNW2225 needs to be increased from 75° to 78°. The modified orientation for this zone will be 120/78.							

Bearing in mind the discussion in sections 4.2 and 4.3, it is apparent that the boundary between rock domains RFM029 and RFM045 (as well as fracture domains FFM01 and FFM06) along KFM08D occurs only c. 30 m deeper than that predicted in the deterministic modelling (Table 4-5). Notwithstanding the occurrence of narrow, low resistivity anomalies in the upper part of the borehole, which are possibly linked to single open fractures, inclusion of this part of the borehole in fracture domain FFM01 (Table 4-6), as carried out in the fracture domain model stage 2.2, is considered to be acceptable, bearing in mind the results from the adjacent borehole KFM08B.

The fracture orientation, fracture mineralogy, alteration and style of deformation of the twelve possible deformation zones identified in the single-hole interpretation /Carlsten et al. 2007b/ support the correlation of nine of these zones with deformation zones already modelled deterministically in stage 2.2 (Figure 4-8 and Table 4-7). These nine zones intersect the possible deformation zones along KFM08D directly, without any need for modification (three zones), or after a minor modification of the dip or strike between 1° and 10° (six zones). The required change for each zone lies predominantly within the range of uncertainty provided in the property tables for the orientation of these zones /Appendices 15 and 16 in Stephens et al. 2007/. It should be kept in mind that several of these modelled zones were assigned a medium confidence of existence and their dip was judged to be highly uncertain (e.g. zone ZFMNNE2308 which corresponds to DZ8 in the SHI). The results from KFM08D confirm the existence of these zones, permit an upgrading to a high level of confidence for their existence, and constrain more tightly their dip. Three possible deformation zones identified in the SHI, with a low or

medium confidence, cannot be matched to a deterministically modelled zone in stage 2.2 or to a low magnetic lineament at the ground surface. These geological features remain as possible deformation zones (Figure 4-8 and Table 4-7).

All the deformation zones are steeply dipping fracture zones that can be included in the ENE and NNE sub-sets /Stephens et al. 2007/. They are either local major zones with a trace length at the ground surface between 1,000 and 3,000 m, or are minor zones with a trace length at the ground surface less than 1,000 m. Sealed fractures and sealed fracture networks dominate in agreement with previous findings at Forsmark.

It is concluded that the results from the drilling of KFM08D verify in a highly satisfactory manner the parts of the stage 2.2 geological models that lie inside the target volume. In particular, no additional zones that have trace lengths longer than 3,000 m have been detected inside the target volume.

5 Borehole KFM011A

5.1 Background

The Singö (ZFMWNW0001), Forsmark (ZFMWNW0004) and Eckarfjärden (ZFMNW0003) deformation zones constitute the most important geological discontinuities in the crystalline bedrock at Forsmark. These zones belong to the WNW to NW set of steeply dipping deformation zones at the site and are situated within the broader belts affected by high ductile strain that envelop the Forsmark tectonic lens /Stephens et al. 2007/. They are retrograde in character and display low-temperature ductile and later, polyphase brittle deformation /Stephens et al. 2007/. The location of these deformation zones and the target area for site investigations in the north-western part of the candidate area are shown in Figure 5-1.

The Singö deformation zone does not intersect the candidate area (Figure 5-1) and was not investigated geologically during earlier site investigation work. Geological data at shallower levels along this zone are available from earlier construction work at the Forsmark site and are summarised in /Carlsson and Christiansson 1987/. However, data from deeper crustal levels along the Singö deformation zone have been lacking up to model stage 2.3.

The drilling of borehole KFM11A during model stage 2.3 aimed to provide base geological information bearing on the character of the Singö deformation zone (ZFMNW0001) at depth, and to acquire hydrogeological and hydrogeochemical information also at depth. Such data have also been lacking up to model stage 2.3. Three complementary percussion boreholes, HFM33, HFM34 and HFM35, were also drilled in the vicinity of drill site 11 (Figure 1-3). These boreholes aimed to investigate both the Singö deformation zone and lineaments to the north-east and south-west of this zone that show traces sub-parallel to the zone. Examination of the hydraulic responses in nearby boreholes as well as at the SFR facility during the drilling operations and the subsequent hydraulic tests was also one of the prime objectives of the drilling campaign at and close to drill site 11.

The decision statement and motivation for borehole KFM11A are provided in document ID 1053022. The position, inclination, bearing and borehole length are summarised in Table 5-1.

Table 5-1. Position, inclination, bearing and length of boreholes KFM11A, HFM33, HFM34 and HFM35. Data extracted from Sicada database: Sicada_08_109 (2008-05-09).

Borehole	Drill site	Easting RT 90, 2.5 gon W (m)	Northing RT 90, 2.5 gon W (m)	Inclination (°)	Bearing (°)	Length (m)
KFM11A	11	1632368	6701105	–61	040	573
HFM33	11	1632223	6701042	–59	220	140
HFM34	11	1632470	6701325	–59	30	201
HFM35	11	1632321	6701556	–59	33	201

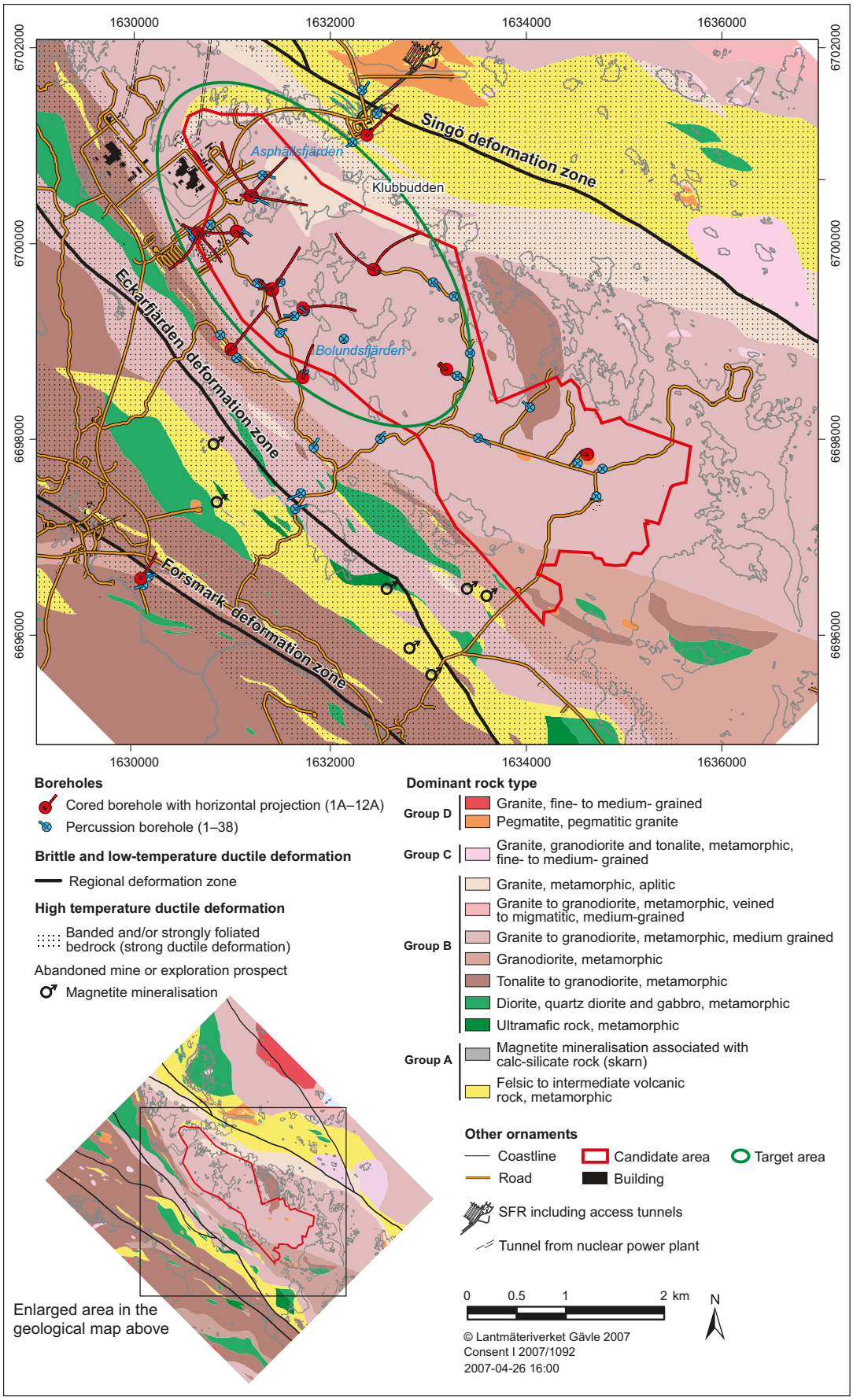

Figure 5-1. *Geological map of the bedrock inside and around the candidate area at Forsmark The Singö, Forsmark and Eckarfjärden regional deformation zones are marked on the map. The horizontal projection of all boreholes as well as the target area are also shown.*

5.2 Prediction of intersections of geological features along borehole KFM11A based on model stage 2.2

With the help of the rock visualisation system (RVS), a prediction of the intersections of rock domains and deformation zones, included in model stage 2.2 /Stephens et al. 2007/, along borehole KFM11A can be carried out. Since the fracture domain model was only constructed inside the target volume at Forsmark /Olofsson et al. 2007/, there are no predicted intersections for fracture domain boundaries in KFM11A.

Borehole KFM11A does not intersect any rock domain boundaries. The entire borehole has been drilled within rock domain 21 (RFM021), which is dominated by strongly foliated and partly tectonically banded, felsic to intermediate metavolcanic rock and subordinate occurrences of different types of metagranitoid, pegmatite, pegmatitic granite and amphibolite /SKB 2005, Appendix 14 in Stephens et al. 2007/. The degree of inhomogeneity of the rock types in this rock domain is high.

The modelling work during stage 2.2 predicts that three, steeply dipping deformation zones that occur in the orientation sub-set referred to as WNW should intersect borehole KFM011A (Table 5-2). These zones are identified in descending order along the borehole as ZFMWNW0813, ZFMWNW0001, which corresponds to the Singö deformation zone, and ZFMWNW1127. The upper intersection of deformation zone ZFMWNW1127, which forms a splay off the Singö zone on its northern side, lies above the lower intersection of the Singö zone close to the bottom of the borehole. This feature arises since the borehole has been drilled very close to where zone ZFMWNW1127 splays off the Singö deformation zone. Selected aspects of all three zones (confidence of existence, orientation, orientation class, trace length at the ground surface and size class) are also shown in Table 5-2.

Since previous surface and borehole data are absent for the medium confidence zones ZFMWNW0813 and ZFMWNW1127, the properties of these two zones are poorly constrained. Most of their properties have been determined by a comparison with the properties of other deformation zones in the same orientation class /Appendix 15 in Stephens et al. 2007/. They have been modelled by simple downward projection of a corresponding low magnetic lineament using a vertical dip. For this reason, the dips of the medium confidence zones and, consequently, their predicted intersections along the borehole have a low level of confidence /Appendix 15 in Stephens et al. 2007/. Furthermore, the revised interpretation of low magnetic lineaments (stage 2.3), presented in chapter 2, suggests that the medium confidence zone ZFMWNW1127 should be removed and replaced by zone ZFMNW0002 (see section 2.3 and Figure 2-3). All these features need to be taken into consideration when the prediction-outcome exercise is assessed (see below).

Table 5-2. Predicted intersection of deformation zones modelled deterministically in model stage 2.2 with borehole KFM11A. Borehole intersections have been extracted with the assistance of RVS, using data on the bearing and inclination of the trace of borehole KFM11A and the geometry of deformation zones in local model, stage 2.2 /Stephens et al. 2007/. Zone confidence, orientation and trace length at the ground surface have been extracted from /Appendix 15 in Stephens et al. 2007/. UI = Upper intercept, LI = Lower intercept. All borehole lengths are adjusted values. All orientations are provided as strike/dip using the right-hand-rule-method.

Modelled deformation zone (ZFM)	Confidence of existence	Strike/dip (°) and orientation class /Stephens et al. 2007/	Inferred trace length at the ground surface (m)	Size class	Borehole length (m)	
					UI	LI
ZFMWNW0813	Medium	116/90 Steep/WNW	1,609	Local major (1 to 10 km)	371	401
ZFMWNW0001	High	120/90 Steep/WNW	30,000	Regional (>10 km)	404	811
ZFMWNW1127	Medium	120/90 Steep/WNW	5,394	Splay from Singö DZ. Local major (1 to 10 km)	784	854

The properties of the Singö deformation zone (ZFMWNW0001) are based on previous work carried out along tunnels and boreholes prior to the present site investigation. This zone is intersected by four tunnels (Table 5-3). Geological data acquired during the investigation and construction phases of these tunnels provide information on the properties of the Singö deformation zone at four shallow locations.

The high confidence zone ZFMWNW0001 has been modelled with a vertical dip that has been inferred from the data along the tunnels and boreholes close to the surface, and that has been adopted in the structural model for SFR /Axelsson and Hansen 1997, Holmén and Stigsson 2001/. Furthermore, the information from the tunnels has been linked to a low magnetic lineament (MFM0804, see chapter 2) that constrains the trace length of the zone at the ground surface (see also /Carlsson et al. 1985, Glamheden et al. 2007/). The regional character of this zone is consistent with the thickness estimated from the tunnel intersections. The thickness of the Singö zone along the discharge tunnel for nuclear power plant 3 has been estimated to 175 m and along the discharge tunnels for the nuclear power plant 1–2, c. 350 m to the south-east, to c. 200 m. The thickness of the zone along the two access tunnels to SFR, c. 1,250 m further to the south-east, has been estimated to 120 m.

Deformation along the Singö deformation zone occurred initially in the ductile regime and it continued to be active later in the brittle regime. The zone occurs in a ductile high-strain belt north-east of the tectonic lens at Forsmark and contains mylonites, cataclastic rocks and cohesive breccias. Sealed fractures dominate but open fractures and incohesive crush rock also occur /Glamheden et al. 2007/. Fractures along the ductile foliation structure dip steeply to the SW and SSW. Fractures that dip steeply to the WNW and to the SSE, dip moderately to the WSW and are gently dipping are also present along the Singö deformation zone. Chlorite, calcite, quartz, clay minerals and sandy material have been documented along fractures.

Kinematic studies along the Eckarfjärden deformation zone /Nordgulen and Saintot 2006/, which belongs to the same set of deformation zones as the Singö deformation zone, indicate a complex brittle evolution along this set of deformation zones. An influence of approximately NW-SE and N-S shortening and a younger, approximately NE-SW compressive period have been inferred /Nordgulen and Saintot 2006, Stephens et al. 2007/. Epidote, which belongs to the oldest generation of fracture filling and coating minerals, is present in all these phases of brittle deformation. Displacement in accordance with an approximately WNW-ENE compressive phase is also apparent along the NW-trending zone ZFMNW1200 /Nordgulen and Saintot 2006, Stephens et al. 2007/.

Table 5-3. Tunnels intersecting the Singö deformation zone. Tunnel design data from /Carlsson et al. 1985/.

Tunnel ID	Depth of zone intersection (m)	Cross-section area (m^2)
Discharge tunnel for cooling water from nuclear power plant 1–2	55–60	80
Discharge tunnel for cooling water from nuclear power plant 3	50–55	55
Construction tunnel for SFR	50	49
Operational tunnel for SFR	50	65

5.3 Single-hole interpretation of borehole KFM11A − outcome

The same critical geological and geophysical data that have been used during the first stage of the single-hole interpretation (SHI) of all the boreholes are presented for borehole KFM11A in Figure 5-2. The results of the SHI work /Carlsten et al. 2007c/ are also shown in this figure. The character and kinematics of the possible deformation zone along this borehole, which were completed during the second stage of the SHI and are addressed in /Nordgulen and Saintot 2008/, are treated together with similar data from other complementary (stage 2.3) boreholes in chapter 8.

Borehole KFM11A has been divided into nine different rock units, RU1–RU9 (/Carlsten et al. 2007c/ and Figure 5-2). Rock units 3 and 6 occur along two separate length intervals (RU3a, RU3b and RU6a, RU6b, respectively). Furthermore, rock unit 7 has been identified in three separate length intervals (RU7a, RU7b and RU7c). All rock units have been recognised with a high degree of confidence, except for RU7c at the bottom of the borehole, which has been recognised with a medium degree of confidence /Carlsten et al. 2007c/.

The bedrock along KFM11A is inhomogeneous. Most units are dominated by more or less tectonically banded and foliated metavolcanic rock with a felsic to intermediate composition (103076). Subordinate occurrences of amphibolite (102017), calc-silicate rock (108019), fine- to medium-grained metagranite (111058) and aplitic metagranite (101058) are present. Four rock units occurring in five separate length intervals show a different dominant rock type: Amphibolite (102017) along RU4 (c. 357–375 m), aplitic metagranite (101058) along RU6a and RU6b (c. 585–660 m and c. 783–822 m, respectively), fine- to medium-grained granite (111058) along RU8 (c. 699–727 m) and fine- to medium-grained metagranitoid (101051) along RU9 (c. 822–846 m). A more detailed description of each rock unit, including variations in the silicate rock density of the metavolcanic rocks, can be found in /Carlsten et al. 2007c/.

A moving average plot for the frequency of fractures along borehole KFM11A (Figure 5-3) indicates that the whole borehole, but particularly between c. 245 and 824 m, is affected by a high frequency of sealed and open fractures as well as sealed fracture networks. This interval also shows an overall reduced bulk resistivity (Figure 5-4), alteration referred to as oxidation (red-staining in the bedrock related to hematite dissemination) and low magnetic susceptibility. On the basis of these observations, the whole interval was classified as a possible deformation and referred to as DZ1 (/Carlsten et al. 2007c/ and Figure 5-2).

Seven borehole intervals with anomalously high fracture frequency are apparent along DZ1. These anomalies occur in the borehole intervals between c. 248–279 m, c. 345–382 m, c. 405–468 m, c. 498–630 m, c. 653–664 m, c. 676–723 m and c. 787–824 m. One or more borehole intervals with incohesive crush rock are also conspicuous at c. 317 m, c. 376–384 m, c. 437–464 m, c. 505–522 m, c. 580–615 m, c. 649–661 m, c. 686–696 m and c. 774–801 m. These correspond to intervals of strongly reduced resistivity in the bedrock (Figure 5-4). The bulk resistivity is very low in the interval 498–630 m. This interval is also characterised by several caliper anomalies and generally low P-wave velocity /Carlsten et al. 2007c/. These features correspond to a high frequency of open fractures and sections of incohesive crush rock. Fracture apertures are generally less than 1 mm, with a few ranging up to 10 mm (/Carlsten et al. 2007c/ and Figure 5-2).

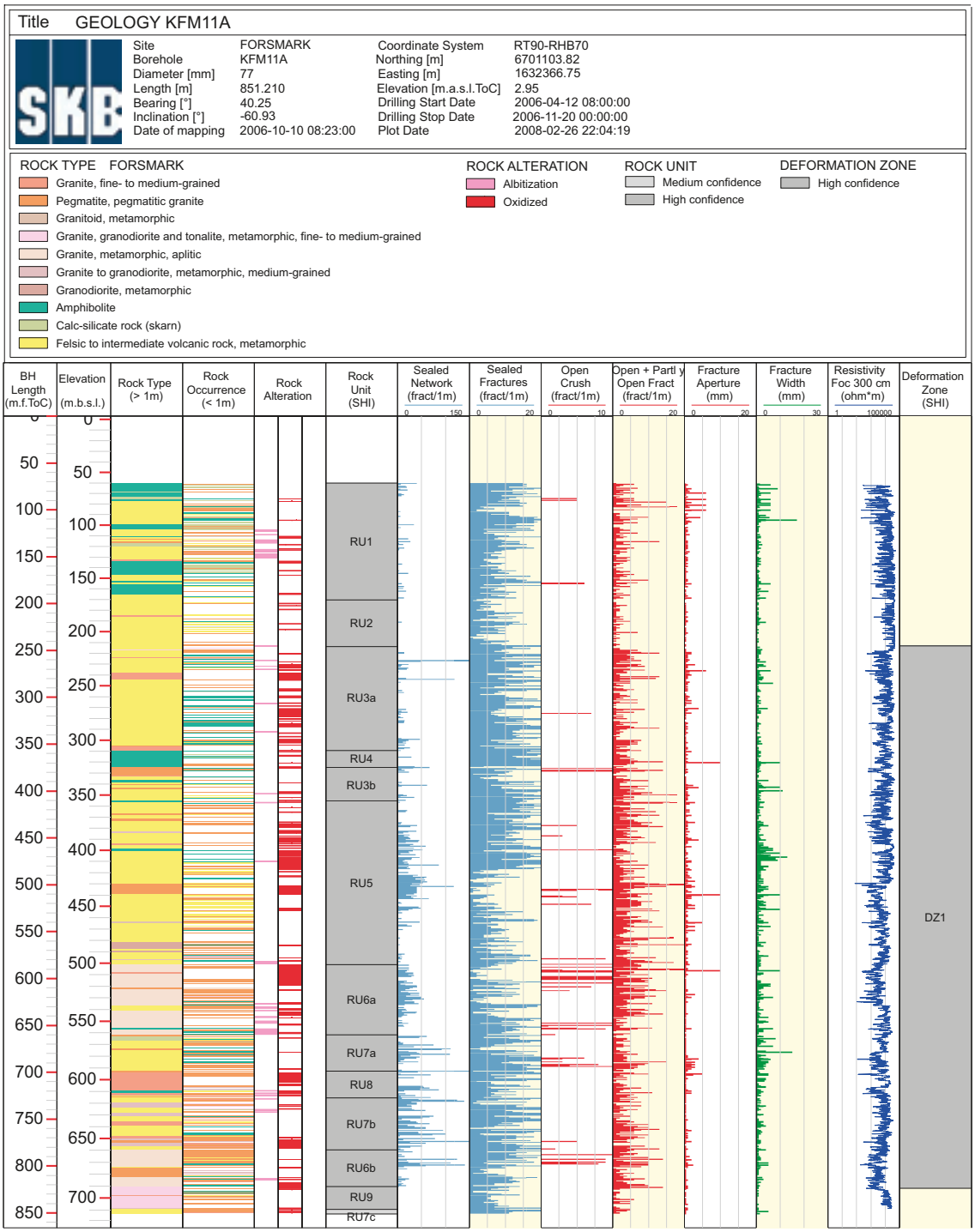

Figure 5-2. *WellCad diagram for the cored borehole KFM11A, showing a selected suite of base geological and geophysical data that have been used to identify rock units and possible deformation zones in the single-hole interpretation of this borehole. The letter after a rock unit helps to distinguish the occurrence of the same rock unit at different intervals along the borehole.*

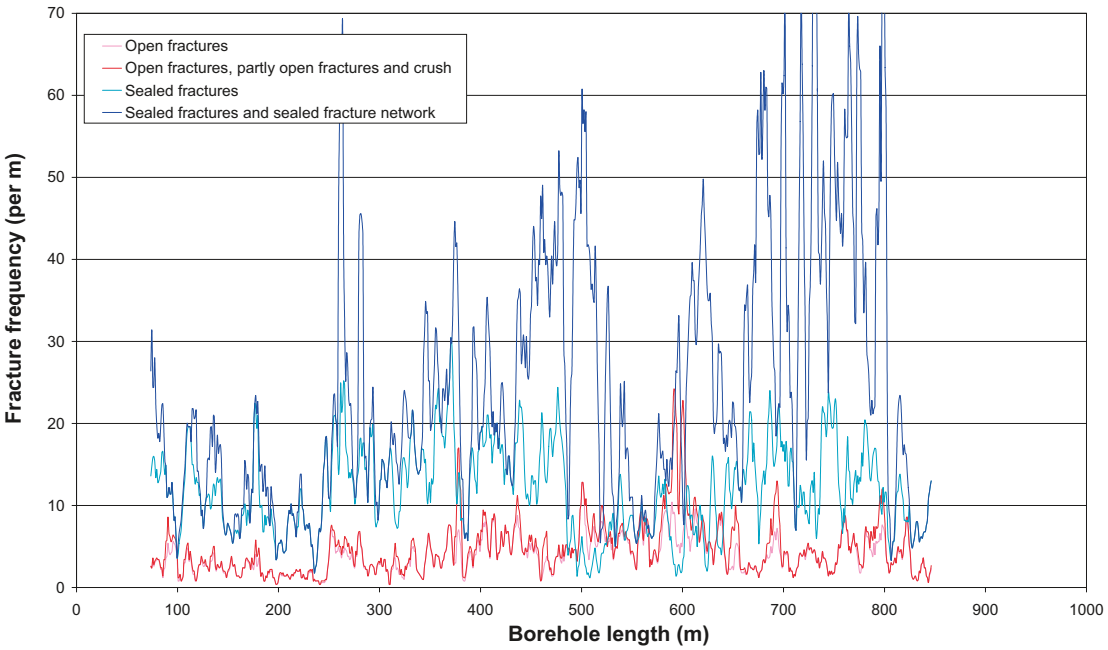

Figure 5-3. *Fracture frequency along borehole KFM11A. Separate moving average plots for open fractures, combined open fractures, partly open fractures and crush zones, sealed fractures, and combined sealed fractures and sealed fracture networks are shown in the diagram. A 5 m window and 1 m steps have been used in the calculation procedure for each plot. Note that the frequency of open fractures is equal to or higher than the frequency of sealed fractures in the interval between 498 and 630 m.*

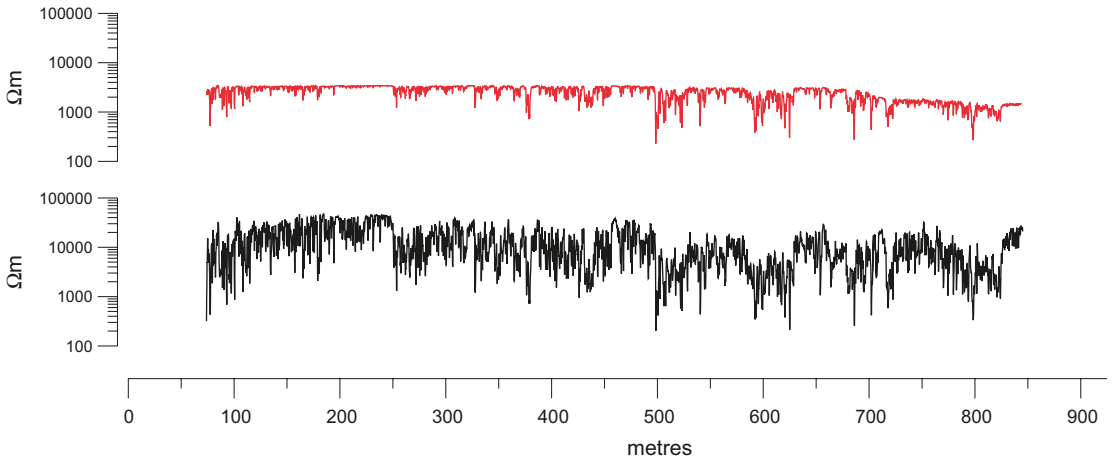

Figure 5-4. *Focused resistivity values along borehole KFM11A. Note the generally good correspondence with the fracture frequency anomalies in Figure 5-3 (see also Figure 5-2).*

The orientation and mineralogy of the fractures along DZ1 are presented in Figure 5-5. These data indicate that this possible zone can be divided into three separate intervals. Three main fracture orientation sets are present in the interval 245–498 m; a set that strikes WNW-ESE and dips steeply, gently dipping fractures and a set that strikes SW to SSW and dips steeply (Figure 5-5a). In the remainder of DZ1, most fractures strike WNW-ESE or ENE-WSW to NE-SW and dip steeply; gently dipping fractures are present but occur less frequently compared with that in the upper part of DZ1 (Figures 5-5b and 5-5c).

The fracture minerals calcite and chlorite occur throughout the borehole interval occupied by DZ1. However, calcite is less common in the central part of the zone along the borehole interval between 498 and 630 m (Figure 5-5b). The early generation mineral epidote and hematite-stained adularia are conspicuous along the fractures in the upper and lower intervals 245–498 m and 630–824 m, respectively (Figure 5-5a and 5-5c). By contrast, epidote is less common and laumontite dominates over adularia/hematite in the central part of DZ1 between 498 and 630 m (Figure 5-5b). Although adularia/hematite and laumontite have been included in the same generation of minerals (see, for example, /Sandström et al. 2008a/), it is notable that they show different relative abundances along different borehole intervals in DZ1. It is inferred that different parts of the zone have been subject to reactivation and fluid movement at different times during the brittle part of the geological evolution. Clay minerals are present along particularly open fractures throughout the entire zone.

The fracture orientation and fracture mineralogy of the three different segments of DZ1, together with the confidence level assigned to DZ1 during the SHI work, are summarised in Table 5-4.

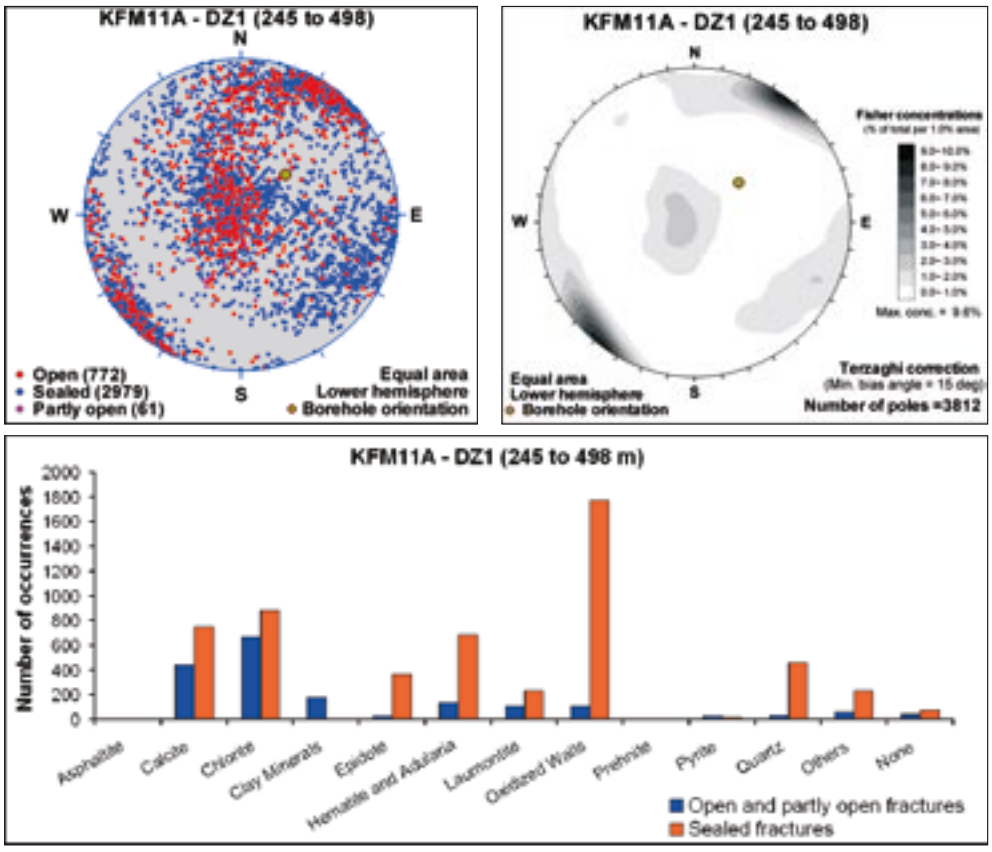

a)

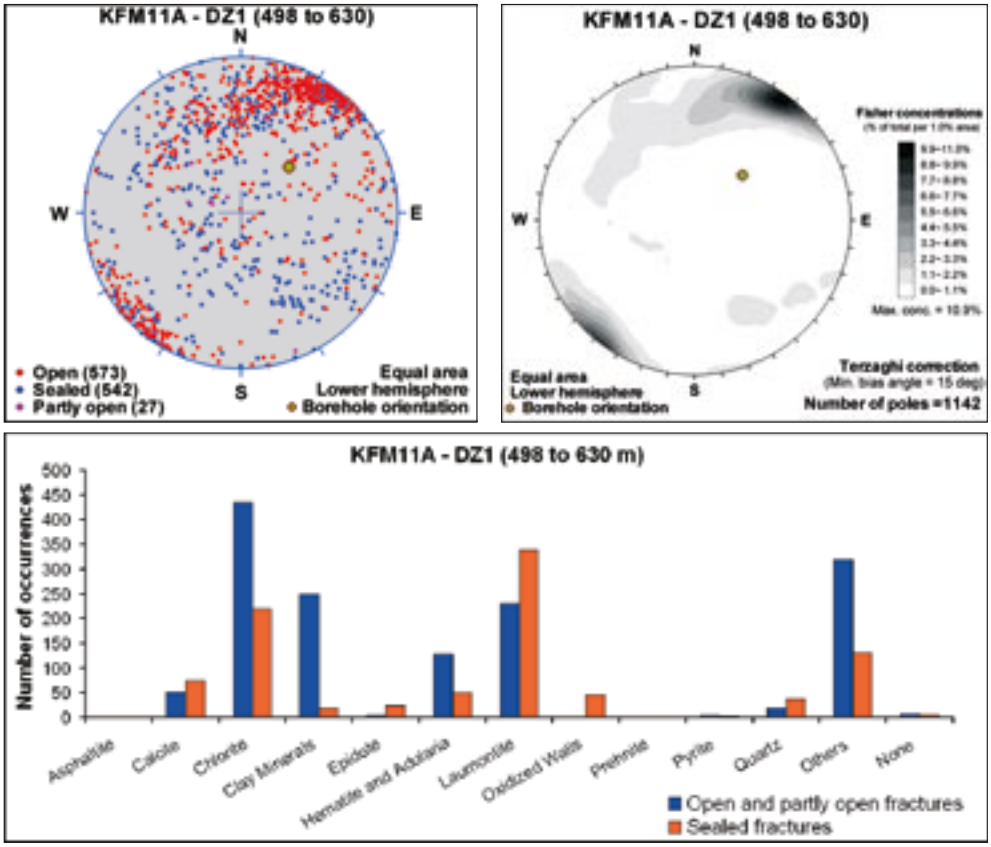

b)

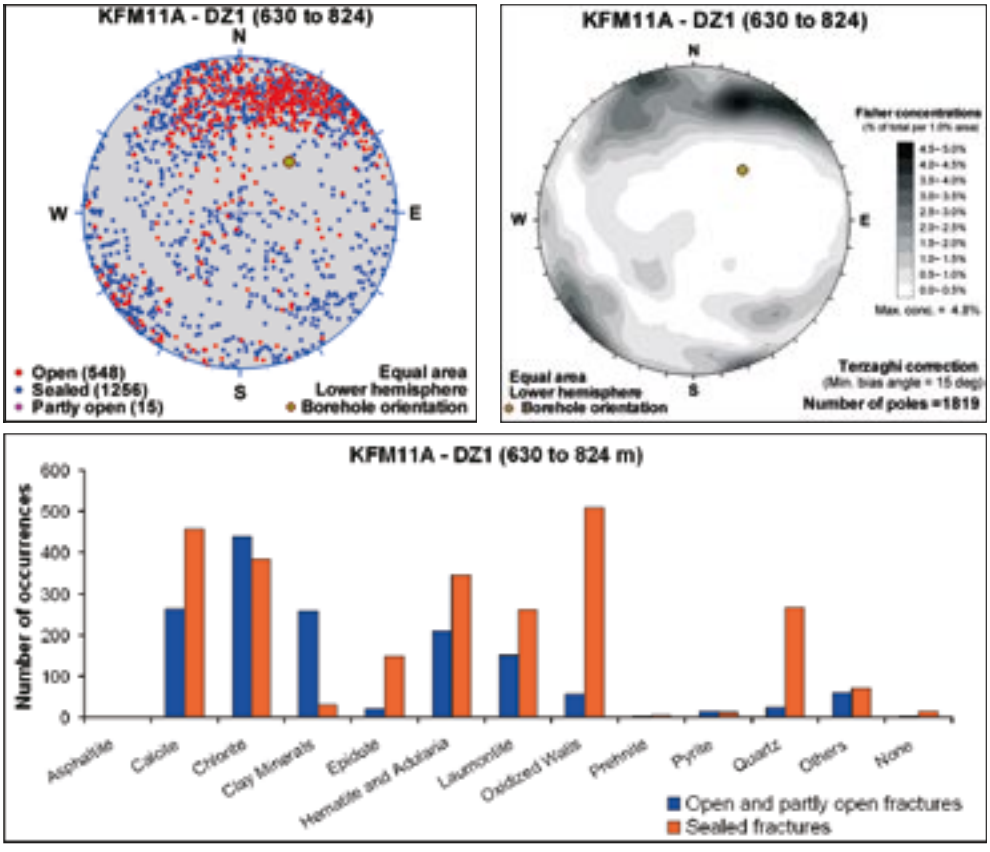

c)

Figure 5-5. *Mean poles to fracture sets and occurrence of different minerals as fillings and coatings along the fractures from three borehole intervals inside the possible deformation zone DZ1 in KFM11A. (a) 245–498 m, (b) 498–630 m and (c) 630–824 m.*

Table 5-4. Confidence level, fracture orientation and fracture mineralogy of the possible deformation zone DZ1 recognised during the single-hole interpretation of borehole KFM11A. All borehole lengths are adjusted values. Strike and dip are presented using the right-hand-rule method. Data extracted from Sicada database: SICADA_07_395 (2007-10-26).

Possible deformation zone	Borehole length (m)		Confidence level	Fracture orientation (strike/dip)	Fracture mineralogy (excluding chlorite, calcite)
	Upper intersection	Lower intersection			
DZ1	245	498	High	1. WNW-ESE/steep dip 2. Gentle 3. SW to SSW/steep dip	Adularia/hematite, quartz, epidote, laumontite, clay minerals Adularia/hematite > laumontite
DZ1	498	630	High	1. WNW-ESE/steep dip 2. Gentle and NE-SW/steep are subordinate	Adularia/hematite, clay minerals, ±quartz, ±epidote Adularia/hematite ≤ laumontite
DZ1	630	824	High	1. WNW-ESE/steep dip 2. ENE-WSW to NE-SW/steep dip 3. Gentle are subordinate	Adularia/hematite, laumontite, quartz, clay minerals, epidote

5.4 Prediction − outcome: A comparison

A comparison between the boundaries of rock domains and deformation zones along borehole KFM11A, as predicted from the deterministic modelling work during stage 2.2 /Stephens et al. 2007/, and the results of the single-hole interpretation of this borehole /Carlsten et al. 2007c/ are presented in Table 5-5 and Table 5-6, respectively. The results of a similar comparative study for the boundaries of deformation zones along the percussion boreholes HFM33, HFM34 and HFM35 are presented in Table 5-7. A statement has been made beneath each geological object in these tables, which specifies the changes that need to be made to the corresponding deterministic model, so that the results from the single-hole interpretation of each borehole are taken into account. Attention in the text below is focused on the results from cored borehole KFM11A and a visualisation of the prediction-outcome test for deformation zones is shown in Figure 5-6.

Table 5-5. Correlation between rock domains (RFM) modelled deterministically in model stage 2.2 /Stephens et al. 2007/ and rock units (RU) in the single-hole interpretation (SHI) of boreholes KFM11A /Carlsten et al. 2007c/. The implications for the local rock domain model, stage 2.2, are summarised in the text beneath the geological object. UI = Upper intercept, LI = Lower intercept. All borehole lengths are adjusted values.

RFM in local model stage 2.2	Confidence level for RFM in local model stage 2.2	Prediction, borehole length (m)		RU in SHI	Confidence level for RU in SHI	Outcome, borehole length (m)	
		UI	LI			UI	LI
RFM021	High at the surface, medium at depth	Start of the cored borehole length	Beneath cored borehole length	RU1, RU2, RU3a, RU4, RU3b, RU5, RU6a, RU7a, RU8, RU7b, RU6b, RU9, RU7c	High	71.60 (top of cored borehole length)	851.21 (base of cored borehole length)
No rock domain boundary has been intersected along KFM11A. No changes are required.							

Table 5-6. Correlation between deformation zones modelled deterministically in model stage 2.2 /Stephens et al. 2007/ and possible deformation zones (DZ) in the single-hole interpretation (SHI) of the borehole KFM11A /Carlsten et al. 2007c/. The implications for the local deformation zone model, stage 2.2, are summarised in the text beneath each geological object. UI = Upper intercept, LI = Lower intercept. All borehole lengths are adjusted values.

ZFM in model stage 2.2	Confidence level for ZFM in model stage 2.2	Prediction, borehole length (m)		DZ in SHI	Confidence level for DZ in SHI	Outcome, borehole length (m)	
		UI	LI			UI	LI
ZFMWNW0813	Medium	371	401	DZ1	High	245	824
ZFMWNW0001 (Singö DZ)	High	404	811				
ZFMWNW1127	Medium	784	854				

Based on the revised lineament interpretation during stage 2.3 (see chapter 2), zone ZFMWNW1127 needs to be removed and replaced by ZFMNW0002. DZ1 in KFM11A probably corresponds to three separate steep WNW-NW zones, ZFMWNW0813, ZFMWNW0001 referred to as the Singö zone and ZFMNW0002. These modifications motivate a need for some minor changes in the regional and local DZ models stage 2.2, including, for example, terminations against the Singö deformation zone and thickness of zones ZFMWNW0813, ZFMWNW0001 and ZFMNW0002. The confidence of existence of zone ZFMWNW0813 can be raised to high.

Table 5-7. Correlation between deformation zones modelled deterministically in model stage 2.2 /Stephens et al. 2007/ and possible deformation zones (DZ) in the single-hole interpretation (SHI) of boreholes HFM34 and HFM35 /Carlsten et al. 2007c/. The implications for the local deformation zone model, stage 2.2, are summarised in the text beneath each geological object. UI = Upper intercept, LI = Lower intercept. All borehole lengths are adjusted values. No possible defomation zones were indentified along HFM33.

Borehole	Confidence level for ZFM in model stage 2.2	ZFM in model stage 2.2	Prediction, borehole length (m)		DZ in SHI	Confidence level for DZ in SHI	Outcome, borehole length (m)	
			UI	LI			UI	LI
HFM34	High	ZFMWNW0001 (Singö DZ)	Above the start of the borehole	Beneath the base of the borehole	DZ1	Medium	37	133
HFM34	High	ZFMWNW0001 (Singö DZ)	Above the start of the borehole	Beneath the base of the borehole	DZ2	Low	180	184
					DZ3	Low	188	192

The entire percussion borehole is drilled inside ZFMWNW0001. See also comments above for KFM11A. Need for minor changes in the DZ models.

HFM35	High	ZFMWNW0001 (Singö DZ)	Above the start of the bore-hole	44	DZ1	High	24	33
					DZ2	High	47	53

See comments above for KFM11A. Need for minor changes in the DZ models.

HFM35	Medium	ZFMWNW1127	79	132	DZ3	Medium	104	200

Possible correlation with low magnetic lineament MFM1035 in revised lineament interpretation (stage 2.3).The length of the lineament is less than 3,000 m. A steep WNW zone probably needs to be added to the DZ local model stage 2.2. No changes in regional DZ model stage 2.2.

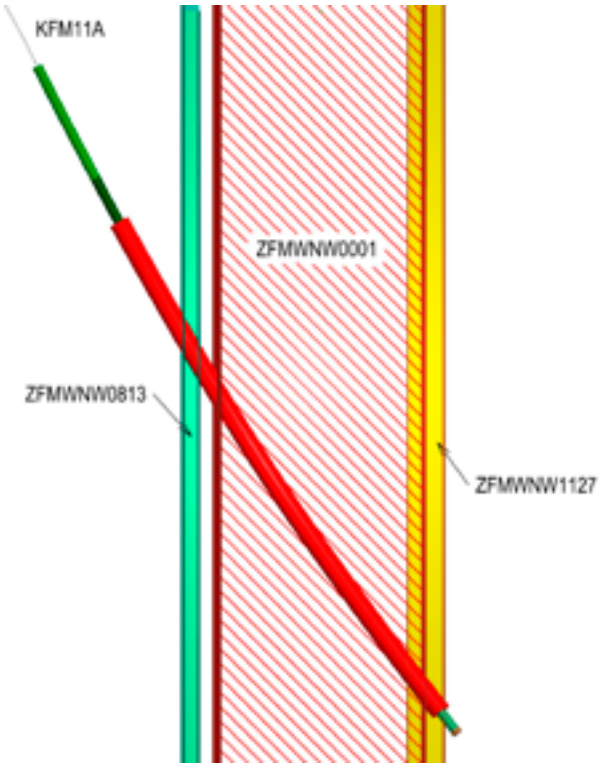

Figure 5-6. *Prediction-outcome visualisation for deformation zones along borehole KFM11A. Modelled deformation zones stage 2.2 (ZFM) are compared with the possible deformation zone DZ1 in the single-hole interpretation. DZ1 is marked with red cylinder along the borehole. The length of the borehole KFM11A is c. 851 m. See text for further discussion.*

On the basis of the discussion earlier in this chapter, the bedrock in borehole KFM11A, as recognised in the single-hole interpretation, can be assigned with high confidence to rock domain RFM021. This is in agreement with the geological rock domain models.

Based on the revised lineament interpretation during stage 2.3 (see chapter 2), zone ZFMWNW1127 needs to be removed and replaced by ZFMNW0002. Bearing this point in mind as well as the style of deformation and fracture characteristics along DZ1 in KFM11A, it is inferred that the latter probably corresponds to three separate steep WNW-NW zones, ZFMWNW0813, ZFMWNW0001 referred to as the Singö zone and ZFMNW0002. Since these zones lie spatially close to each other in the vicinity of borehole KFM11A (Figure 2-3), it is difficult to separate them along DZ1. These observations motivate a need for some minor changes in the regional and local DZ models stage 2.2, including, for example, terminations against the Singö deformation zone and estimates of the thickness of zones ZFMWNW0813, ZFMWNW0001 and ZFMNW0002. The complementary stage 2.3 data also permit a high confidence assessment for the existence of zone ZFMWNW0813.

The evaluation of the data from the single-hole interpretation together with the revised interpretation of lineaments from the high resolution ground magnetic survey (see chapter 2) support the prediction that the Singö deformation zone is a complex zone which has an intricate interplay with splay structures, e.g. ZFMNW0002. It is also apparent that the Singö deformation zone has had a long period of geological evolution, which started in the ductile regime and continued throughout several phases of brittle reactivation. These features are in good agreement with the evaluation of the WNW to NW set of steeply dipping deformation zones in the geological model.

6 Borehole KFM012A

6.1 Background

As stated in chapter 5, the Forsmark deformation zone (ZFMWNW0004) together with the Singö (ZFMWNW0001) and Eckarfjärden (ZFMNW0003) deformation zones constitute the regionally most significant geological discontinuities in the crystalline bedrock at Forsmark. These zones belong to the WNW to NW set of steeply dipping zones at the site and are situated within the broader belts affected by high ductile strain that envelop and form the margins to the Forsmark tectonic lens /Stephens et al. 2007/. Both ductile and polyphase brittle deformation has been inferred to be present along these zones. The location of the Forsmark deformation zone is shown in Figure 5-1. It is situated c. 2 km to the south-west of the target area at the site.

There are few outcrops inside that part of the regional model area where the Forsmark deformation zone intersects the ground surface. These outcrops have only provided information on the ductile deformation in the high-strain belt within which the zone is situated. Furthermore, drill core information across this regionally important zone has been lacking up to model stage 2.3. The position, orientation and properties such as length, thickness, style of deformation and alteration are based solely on the interpretation of geophysical and topographic data, and a comparison with especially the Singö deformation zone /Appendix 15 in Stephens et al. 2007/.

The drilling of borehole KFM12A during model stage 2.3 aimed to provide base geological information bearing on the character of the Forsmark deformation zone, and to acquire hydrogeological and hydrogeochemical data along the borehole trajectory through the zone. Two complementary percussion boreholes were also drilled in the vicinity of drill site 12. HFM36 aimed to provide flushing water for the drilling of borehole KFM12A and to investigate the character of a lineament to the south-west of the Forsmark deformation zone. Percussion borehole HFM37 was drilled in the inferred position of the Forsmark deformation zone so as to improve our understanding of the geological significance of this structure and to monitor possible pressure responses during the core drilling.

The decision statement and motivation document for borehole KFM12A are provided in document ID 1053022. The position, inclination, bearing and borehole length are summarised in Table 6-1.

Table 6-1. Position, inclination, bearing and length of borehole KFM12A, HFM36 and HFM37. Data extracted from Sicada database: Sicada_08_109 (2008-05-09).

Borehole	Drill site	Easting RT 90, 2.5 gon W (m)	Northing RT 90, 2.5 gon W (m)	Inclination (°)	Bearing (°)	Length (m)
KFM12A	12	1630052	6696578	–61	036	601
HFM36	12	1630137	6696592	–59	257	153
HFM37	12	1630138	6696594	–59	041	192

6.2 Prediction of intersections of geological features along borehole KFM12A based on model stage 2.2

With the help of the rock visualisation system (RVS), a prediction of the intersections of rock domains and deformation zones, included in model stage 2.2 /Stephens et al. 2007/, along borehole KFM12A can be carried out. It needs to be kept in mind that drill site 12 is situated inside the regional model volume but outside the local model volume. For this reason, only zones with a trace length at the ground surface longer than 3,000 m can be predicted to intersect this borehole /Stephens et al. 2007/. Furthermore, since the fracture domain model was only constructed inside the target volume at Forsmark /Olofsson et al. 2007/, there are no predicted intersections for fracture domain boundaries in KFM12A.

Borehole KFM12A does not intersect any rock domain boundaries. The entire borehole is drilled within rock domain 30 (RFM030), which is dominated by strongly foliated metatonalite or metagranodiorite. Subordinate occurrences of different types of metagranitoid, metadiorite or metagabbro, pegmatite, pegmatitic granite, amphibolite and felsic to intermediate metavolcanic rock are also present /SKB 2005/. As in the vicinity of drill site 11, the degree of inhomogeneity of the rock types in this rock domain is high.

The modelling work during stage 2.2 predicts that one, steeply dipping deformation zone (ZFMWNW0004 corresponding to the Forsmark zone), which belongs to the orientation sub-set referred to as WNW, intersects borehole KFM012A (Table 6-2). The predicted upper and lower borehole intersections of this zone are shown in Table 6-2. The properties of this zone are provided in /Appendix 15 in Stephens et al. 2007/ and selected aspects (confidence of existence, orientation, orientation class, trace length at the ground surface and size class) are also shown in Table 6-2.

The predicted high confidence zone ZFMWNW0004 is significantly longer than 10,000 m in trace length at the ground surface. Based on the inferred trace length, the zone has been classified as regional in character (Table 6-2). The properties of the Forsmark deformation zone are described in some detail in /SKB 2002/ and summarised in the property tables in /Appendix 15 in Stephens et al. 2007/. The position and length (c. 70 km) of the zone have been inferred with the help of ground geophysical data, including seismic and electromagnetic measurements, and the interpretation of lineaments using both airborne geophysical and topographic data. The strike of the Forsmark deformation zone is based on the trend of the corresponding low magnetic lineament (MFM0014) and the dip is assumed to be 90° on the basis of a comparison with the Singö deformation zone. The thickness has also been interpreted by a comparison with the Singö zone.

Table 6-2. Predicted intersection of deformation zones modelled deterministically in model stage 2.2 with borehole KFM12A. Only one zone, ZFMWNW0004 corresponding to the Forsmark deformation zone, is indicated. Borehole intersections have been extracted with the assistance of RVS, using data on the bearing and inclination of the trace of borehole KFM12A and the geometry of deformation zones in regional model, stage 2.2 /Stephens et al. 2007/. Zone confidence, orientation and trace length at the ground surface have been extracted from /Appendix 15 in Stephens et al. 2007/. UI = Upper intercept, LI = Lower intercept. All borehole lengths are adjusted values. All orientations are provided as strike/dip using the right-hand-rule-method.

Modelled deformation zone (ZFM)	Confidence of existence	Strike/dip (°) and orientation class /Stephens et al. 2007/	Trace length at the ground surafce (m)	Size class	Borehole length (m)	
					UI	LI
ZFMWNW0004	High	125/90 Steep/WNW	70,000	Regional (>10 km)	104	416

The style of deformation, with both ductile and brittle strain, as well as alteration along the zone are based on observations in outcrop predominantly outside the regional model area /see SKB 2002/. In particular, fault rock including mylonites and fault breccias has been documented in the vicinity of Östhammar to the south-east. Close to Forsmark, the topographic surface, which is inferred to mark the sub-Cambrian unconformity (peneplain), lies up to c. 10 m lower on the south-western relative to the north-eastern side of the zone /Bergman et al. 1999, SKB 2002/. A bulk southwest-side-down sense of movement has tentatively been inferred along the zone and it is inferred that at least some normal displacement has occurred after the establishment of this unconformity. Data bearing on the character of fractures along the zone have been totally lacking up to model stage 2.3.

6.3 Single-hole interpretation of borehole KFM12A − outcome

Key geological and geophysical data in this borehole that have been used during the first stage of the single-hole interpretation (SHI) of KFM12A, including rock alteration, the frequency of different types of fractures and focused resistivity, are shown in Figure 6-1 together with the results of the interpretation /Carlsten et al. 2007d/. The character and kinematics of the possible deformation zones along this borehole, which were completed during the second stage of the SHI and are addressed in /Nordgulen and Saintot 2008/, are treated together with similar data from other complementary (stage 2.3) boreholes in chapter 8.

Borehole KFM12A has been divided into twelve different rock units (RU1–RU12) with a high confidence of existence (Figure 6-1). Each of the three rock units RU3, RU4 and RU8 occur in two separate length intervals (RU3a and RU3b, RU4a and RU4b, and RU8a and RU8b, respectively). Furthermore, rock unit RU9 has been identified in three separate length intervals (RU9a, RU9b and RU9c) /Carlsten et al. 2007d/. These features illustrate the inhomogeneity of the bedrock along the borehole.

Nearly all the rock units in borehole KFM12A are inhomogeneous in rock composition (/Carlsten et al. 2007d/ and Figure 6-1). The more homogeneous units, RU1, RU3, RU8, RU10 and RU12, are dominated by metagranodiorite (101056), which shows variable texture and degree of foliation development, and is partly affected by grain-size reduction related to high ductile strain. In the upper part of the borehole, in RU1, rotated megacrysts in metagranodiorite indicate ductile shear strain in the bedrock. However, the general asymmetry of these megacrysts and the presence of poorly defined shear bands, typical of deformation under amphibolite facies metamorphic conditions, have not permitted the sense of shear to be determined /Nordgulen and Saintot 2008/.

The development of the fault rock cataclasite (108003) in rock units RU6 and RU7 is so extensive that it has not been possible to identify the protolith along these sections (see also chapter 8). However, borehole intervals with calc-silicate rock are present along rock unit RU6. Silicification and epidotization of variable intensity occur throughout rock unit RU7. Felsic to intermediate metavolcanic rock (103076) becomes increasingly more prominent towards the bottom of the borehole and dominates in rock unit RU9. Banded metatonalite to granodiorite (101054) dominates in rock unit RU11.

A moving average plot for the frequency of fractures along borehole KFM12A (Figure 6-2) indicates a marked increase in sealed fractures and sealed fracture networks in the long borehole interval c. 170–402 m. Open fractures are also conspicuous in particularly the borehole interval c. 170–338 m. The whole interval between c. 170–402 m also shows an overall reduced bulk resistivity (Figure 6-3), alteration referred to as oxidation (red-staining in the bedrock related to hematite dissemination) and low magnetic susceptibility. On the basis of these observations, it was classified as a possible deformation (DZ1 in /Carlsten et al. 2007d/ and Figure 6-1). Similar highly fractured and altered bedrock has been identified at c. 125–158 m and c. 513–523 m (DZ1 and DZ3, respectively, in /Carlsten et al. 2007d/ and Figure 6-1).

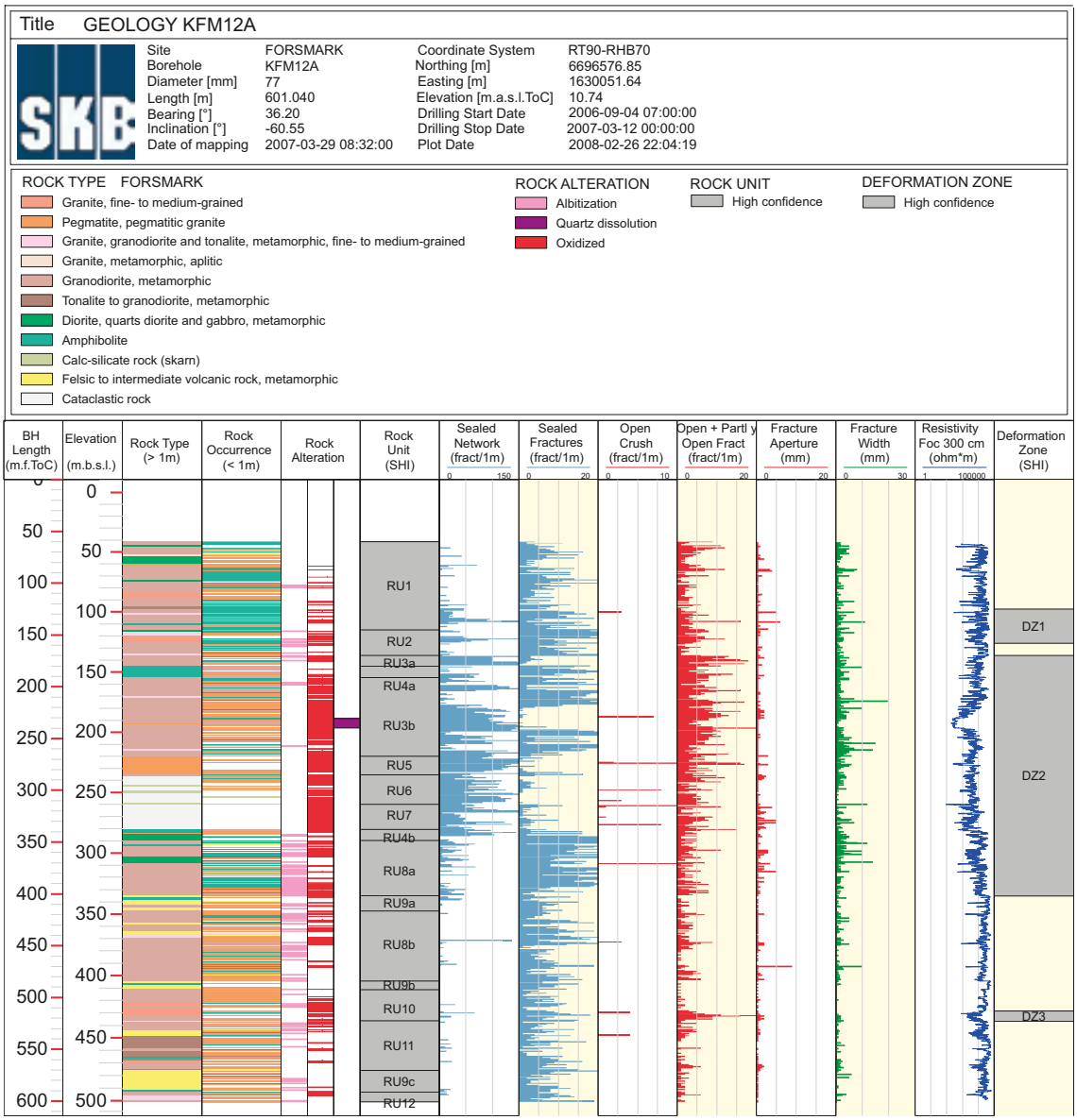

Figure 6-1. *WellCad diagram for the cored borehole KFM12A, showing a selected suite of base geological and geophysical data that have been used to identify rock units and possible deformation zones in the single-hole interpretation of this borehole. The letter after a rock unit helps to distinguish the occurrence of the same rock unit at different intervals along the borehole.*

Short borehole sections with incohesive crush rock are also present along all three possible deformation zones (/Carlsten et al. 2007d/ and Figure 6-1). These occurrences correspond to intervals of more strongly reduced focused resistivity in the bedrock (Figure 6-3). In the upper part of the borehole, between c. 230 and 240 m along DZ2, altered vuggy rock is affected by cataclasis. The altered vuggy rock is associated with very low resistivity, low P-wave velocity, low density and increased gamma radiation.

Bearing in mind the character of the rock units along borehole KFM12A /Carlsten et al. 2007d/, it is apparent that the possible deformation zones DZ1, DZ2 and DZ3 are composite structures with both ductile and brittle deformation. In particular, the possible deformation zone DZ2 exhibits both high ductile strain and a conspicuous interval between c. 285 and 338 m of cataclastic fault rock. The latter corresponds to the two rock units RU6 and RU7. However, there are some difficulties to distinguish the ductile deformation attributed to the Forsmark zone from that associated with the broader high-strain belt in which this zone is located (see Figure 5-1).

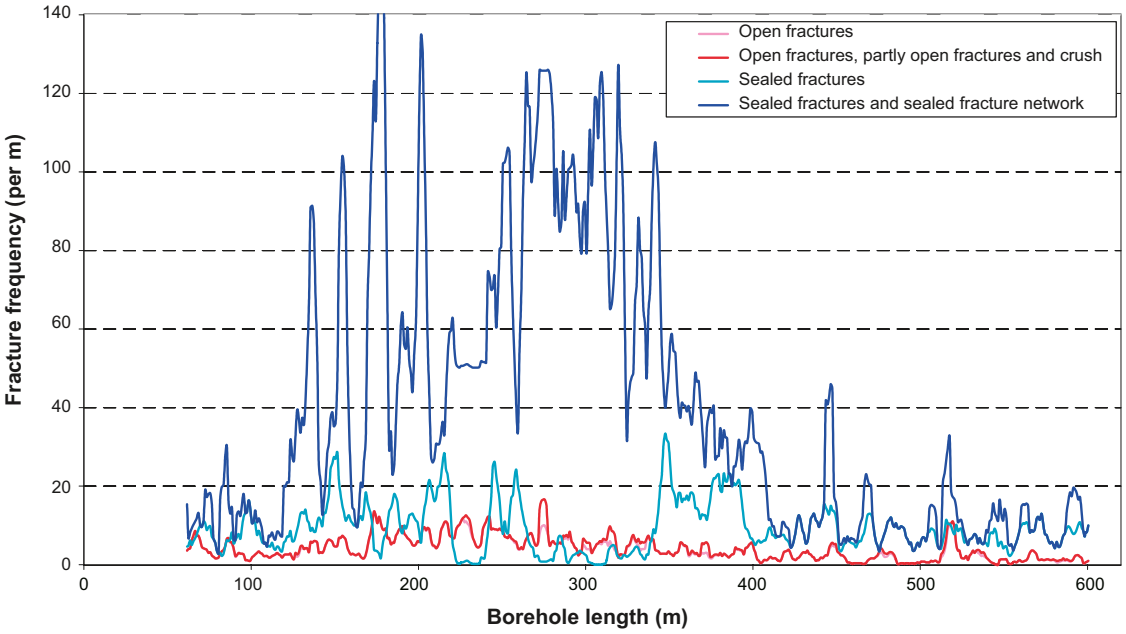

Figure 6-2. *Fracture frequency along borehole KFM12A. Separate moving average plots for open fractures, combined open fractures, partly open fractures and crush zones, sealed fractures, and combined sealed fractures and sealed fracture networks are shown in the diagram. A 5 m window and 1 m steps have been used in the calculation procedure for each plot.*

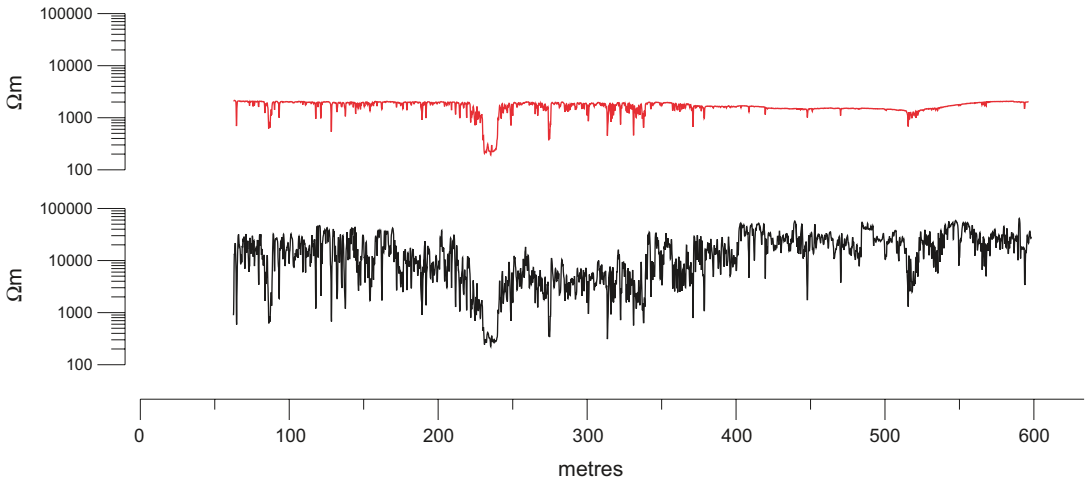

Figure 6-3. *Focused resistivity values along borehole KFM12A. Note the generally good correspondence with the fracture frequency anomalies in Figure 6-2. The very low resistivity between c. 230 and 240 m corresponds to altered vuggy rock.*

The orientation and mineralogy of the fractures along the possible deformation zone are shown in Figure 6-4. Two main fracture orientation sets are present in the possible deformation zone DZ1, a steeply dipping set that strikes NW-SE and a set that dips more gently to the south-east (Figure 6-4a). Similar distributions in the orientation of fractures are observed at different depths along DZ2 (Figure 6-4b, c and d) However, in the lower part of the zone, beneath the cataclastic rocks in RU6 and RU7, the steeply dipping fractures strike predominantly NW-SE to ESE and a new steeply dipping set that strikes NE-SW or ENE-WSW is also present (Figure 6-4d). Open fractures that dip steeply to the SSW or are gently dipping are present along DZ3 (Figure 6-4e). The sealed fractures show a variable orientation (Figure 6-4e).

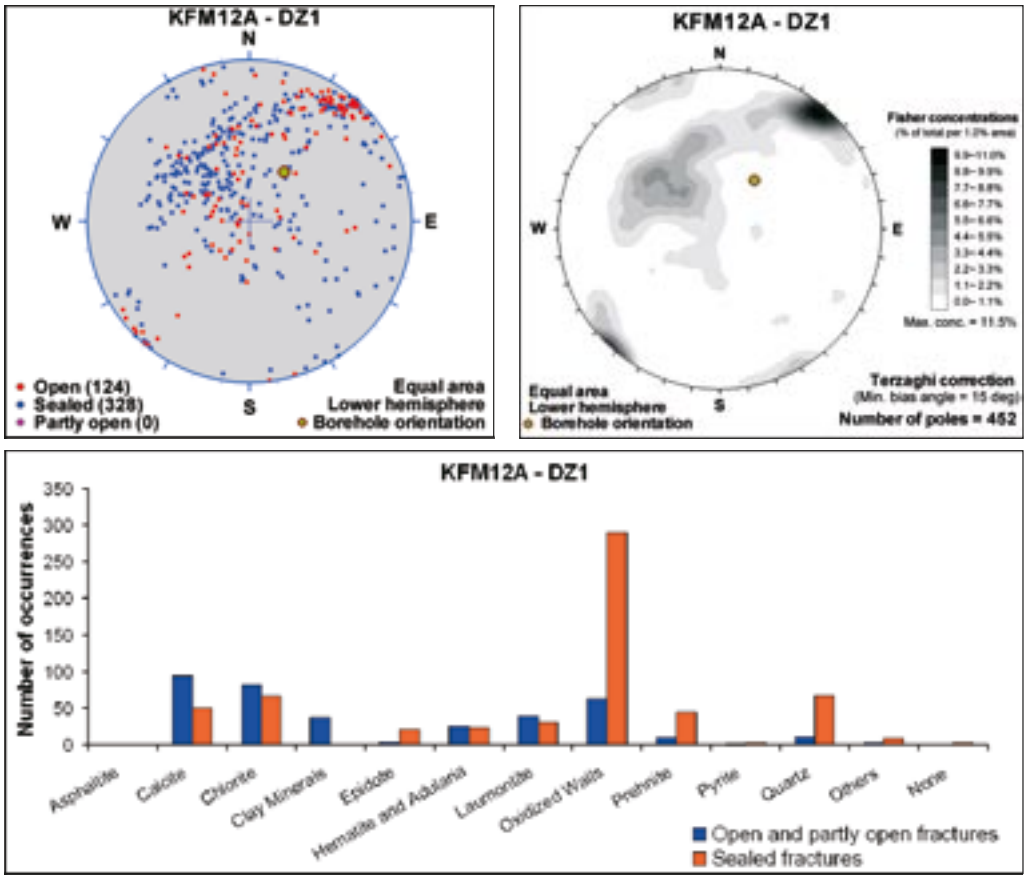
KFM12A - DZ1
N
W
E
S
Open (124)
Sealed (328)
Partly open (0)
Equal area
Lower hemisphere
Borehole orientation
KFM12A - DZ1
Fisher concentrations
Max. conc. = 11.5%
Terzaghi correction
Number of poles = 452
KFM12A - DZ1
Number of occurrences
Asphaltite
Calcite
Chlorite
Clay Minerals
Epidote
Hematite and Adularia
Laumontite
Oxidized Walls
Prehnite
Pyrite
Quartz
Others
None
Open and partly open fractures
Sealed fractures

a)

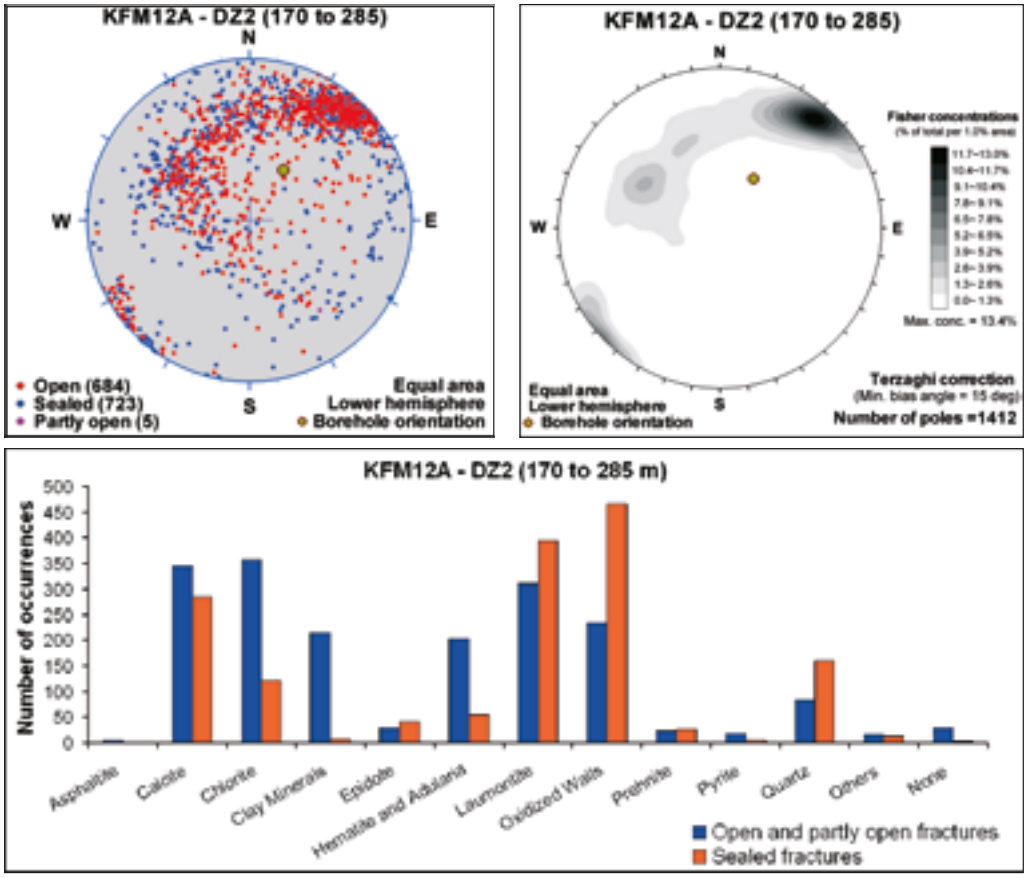
KFM12A - DZ2 (170 to 285)
N
W
E
S
Open (684)
Sealed (723)
Partly open (5)
Equal area
Lower hemisphere
Borehole orientation
KFM12A - DZ2 (170 to 285)
Fisher concentrations
Max. conc. = 13.4%
Terzaghi correction
Number of poles =1412
KFM12A - DZ2 (170 to 285 m)
Number of occurrences
Asphaltite
Calcite
Chlorite
Clay Minerals
Epidote
Hematite and Adularia
Laumontite
Oxidized Walls
Prehnite
Pyrite
Quartz
Others
None
Open and partly open fractures
Sealed fractures

b)

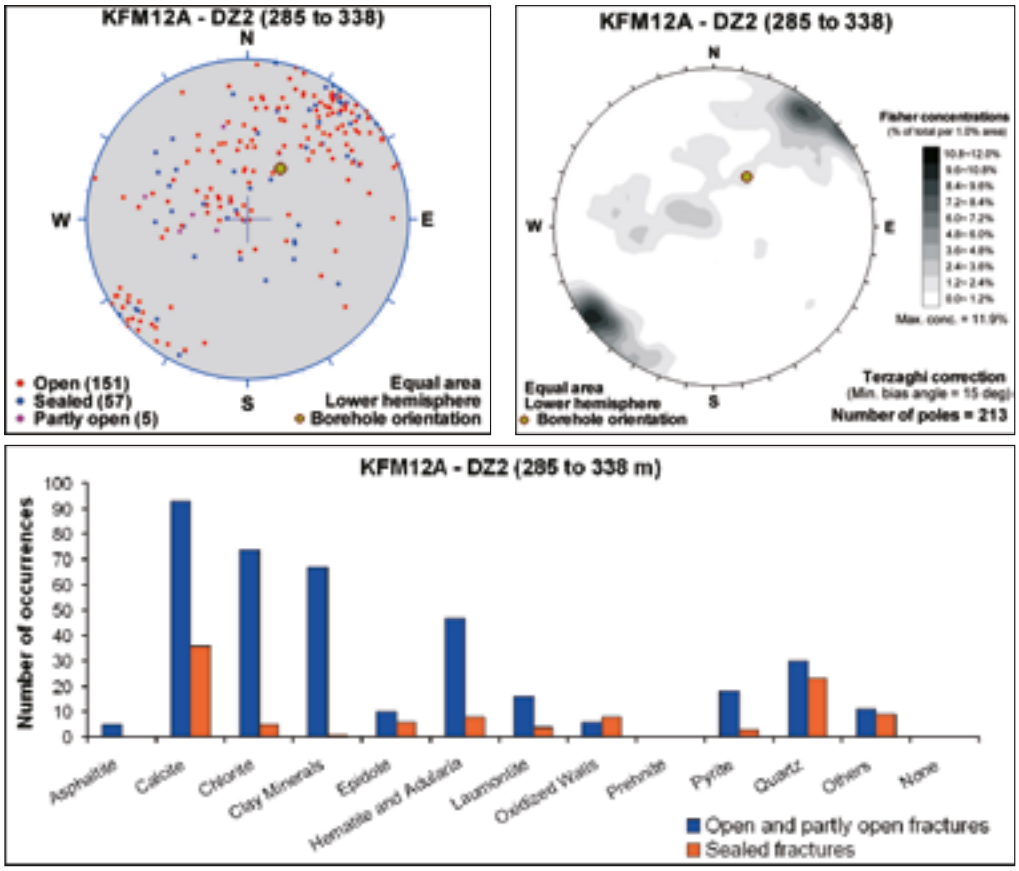
KFM12A - DZ2 (285 to 338)
N
W
E
S
Open (151)
Sealed (57)
Partly open (5)
Equal area
Lower hemisphere
Borehole orientation
KFM12A - DZ2 (285 to 338)
Fisher concentrations
Max. conc. = 11.9%
Terzaghi correction
Number of poles = 213
KFM12A - DZ2 (285 to 338 m)
Number of occurrences
Asphaltite
Calcite
Chlorite
Clay Minerals
Epidote
Hematite and Adularia
Laumontite
Oxidized Walls
Prehnite
Pyrite
Quartz
Others
None
Open and partly open fractures
Sealed fractures

c)

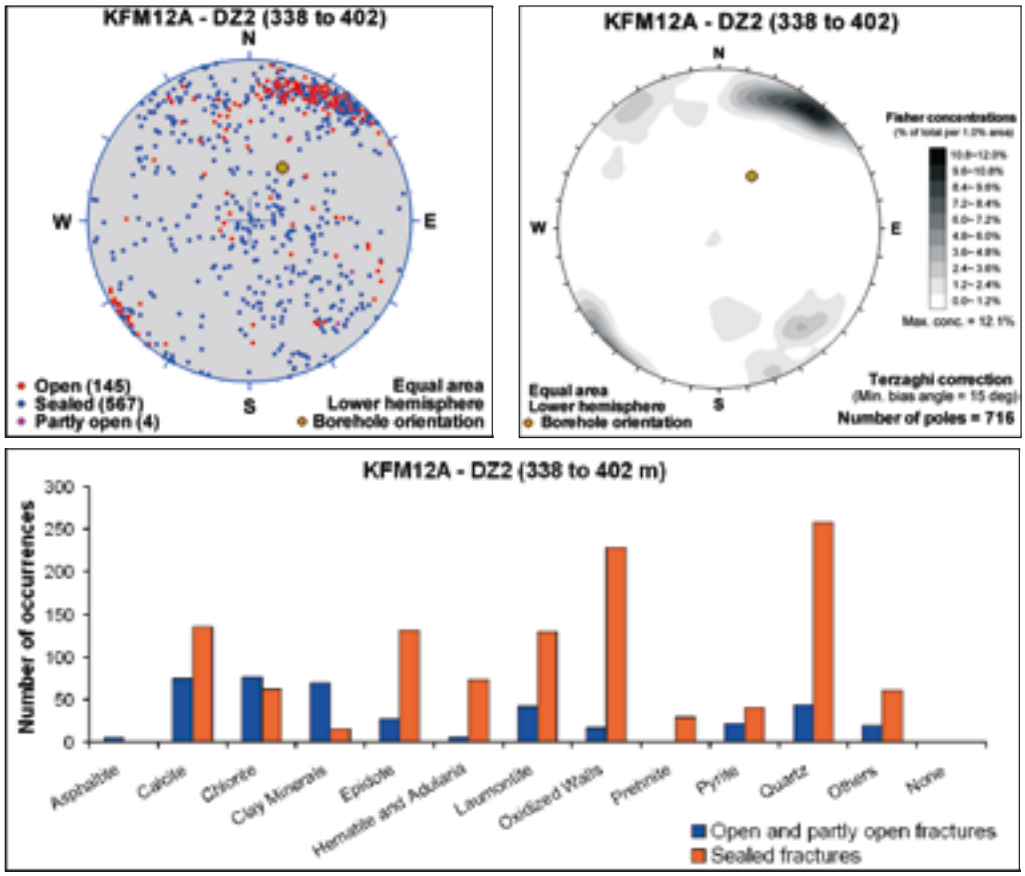
KFM12A - DZ2 (338 to 402)
N
W
E
S
Open (145)
Sealed (567)
Partly open (4)
Equal area
Lower hemisphere
Borehole orientation
KFM12A - DZ2 (338 to 402)
Fisher concentrations
Max. conc. = 12.1%
Terzaghi correction
Number of poles = 716
KFM12A - DZ2 (338 to 402 m)
Number of occurrences
Asphaltite
Calcite
Chlorite
Clay Minerals
Epidote
Hematite and Adularia
Laumontite
Oxidized Walls
Prehnite
Pyrite
Quartz
Others
None
Open and partly open fractures
Sealed fractures

d)

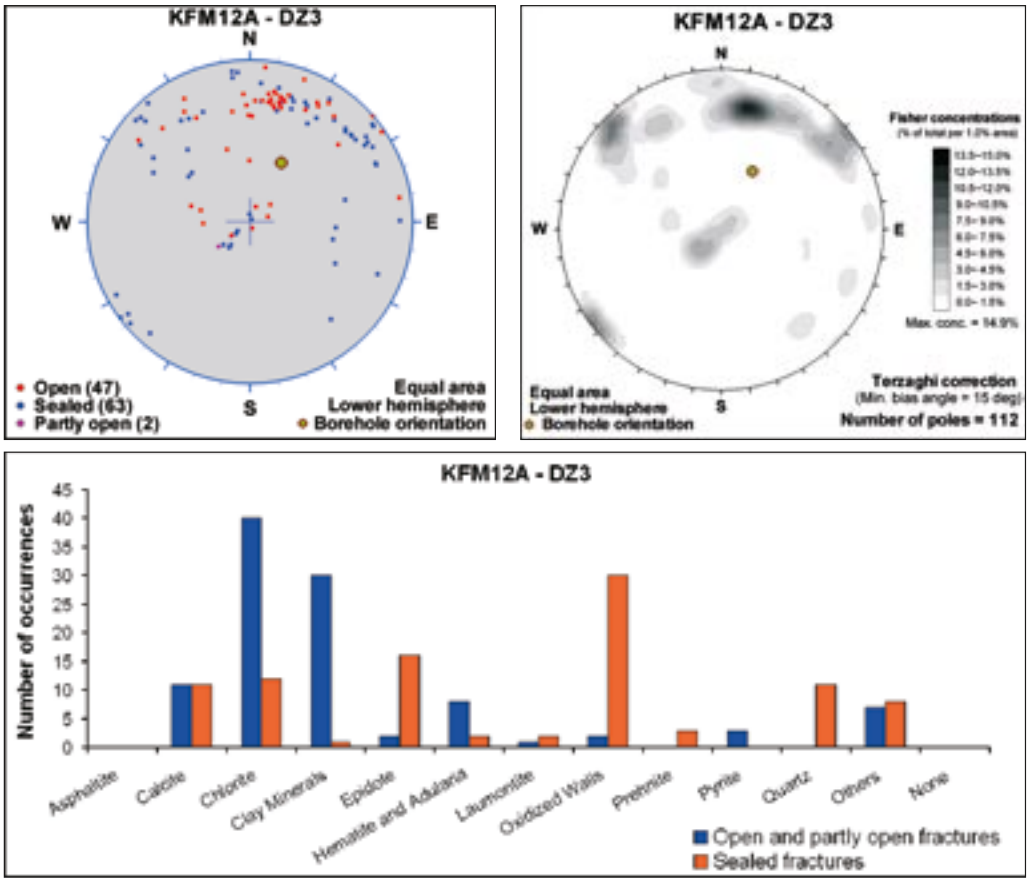

e)

Figure 6-4. *Mean poles to fracture sets and occurrence of different minerals as fillings and coatings along (a) DZ1, (b) section c. 170–285 m in DZ2, (c) section c. 285–338 m in DZ2, (d) section c. 338–402 m in DZ2 and (e) DZ3 in KFM12A.*

The fracture filling and coating minerals calcite and chlorite occur throughout the borehole intervals along all three possible deformation zones (DZ1–DZ3). Furthermore, the early generation mineral epidote is also present along the fractures in all three zones (Figure 6-4). Both laumontite and hematite/adularia, which belong to a younger generation of fracture minerals /Sandström et al. 2008a/, are prominent particularly along DZ2 (Figure 6-4b, c and d). Clay minerals are noticeable along open fractures in all three fracture zones. Furthermore, the late generation mineral asphaltite is a minor but conspicuous component along DZ2. This mineral is also present along fractures down to c. 400 m depth in this borehole, i.e. between DZ2 and DZ3. It is inferred that different parts of the zones have been subject to reactivation and fluid movement at different times during the brittle deformational history of the site.

The fracture orientation and fracture mineralogy of the three different segments of DZ1, DZ2 and DZ3, together with the confidence level assigned to these zones during the SHI work, are summarised in Table 6-3.

Table 6-3. Confidence level, fracture orientation and fracture mineralogy of the possible deformation zones recognised during the single-hole interpretation of borehole KFM12A. All borehole lengths are adjusted values. Data extracted from Sicada database: SICADA_07_395 (2007-10-26).

Possible deformation zone	Borehole length (m)		Confidence level	Fracture orientation (strike dip/)	Fracture mineralogy (excluding chlorite, calcite)
	Upper intersection	Lower intersection			
DZ1	125	158	High	1. NW-SE/steep dip 2. Moderate to gentle dip to the SE	Laumontite, adularia/hematite, quartz, prehnite, clay minerals, epidote
DZ2	170	402	High	1. NW-SE to WNW-ESE/steep dip 2. Moderate to gentle dip to the SE 3. In lower part, NE-SW or ENE-WSW/steep dip	Laumontite, adularia/hematite, quartz, clay minerals, epidote. Asphaltite is also present
DZ3	513	523	High	Sealed fractures: Variable orientation Open fractures: Steep dip to the south or gently dipping	Clay minerals, epidote, quartz, adularia/hematite

6.4 Prediction − outcome: A comparison

A comparison between the boundaries of rock domains and deformation zones along borehole KFM12A, as predicted from the deterministic modelling work during stage 2.2 /Stephens et al. 2007/, and the results of the single-hole interpretation of this borehole /Carlsten et al. 2007d/ are presented in Table 6-4 and Table 6-5, respectively. The results of a similar comparative study for the boundaries of deformation zones along the percussion boreholes HFM36 and HFM37 are presented in Table 6-6. A statement has been made beneath each geological object in these tables, which specifies the changes that need to be made to the corresponding deterministic model, so that the results from the single-hole interpretation of each borehole are taken into account. Attention in the text below is focused only on the results from cored borehole KFM12A and a visualisation of the prediction-outcome test for deformation zones is shown in Figure 6-5.

Table 6-4. Correlation between rock domains (RFM) modelled deterministically in model stage 2.2 /Stephens et al. 2007/ and rock units (RU) in the single-hole interpretation (SHI) of borehole KFM12A /Carlsten et al. 2007d/. The implications for the regional rock domain model, stage 2.2, are summarised in the text beneath the geological object. UI = Upper intercept, LI = Lower intercept. All borehole lengths are adjusted values.

RFM in local model stage 2.2	Confidence level for RFM in local model stage 2.2	Prediction, borehole length (m)		RU in SHI	Confidence level for RU in SHI	Outcome, borehole length (m)	
		UI	LI			UI	LI
RFM030	High at the surface, medium at depth	Above the start of the cored borehole length	Beneath the cored borehole length	RU1, RU2, RU3a, RU4a, RU3b, RU5, RU6, RU7, RU4b, RU8a, RU9a, RU8b, RU9b, RU10, RU11, RU9c, RU12	High	60.21 (top of cored borehole length)	600.95 (base of cored borehole length)
No rock domain boundary has been intersected along KFM12A. No changes are required.							

Table 6-5. Correlation between deformation zone ZFMWNW0004 (Forsmark zone) modelled deterministically in model stage 2.2 /Stephens et al. 2007/ and possible deformation zones (DZ) in the single-hole interpretation (SHI) of the borehole KFM12A /Carlsten et al. 2007d/. The implications for the regional deformation zone model, stage 2.2, are summarised in the text beneath the geological object. UI = Upper intercept, LI = Lower intercept. All borehole lengths are adjusted values.

ZFM in model stage 2.2	Confidence level for ZFM in model stage 2.2	Prediction, borehole length (m)		DZ in SHI	Confidence level for DZ in SHI	Outcome, borehole length (m)	
		UI	LI			UI	LI
ZFMWNW0004 (Forsmark DZ)	High	104	416	DZ1	High	125	158
ZFMWNW0004 (Forsmark DZ)	High	104	416	DZ2	High	170	402
No changes to the deformation zone model. Thickness along KFM12A is 140 m.							
				DZ3	High	513	523

Table 6-6. Correlation between deformation zones modelled deterministically in model stage 2.2 /Stephens et al. 2007/ and possible deformation zones (DZ) in the single-hole interpretation (SHI) of boreholes HFM36 and HFM37 /Carlsten et al. 2007d/. The implications for the regional deformation zone model, stage 2.2, are summarised in the text beneath the geological object. UI = Upper intercept, LI = Lower intercept. All borehole lengths are adjusted values.

Borehole	Confidence level for ZFM in model stage 2.2	ZFM in model stage 2.2	Prediction, borehole length (m)		DZ in SHI	Confidence level for DZ in SHI	Outcom, borehole length (m)	
			UI	LI			UI	LI
HFM36					DZ1	Medium	42	147
Possible correlation with linked lineament 95 in older lineament interpretation 1.2. The trace length of this lineament is less than 3,000 m. For this reason, there is no modification to the regional deformation zone model, stage 2.2. Since drill site 12 lies outside the local model area, no change is necessary in the local deformation zone model.								
HFM37	High	ZFMWNW0004 (Forsmark DZ)	Start of borehole length	Beneath borehole length	DZ1	Medium	15	23
					DZ2		72	104
					DZ3		130	191
The entire percussion borehole is drilled inside ZFMWNW0004. Need for minor changes in the regional deformation zone model stage 2.2. See comments for KFM12A.								

Based on the earlier discussion, the bedrock in borehole KFM12A, as recognised in the single-hole interpretation, can be assigned to rock domain RFM030. This is in agreement with the regional rock domain model for the site.

The fracture orientation, fracture mineralogy, alteration and style of deformation of the two possible deformation zones (DZ1 and DZ2) identified in the single-hole interpretation of the cored borehole KFM12A support the correlation of these two zones with the deformation zone ZFMWNW0004 (Forsmark deformation zone), as modelled deterministically in stage 2.2. The modelled Forsmark zone intersects DZ1 and DZ2 in KFM12A after only minor modification in thickness. The required change lies within the range of uncertainty provided in the property tables /Appendix 15 in Stephens et al. 2007/.

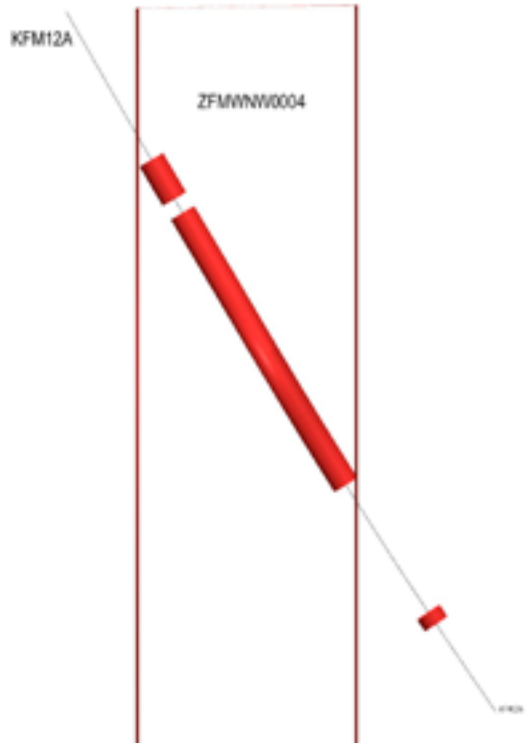

Figure 6-5. *Prediction-outcome visualisation for deformation zones along borehole KFM12A. Modelled deformation zone ZFMWNW0004 (Forsmark zone) stage 2.2 compared with the possible deformation zones in the single-hole interpretation, marked with red cylinder along the borehole. See text for further description. The length of the borehole KFM12A is c. 601 m.*

The evaluation of the data from the single-hole interpretation, in combination with the lineament model, supports the prediction that the Forsmark deformation zone is a complex structure with deformation under both ductile and brittle conditions. Furthermore, the fracture mineralogy indicates that brittle deformation occurred at several times during the long geological history at the site. As for the Singö deformation zone, these features are in good agreement with the evaluation of the WNW to NW set of steeply dipping deformation zones in the geological model /Stephens et al. 2007/.

The possible deformation zone DZ3 does not correlate with any modelled zone presently included in the regional model for the site. The status of this zone remains unclear. However, since it occurs along a short borehole interval, it is highly unlikely that it should be included in the regional model. For this reason, the regional deformation zone model is supported by the results from borehole KFM12A.

7 Assessment of the validity of the regional rock domain model based on the modelling of gravity and petrophysical data

7.1 Opening remarks

During the work with model stage 2.2, a study was carried out that aimed to assess the validity of the regional rock domain model at Forsmark based on modelling gravity and petrophysical data. This approach was considered viable since the modelling of rock domains at Forsmark had been developed without the use of gravity data. The results of this study were presented in /Isaksson and Stephens 2007/, following the release of the stage 2.2 geological models /Stephens et al. 2007/. A short summary of these results are presented in this chapter.

The regional rock domain model used in the interpretation work originates from the preliminary site description, model version 1.2 /SKB 2005/. The petrophysical data for each rock domain in that model were derived from /Isaksson et al. 2004, Mattsson et al. 2004, 2005, Lanaro 2005/. The three-dimensional model geometry in version 1.2 is very similar to that presented in model stage 2.2 /Stephens et al. 2007/. A two-dimensional slice at the ground surface that shows rock units identified on the basis of composition is shown in Figure 7-1. Consequently, the modelling of gravity and petrophysical data is also well suited as a test for the validity of the stage 2.2 regional rock domain model.

The validity of the regional rock domain model was assessed by comparing the calculated gravity model response, which takes account of the geological model, with a local gravity anomaly that represents the measured data (Figure 7-2). In particular, attention was focused on feasible discrepancies between these two components /Isaksson and Stephens 2007/. These are visualised as point information at each survey station (Figure 7-1). Due to model boundary conditions, the comparison was carried out in a smaller area within the regional model area.

The modelling work is strongly restricted by the paucity of quantitative data that bear on the volumetric proportions of subordinate rock types in each rock domain /SKB 2005, Stephens et al. 2007/. This problem has been addressed to some extent by the development of alternative models that do not solely take account of the average density of the dominant rock type for each rock domain. Gravity model responses were calculated in three stages; an initial model, a base model and a refined base model. The refined base model was preferred and used for comparison purposes /Isaksson and Stephens 2007/.

7.2 Implications for the regional rock domain model

In general, there is a good agreement between the refined base model that makes use of the version 1.2 regional rock domain model and the measured gravity data (Figure 7-1 and Figure 7-2), not least where it concerns the depth extension of the critical rock domain RFM029. The most significant discrepancy occurs in the area extending from the SFR office to the SFR underground facility and further to the north-west.

It is speculated that the discrepancy close to SFR is caused by a combination of an overestimation of the volume of gabbro in rock domain RFM016, that plunges towards the south-east in the rock domain model, and an underestimation of the volume of occurrence of pegmatite and pegmatitic granite that are known to be present and occur as larger bodies around SFR, especially within rock domain RFM021. Other discrepancies are noted in rock domain RFM022, which is considered to be volumetrically overestimated in the geological model, and in rock domain RFM017, where the gravity model response shows a somewhat different extension of the gravity anomaly (Z-shape) than that indicated by the original data. A small mass deficiency

is also apparent in RFM017, indicating that the rock domain is slightly underestimated in density and/or volume compared with that in rock domain RFM029. In the south-eastern part of rock domain RFM023, the occurrence of less dense, subordinate granitic rocks has probably not been sufficiently accounted for. However, all these rock domains are situated more or less completely outside the local model volume (Figure 7-1) and the discrepancies outlined here have no implications for the rock domain model inside this volume.

A strong gravity anomaly (5–7 mgal) that is situated c. 3 km north-west of the Forsmark nuclear power plant merits special attention, even though it is located outside the regional model area (square 1625000–1630000, 6700000–6705000 on Figure 7-2) and does not affect directly the geological model inside the local model volume. A continuation of rock domain RFM025, which contains abundant metadiorite and metagabbro, towards the north-west, and the inclusion of rocks with a higher density, corresponding to rocks with more mafic or even ultramafic composition, may explain this gravity high. However, the shape and wavelength of this anomaly, and the fact that iron oxide mineralisation is known in the area, permit an alternative interpretation that the anomaly is associated with a metallic but non-magnetic ore body.

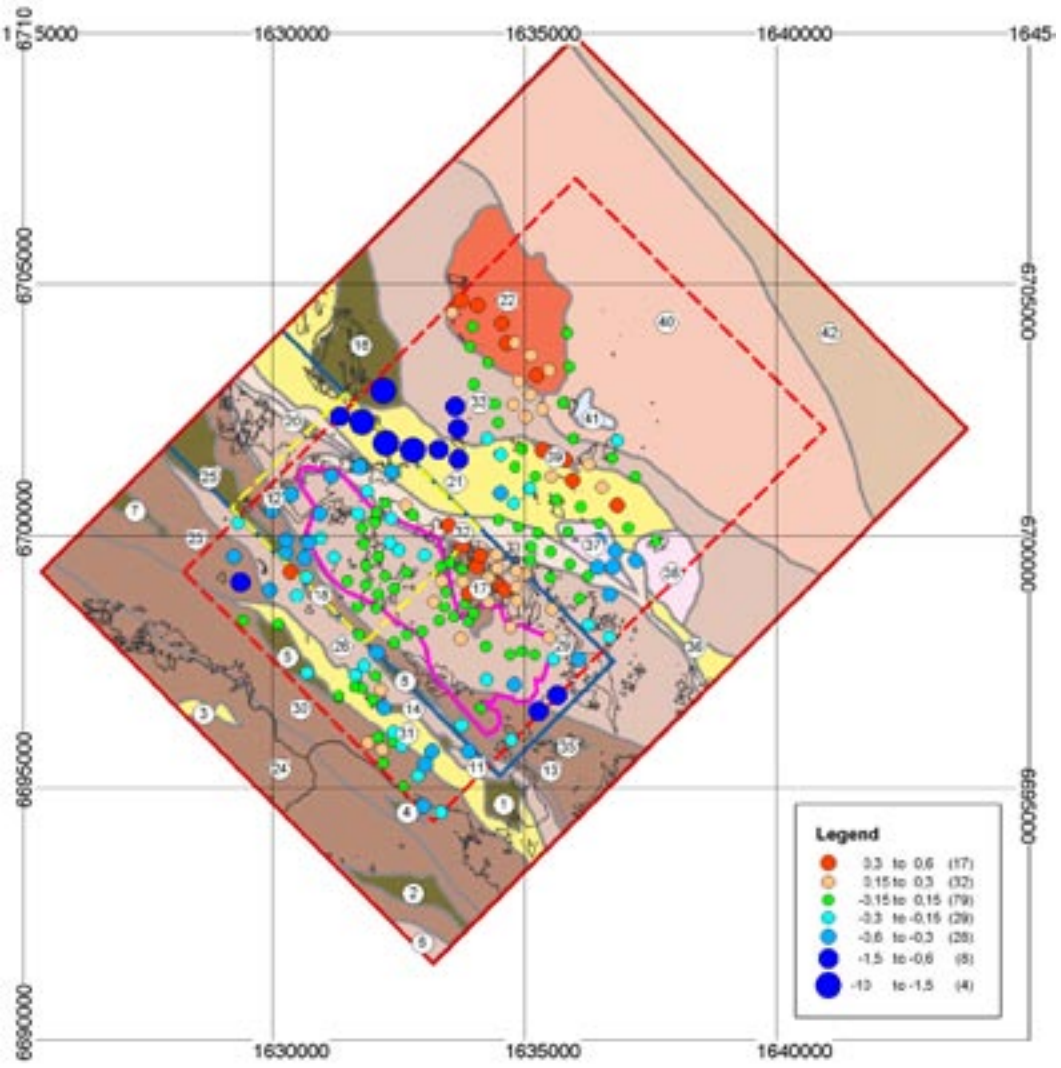

Figure 7-1. *Refined base model for modelling the gravity response from rock domains, version 1.2, inside the regional model area (solid red line). Rock domains are numbered; ⑧=RFM008, etc. Responses are only shown within the boundary buffer area (dashed red line). The residual between the input gravity anomaly and the model anomaly [mgal] is calculated for each survey station; blue colours indicate a mass surplus in the regional rock domain model and red colours indicate a mass deficiency in this model. The candidate area is shown with a solid magenta line. The local model areas in version 1.2 and stage 2.2 are shown with a solid blue line and a dashed yellow line, respectively.*

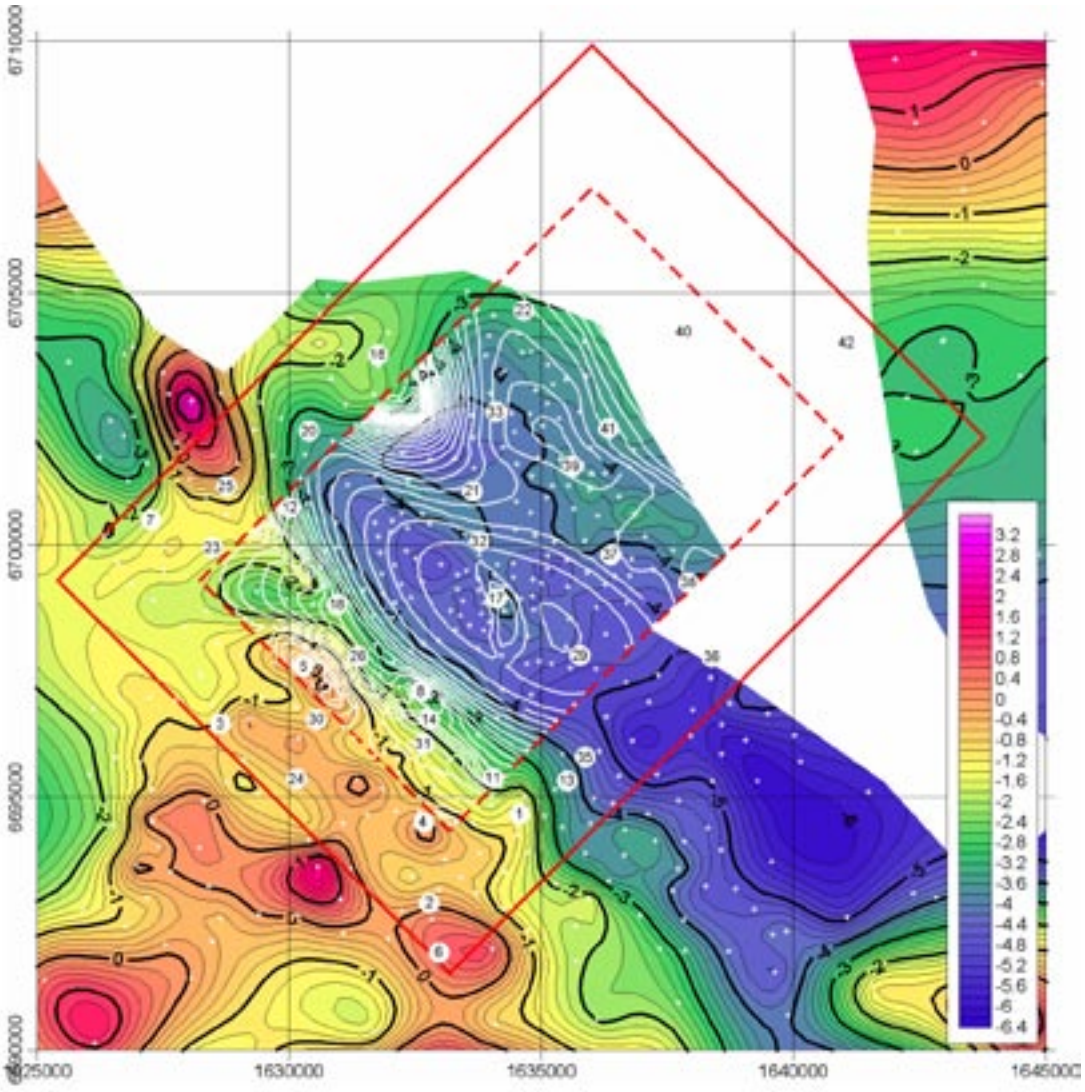

Figure 7-2. *Refined base model for the gravity response from rock domains, model version 1.2, inside the regional model area (solid red line). Rock domains are numbered; ⑧=RFM008, etc. Responses shown are valid within the boundary buffer area (dashed red line). For purposes of comparison, the response from the geological model [mgal] is shown as white contours that are inserted on the local gravity anomaly inferred from the measured gravity data; red indicates gravity high and blue gravity low.*

8 Character and kinematics of deformation zones − complementary data

Data bearing on the character and kinematics of the possible deformation zones that were identified with high confidence in the single-hole interpretations have been acquired in three separate phases /Nordgulen and Saintot 2006, 2008, Saintot and Nordgulen 2007/. This work has included the identification and description of fault core intervals and an assessment of the kinematics along each zone. Bearing in mind the focused nature of the drilling activity, most of these data come from intersections of zones along boreholes that are present inside the targeted, north-western part of the tectonic lens at Forsmark. It is important to keep in mind that the analysis in this report addresses solely deformation in the brittle regime. This point is particularly relevant for the structures that are steep and strike WNW-ESE to NW-SE.

Data acquired during phase 1 come from fourty-one (41) possible deformation zones in twelve (12) boreholes /Nordgulen and Saintot 2006/. These data were available during model stage 2.2 and were compiled, evaluated and utilised in the modelling work at this stage /Stephens et al. 2007, sections 3.7 and 5.2/. The phase 2 and phase 3 data /Saintot and Nordgulen 2007, Nordgulen and Saintot 2008/, acquired during model stage 2.3, come from fourty-eight (48) possible deformation zones, which have been identified with high confidence in the single-hole interpretation of an additional thirteen (13) cored boreholes (KFM02B, KFM01C, KFM01D, KFM06C, KFM07B, KFM07C, KFM08C, KFM08D, KFM09A, KFM09B, KFM10A, KFM11A and KFM12A). Together with the phase 1 data, these data are compiled and evaluated for the first time here (see Table A-4, Table A-5 and Table A-6 in the appendix). An assessment of the consequences for the stage 2.2 modelling work of the increased data quantity during stage 2.3 is also addressed in the text below.

The data evaluation carried out here builds on the results and interpretations presented in /Nordgulen and Saintot 2006, 2008, Saintot and Nordgulen 2007/ as well as extractions from the Sicada database completed in two deliveries (Sicada_07_186 and Sicada_08_143).

8.1 Occurrence and character of fault core

Fault core sections have been identified along 55% of all the possible deformation zones studied in the boreholes (Table A-4 in the appendix). These sections are narrow features, generally up to a few metres in borehole length (apparent thickness). The remaining part of each possible deformation zone as well as the possible deformation zones where no fault core has been recognised are classified as transitional in character (the reader is referred to section 5.2.1 in /Stephens et al. 2007/ for a terminological discussion). The overall frequency of sections with fault core along possible deformation zones has reduced somewhat compared with that estimated from the more limited data set during model stage 2.2 (55% compared with 75%). It is difficult to assess whether this is simply an affect of the character of the zones that have been studied or whether different judgements have been made through time in connection with the inspection of the boreholes. Suffice it to say that the same team of geologists have been used throughout the data assembly.

The character of the fault core in all the eighty-nine (89) possible deformation zones that have been investigated in the boreholes is documented in Table A-4 in the appendix. The fault core sections consist of an anomalously high frequency of fractures, especially sealed fractures commonly in the form of complex networks, and the occurrence of cohesive breccia and cataclasite (Figure 8-1). Rock alteration (oxidation) is also conspicuous (Figure 8-1). Although incohesive crush rock is locally present (see Figure 8-1a), fault gouge has not been documented along any of the possible zones.

These observations bearing on the character of the fault core from all the data are very similar to those made on the basis of the first data batch that was used during stage 2.2. The apparent absence of fault gouge along the zones at Forsmark and the possibility that this feature is related to loss of drill core during drilling was discussed in /Stephens et al. 2007, section 3.7/. It was concluded that the absence of fault gouge cannot simply be explained by removal during drilling.

a

b

Figure 8-1. *Character of fault core in the regionally important Singö and Forsmark deformation zones. a) Incohesive crush rock, laumontite-sealed cataclasites and networks, and wall-rock alteration defined by dissemination of hematite and red staining, along part of a fault core interval in the central part of the Singö deformation zone (ZFMWNW0001) in borehole KFM11A (borehole interval c. 597 to 608 m). b). Cataclasite and fault breccia cut by younger fractures and networks sealed with quartz, calcite and other fracture minerals, along part of a pronounced fault core interval in the central part of the Forsmark deformation zone (ZFMWNW0004) in borehole KFM12A (borehole interval c. 315 to 326 m)*

8.2 Kinematics

8.2.1 Data quality and compilation

A synthesis of the kinematic data from all zone intersections in the cored boreholes (DZ) is presented in two tabular compilations in the appendix (Table A-5 and Table A-6). The evaluation of data presented below is founded on these two compilations.

As observed on the basis of the first data batch /Stephens et al. 2007/, the quality of the kinematic determinations varies considerably and is not always sufficient to constrain, in more detail, the strike-slip (dextral or sinistral) or dip-slip (normal or reverse) sense of movement. Furthermore, direct observational data that show the possible geometric relationship between shear fractures (minor faults) with different orientations (e.g. conjugate sets, Riedel shears) or between shear fractures and marker units are more or less absent. In this respect, borehole data are of considerably less help to determine the kinematics along deformation zones compared with data from outcrops.

The borehole data are grouped in Table A-5 on the basis of their occurrence in the different sets and sub-sets of deterministically modelled deformation zones (ZFM) /Stephens et al. 2007, section 5.2.2/. Even the fourteen (14) possible deformation zones that have not been modelled deterministically (PDZ) are included in this table. Data identification is presented in columns 1, 2 and 3. Since many zones contain different sets of minor faults with different orientations /see Stephens et al. 2007/, along which kinematic data have been acquired, the sense of movement is provided for each fracture orientation set within a zone. For this reason, the fracture set is specified in column 4 in Table A-5, the mineral (or minerals) present along the shear striae or steps in column 5, the inferred sense of movement in column 6 and, finally, the number of fractures with kinematic data in column 7.

In order to provide a more quantitative evaluation, the data from all zone intersections in the cored boreholes are presented in an alternative synthesis in Table A-6 in the appendix. The data are grouped in this table firstly on a fracture orientation and secondly on a deterministically modelled deformation zone basis. A quantitative compilation of the kinematics of each intersection in the cored boreholes for each fracture orientation set (strike-slip, dip-slip or oblique-slip; dextral or sinistral, reverse or normal) completes the compilation in Table A-6.

A characteristic feature of the data is that the minerals chlorite, calcite and hematite commonly define the kinematic indicators (Figure 8-2). Since these minerals are not restricted to a single fracture mineral generation (see, for example, /Sandström et al. 2008a/), the kinematic data are not easily related to a particular mineral phase and, as a consequence, to the possible timing of formation. This observation precludes division of the kinematics data according to timing of movement and, thereafter, a study of the possible geometric relationships between the kinematics of shear fractures with different orientations on, for example, a stereographic projection. Bearing in mind this consideration, no such analysis has been attempted. Instead, some general comments on the kinematics of each orientation set of shear fractures are presented below on the basis of the compilation in Table A-6.

8.2.2 Occurrence of shear fractures

Virtually all the possible deformation zones (85% of 89 possible zones) contain one or more broken fractures, along which kinematic data are present. Thus, evidence for shear displacement along minor faults within the zones is apparent. It needs to be kept in mind that since unbroken and sealed fractures are very common along these structures, the identification of kinematic data along the boreholes is strongly restricted by the character of the fractures along the zones. However, the proportion of deterministically modelled, gently dipping zones that completely lack fault-slip data is higher (30% of 29 deterministically modelled, gently dipping zones) relative to that in all the other zone sets and sub-sets. At least some of the broken fractures along these zones are joints. These observations confirm those presented in /Stephens et al. 2007, section 3.7/ that were based on a more limited data set.

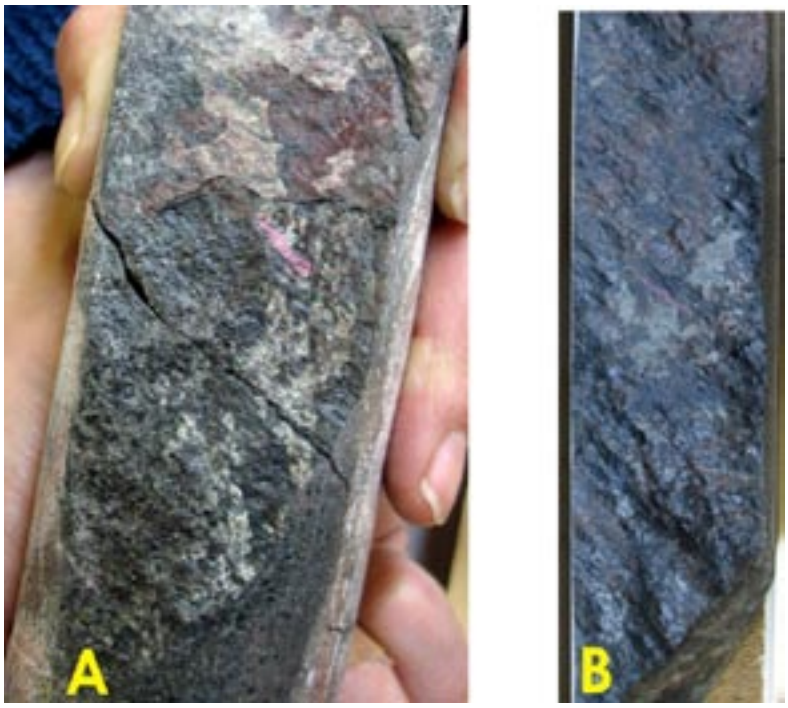

Figure 8-2. *Examples of shear fractures that represent minor fault planes and kinematic indicators along these planes in DZ1 along KFM09B. a) Sinistral calcite steps and shear striae on hematite (strike/dip/pitch of striae is 350/80/15. Borehole length = 20.035 m). b) Dextral shear striae on chlorite, hematite and clay mineral (strike/dip/pitch of striae is 338/85/-5. Borehole length = 65.043 m). After /Saintot and Nordgulen 2007/.*

8.2.3 Steeply dipping shear fractures with WNW-ESE to NW-SE strike

Kinematic data from steeply dipping shear fractures with WNW-ENE to NW-SE strike have been documented along 26 different zone intersections in the cored boreholes. These intersections include all the deterministically modelled sets and sub-sets of deformation zones. Fractures from three zone intersections that were neither modelled deterministically in stage 2.2 nor have been correlated with a modelled zone in the present report are also included in this group. A conspicuous number of shear fractures were observed along the Singö and Forsmark deformation zones (ZFMWNW0001 and ZFMWNW0004, respectively) as well as along zone ZFMWNW0123. These structures lie outside (Singö and Forsmark) or along the south-western margin (ZFMWNW0123) of the target volume.

The data indicate a strong component of strike-slip displacement along the shear fractures. Even where the sense of movement is more oblique, the strike-slip component is once again more conspicuous. Both sinistral and dextral strike-slip displacement have occurred with a clear bias in the data towards sinistral strike-slip movement. This feature differs from the dextral sense of shear observed along ductile structures with the same orientation /Stephens et al. 2007/. Although subordinate in character, both reverse and normal dip-slip movement has taken place along this group of shear fractures. Different senses of movement are present along the same deformation zone (see, for example, the Singö and Forsmark deformation zones). It is apparent that at least these zones were reactivated at different times during the long geological evolution in the area /Söderbäck (ed.) 2008/ under contrasting stress regimes /Nordgulen and Saintot 2008/.

The observations above are consistent with those reported for the Eckarfjärden deformation zone (ZFMNW0003) and for the sub-parallel zone ZFMNW1200 on the basis of outcrop data /Nordgulen and Saintot 2006, section 3.7 in Stephens et al. 2007/. The kinematic data from the Eckarfjärden zone indicate a complex evolution with the influence of approximately NW-SE

and N-S compressive phases and a younger, approximately NE-SW compressive phase, all of which occurred while epidote formed along the fractures in the zone. A shortening phase in an approximately WNW-ENE direction is also indicated from the data along zone ZFMNW1200, to explain the significant sinistral strike-slip brittle deformation along this zone.

8.2.4 Steeply dipping shear fractures with NNW-ESE strike

Kinematic data from steeply dipping shear fractures with NNW-SSE strike have been documented along 27 different zone intersections. These intersections once again include all the deterministically modelled sets and sub-sets of deformation zones, particularly the sub-set of zones referred to as steep ENE(NE) /Stephens et al. 2007, section 5.2.2/. Fractures from one zone intersection, which was neither modelled deterministically in stage 2.2 nor has been correlated with a modelled zone in the present report are also included in this group. A conspicuous number of shear fractures were observed along zone ZFMNNW0100 that intersects boreholes KFM07A and KFM09A outside the target volume.

The data indicate a very strong component of strike-slip deformation along the shear fractures. Sinistral strike-slip displacement dominates strongly over dextral strike-slip. This is consistent with an approximately NW-SE compression. Although subordinate in character, both normal and reverse dip-slip movements have taken place along this group of shear fractures. These observations are similar to those documented earlier for this group of shear fractures /Stephens et al. 2007, section 3.7/.

8.2.5 Steeply dipping shear fractures with ENE-WSW to NNE-SSW strike

In Table A-6, the steeply dipping shear fractures that strike ENE-WSW and NE-SW are separated from those with a more NNE-SSW strike. All these fractures are treated together in the text below.

Kinematic data from the steeply dipping shear fractures that strike between ENE-WSW and NNE-SSW have been documented along 62 different zone intersections. As for the other fracture orientation groups, these intersections include all the deterministically modelled sets and sub-sets of deformation zones. However, most of these intersections have been modelled in the zone sub-sets referred to as steep ENE(NE) and steep NNE /Stephens et al. 2007/. The common occurrence of borehole intersections that contain fractures with this orientation is consistent with the importance of zones with this orientation in especially the target volume. Fractures from 12 zone intersections that were neither modelled deterministically in stage 2.2 nor correlated with a modelled zone in the present report are also included in the group of 62 intersections. Apart from a zone (ZFMNE1188) that is present outside and to the south-west of the target volume, there is an absence of zone intersections with a high number of shear fractures in this group. It is suggested that this reflects the character of the steep ENE (NE) and NNE zones inside the target volume, i.e. local in size and with a high frequency of sealed fractures which are not suitable for kinematic study.

As for the other fracture orientation groups discussed above, the data indicate a very strong component of strike-slip displacement. Both sinistral and dextral strike-slip displacement has occurred along the steeply dipping ENE-WSW and NE-SW fractures, consistent with bulk shortening between N-S and NE-SW, and approximately WNW-ESE, respectively. By contrast, sinistral displacement is more dominant along the steeply dipping NNE-SSW shear fractures. This kinematics may be explained by NW-SE to N-S compression. The subordinate dip-slip or oblique-slip movement with a strong dip-slip component is more frequently normal in character along the steeply dipping ENE-WSW and NE-SW fractures and solely reverse in character along the steeply dipping NNE-SSW fractures. All these observations are strongly reminiscent of those that were recognised on the basis of the phase 1 data /Stephens et al. 2007, section 3.7/.

8.2.6 Gently dipping shear fractures

Kinematic data from gently dipping shear fractures have been documented along 39 different zone intersections. As for the other fracture orientation groups, these intersections correspond to all the deterministically modelled sets and sub-sets of deformation zones, particularly the gently dipping zones and the steep ENE(NE) sub-set that are common inside the candidate volume /Stephens et al. 2007/. Fractures from only two zone intersections that were neither modelled deterministically in stage 2.2 nor correlated with a modelled zone in the present report are also included in this group of fractures. Zones ZFMA2, ZFMA3 and ZFMF1 are conspicuous since they contain an increased number of shear fractures relative to all the other zones.

In contrast to the other fracture orientation groups discussed above, the data indicate a strong component of reverse dip-slip displacement along the gently dipping fractures. Even where the sense of movement is more oblique dip-slip, reverse displacement is dominant. Shear fractures with strike-slip displacement or with oblique-slip displacement that includes a prominent strike-slip component are present but are subordinate. Different senses of strike-slip movement have been observed. The kinematic data are consistent with the influence of one or more phases of compressional tectonics in the area /Juhlin and Stephens 2006/. These observations are identical to those documented earlier for this group of shear fractures /Stephens et al. 2007, section 3.7/.

8.2.7 Concluding statement

It is apparent that the additional kinematic data obtained during stage 2.3 /Saintot and Nordgulen 2007, Nordgulen and Saintot 2008/ are consistent with the data from phase 1 /Nordgulen and Saintot 2006/. For this reason, it is concluded that the stage 2.3 data strengthen the conclusions drawn earlier that bear on the conceptual understanding of deformation zones in the brittle regime at the Forsmark site /Stephens et al. 2007, sections 3.7 and 5.2/.

9 Mineral coating and mineral filling along fractures in cored boreholes − complementary data

The identification of mineral coatings and fillings in fractures is a standard procedure adopted during the mapping of cored boreholes. A more detailed study of the fracture mineralogy along such boreholes, which has involved the identification of different families of minerals with an inferred similar age, i.e. mineral paragenesis, the establishment of the relative age relationship between the different mineral paragenesis and even the absolute ages of the fracture mineral adularia, has been carried out during the site investigation programme. The geological implications of the data available at data freeze 2.2 were evaluated in /Stephens et al. 2007, section 3.6.5/. Complementary data for boreholes KFM01C, KFM01D, KFM02B, KFM08C, KFM08D, KFM09A, KFM09B, KFM10A and KFM11A were acquired in connection with data freeze 2.3 /Sandström et al. 2008b/.

All data on fracture minerals at the Forsmark site, including the stage 2.3 data, have been evaluated in an overview report /Sandström et al. 2008a/. Furthermore, the specific implications of these data for the geological understanding of the site have been addressed in /Söderbäck (ed.) 2008/. Since the complementary data in /Sandström et al. 2008b/ are consistent with the conclusions drawn earlier concerning the fracture mineralogy at the site, no further evaluation of these data is carried out here and the reader is referred to /Sandström et al. 2008a, Söderbäck (ed.) 2008/ for more detailed discussions.

10 Fracture orientation data − revision and consequences for the deterministic geological models

The orientation of geological features at depth, including fractures, rock contacts and ductile structures, are estimated with the help of the Boremap methodology adopted by SKB. The input data used to calculate the orientation of a geological feature include deviation measurements of the boreholes, oriented images of the borehole walls obtained by the Borehole Image Processing System (BIPS) and the borehole diameter.

Between autumn 2006 and autumn 2007, SKB carried out a critical review of the methodology of the Boremap system, in order to identify potential errors and to quantify uncertainties in the orientation of geological entities in boreholes /Munier and Stigsson 2007/. An important consequence of this critical review has been that all orientation data for geological structures in the cored boreholes, which were available at the data freeze 2.2, were recalculated and provided with numerical estimates of uncertainty. Data corrected up to mid-May 2007 were used in the stage 2.2 geological modelling work. Unfortunately, further revision of orientation data occurred later during 2007, after the delivery of model stage 2.2. For this reason, it was judged necessary to assess here the implications of this late revision for the stage 2.2 modelling work.

As pointed out in /Stephens et al. 2007/, the deterministic modelling work in geology has only used the orientation of geological structures in boreholes (e.g. fractures) as a support in the correlation of a large-scale geological or geophysical feature (e.g. a low magnetic lineament at the ground surface) with a fixed point intersection in a borehole (e.g. a possible deformation zone). For example, the mean pole and the Fisher κ concentration parameter were calculated for all the fractures in a particular fracture set along a deformation zone and compared with the modelled orientation of the zone. The latter was derived by linking a geophysical anomaly with the fixed point intersection in the borehole. It is important to emphasise that the modelled orientation of a deformation zone or the boundary between two rock domains is calculated independently of the orientation of the geological structures in boreholes and, for this reason, these data are supportive rather than deterministic in character. However, they are of more significance in the establishment of the properties of geological features. The orientation model in the discrete fracture network (DFN) work /Fox et al. 2007/ also involved the identification and parameterization of fracture orientation sets, without direct focus on the orientation of specific fractures.

In order to assess the implications of the late revision of borehole orientation data for the properties of geological features in the stage 2.2 model, a revised parameterization of fracture sets in five deformation zones has been carried out. These zones were chosen since they either form the boundary to or are present within the target volume at Forsmark, and are all included in the regional deformation zone model. They include two steeply dipping zones that have a trace length at the ground surface that is longer than 3,000 m (ZFMWNW0123, ZFMENE0060A) and three gently dipping zones (ZFMA2, ZFMA8 and ZFMF1). Revised orientation data were extracted from the Sicada database in the delivery labelled Sicada_07_395 (2007-10-26). The methodology used to parameterize each fracture set was identical to that used in /Appendix 15 in Stephens et al. 2007/.

The revised parameters for each fracture set in each zone are compared in Table 10-1 with the equivalent parameters included in the stage 2.2 property tables /Appendix15 in Stephens et al. 2007/. Inspection of this table reveals that the data revision that was carried out after the completion of the geological models during stage 2.2 has had only very minor affects on the orientation parameters for at least the fractures in these five zones. The visualization for zone ZFMENE0060A (Figure 10-1) further emphasizes the insignificance of the data revision after model stage 2.2, at least for this zone.

Table 10-1. Comparison of the mean pole trend and plunge and Fisher κ value for the fracture sets in deformation zones ZFMWNW0123, ZFMENE0060A, ZFMA2, ZFMA8 and ZFMF1 on the basis of two different orientation data sets. The parameters calculated from the revised fracture orientation data in delivery Sicada_07_395 on 2007-10-26 (values without brackets) are compared with the equivalent parameters in the published property tables extracted from /Appendix 15 in Stephens et al. 2007/ (values inside brackets). Set G = Gently dipping set. Set NNE = Steeply dipping set with strike between 005 and 035. Set NE = Steeply dipping set with strike between 035 and 055. Set SW = Steeply dipping set with strike between 215 and 235. Set SE = Steeply dipping set with strike between 125 and 145.

ZFM	Fracture group	Data count	Trend	Plunge	Fisher κ
ZFMA2	Set G	414 (414)	270.4 (282.4)	80.7 (77.6)	7.3 (6.3)
	Unassigned fractures	398 (398)			
ZFMA8	Set G	183 (182)	334.0 (331.9)	72.3 (72.4)	9.1 (8.2)
	Set NNE	93 (93)	304.0 (304.2)	12.6 (12.8)	52.5 (58.8)
	Unassigned fractures	51 (52)			
ZFMENE0060A	Set G	149 (138)	340.8 (342.3)	78.3 (78.1)	13.8 (13.6)
	Set SW	312 (315)	130.7 (132.5)	5.4 (4.9)	11.4 (10.8)
	Unassigned fractures	128 (136)			
ZFMF1	Set G	189 (185)	297.5 (317.8)	53.4 (53.7)	9.2 (9.3)
	Unassigned fractures	75 (79)			
ZFMWNW0123	Set G	223 (231)	246.8 (252.5)	78.6 (80.2)	8.8 (8.0)
	Set NE	111 (107)	311.7 (311.6)	6.4 (5.2)	24.5 (26.9)
	Set SE	274 (268)	44.6 (45.1)	12.5 (12.3)	21.8 (22.5)
	Unassigned fractures	201 (201)			

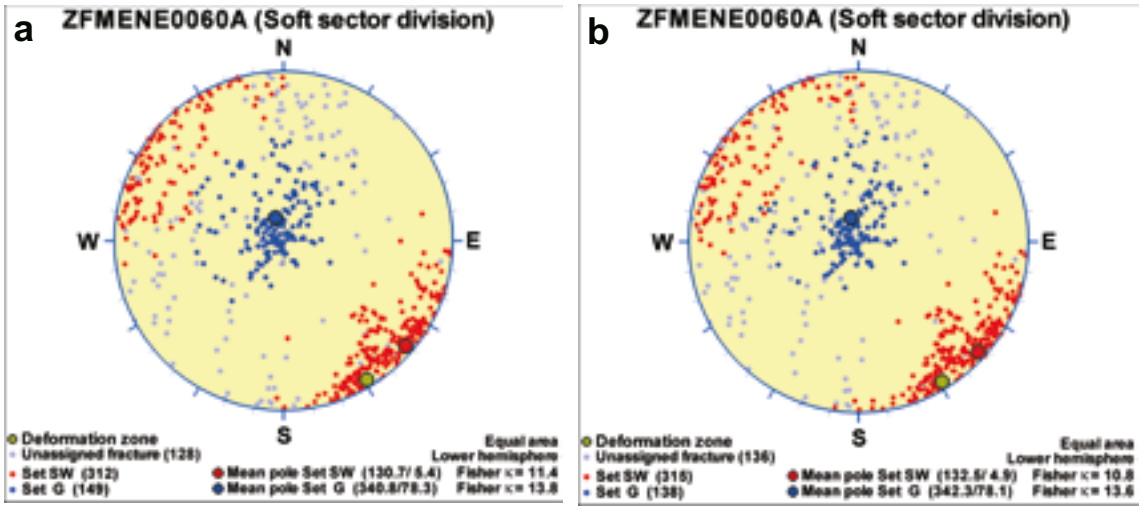

Figure 10-1. *Equal-area stereoplot visualization of the two fracture sets in zone ZFMENE0060A. The fracture clusters identified on the basis of the orientation data revised after model stage 2.2 are shown in (a) and the fracture clusters identified during model stage 2.2 and published in the property table for this zone in /Appendix 15 in Stephens et al. 2007/ are shown in (b). The identical soft sectoring technique (see /Appendix 15 in Stephens et al. 2007/) was used to identify fracture clusters in both sets of data.*

11 Validity of the deterministic geological models − concluding remarks

A large proportion of the complementary stage 2.3 geological and geophysical data provides information on the bedrock outside the target volume. The additional ground magnetic data (chapter 2) and the data from the boreholes KFM02B, KFM11A, KFM12A and HFM33 to HFM37 (chapters 3, 5 and 6) can be included in this group. Other data simply complement older information of identical character, both inside and outside the target volume. These include the character and kinematics of deformation zones (chapter 8) and fracture mineralogy (chapter 9).

In general terms, it can be stated that all the new data identified above either confirm the geological modelling work completed during stage 2.2 /Stephens et al. 2007/ or are in good agreement with the data that were used in this work. For example, although the additional ground magnetic data modify slightly the position and trace length of some stage 2.2 deformation zones at the ground surface, no new or modified deformation zones with a trace length longer than 3,000 m at the ground surface have emerged. Thus, the prediction made in model stage 2.2 regarding this point has been confirmed. The abundant new kinematic data strengthen the conceptual understanding of the brittle deformation at the site (see Stephens et al. 2007, section 5.2), while borehole data from KFM11A and KFM12A confirm the regional significance of the Singö and Forsmark deformation zones, respectively. It is also apparent that the revision of fracture orientation data (chapter 10), which was carried out after the completion of the geological models during stage 2.2, has had little affect on the orientation parameters for the fractures along some important deformation zones that intersect the local model volume.

By contrast, borehole KFM08D is situated inside the target volume and intersects the bedrock a considerable distance from other boreholes. For this reason, the new data from this borehole (chapter 4) provide the means to carry out a stringent test of the validity of the stage 2.2 deterministic geological models for rock domains, fracture domains and deformation zones inside the target volume. The predictions provided by local model stage 2.2 /Stephens et al. 2007/ for the position and character of the intersections of these geological entities along borehole KFM08D have been verified highly satisfactorily by the outcome of the single-hole interpretation of this borehole during model stage 2.3 /Carlsten et al. 2007b/. In addition, the gravity modelling work (chapter 7 and /Isaksson and Stephens 2007/) provides a good support to the regional rock domain model for the site, at least where it concerns the critical rock domain RFM029.

In summary, it can be stated that all these observations provide a basis for confidence in the deterministic geological models, notwithstanding the intrinsic methodological weaknesses in the modelling work (see sections 4.1.1 and 5.1.1 in /Stephens et al. 2007/). It is suggested that the successful predictability of the occurrence and character of deformation zones is related to the significant bedrock anisotropy that was established over 1,850 million years ago, when the bedrock was situated at mid-crustal depths and was affected by penetrative, ductile deformation under high-temperature metamorphic conditions. However, if Forsmark is selected as a site for the deep geological repository, then it will be necessary to complete minor modifications to the deterministic geological models prior to construction work using the data acquired during model stage 2.3.

12 References

Axelsson C-L, Hansen L, 1997. Update of structural models at SFR nuclear waste repository, Forsmark, Sweden. SKB R-98-05, Svensk Kärnbränslehantering AB.

Bergman T, Isaksson H, Johansson R, Lindèn A H, Lindroos H, Rudmark L, Stephens M, 1999. Förstudie Tierp. Jordarter, bergarter och deformationszoner. SKB R-99-53, Svensk Kärnbränslehantering AB.

Carlsson A, Olsson T, Stille H, 1985. Submarine tunnelling in poor rock. Tunnels and Tunnelling, Vol.17, No. 12. London.

Carlsson A, Christiansson R, 1987. Geology and tectonics at Forsmark, Sweden. SKB SFR-87-04, Svensk Kärnbränslehantering AB.

Carlsten S, Döse C, Samuelsson E, Gustafsson J, Petersson J, Stephens M B, Thunehed H, 2007a. Forsmark site investigation. Geological single-hole interpretation of KFM02B. SKB P-07-107, Svensk Kärnbränslehantering AB.

Carlsten S, Gustafsson J, Samuelsson E, Stephens M B, Thunehed H, 2007b. Forsmark site investigation. Geological single-hole interpretation of KFM08D. SKB P-07-108, Svensk Kärnbränslehantering AB.

Carlsten S, Döse C, Samuelsson E, Gustafsson J, Petersson J, Stephens M B, Thunehed H, 2007c. Forsmark site investigation. Geological single-hole interpretation of KFM11A, HFM33, HFM34 and HFM35. SKB P-07-109, Svensk Kärnbränslehantering AB.

Carlsten S, Gustafsson J, Petersson J, Samuelsson E, Stephens M B, Thunehed H, 2007d. Forsmark site investigation. Geological single-hole interpretation of KFM12A, HFM36 and HFM37. SKB P-07-110, Svensk Kärnbränslehantering AB.

Follin S, Levén J, Hartley L, Jackson P, Joyce S, Roberts D, Swift B, 2007. Hydrogeological characterisation and modelling of deformation zones and fracture domains, Forsmark modelling stage 2.2. SKB R-07-48, Svensk Kärnbränslehantering AB

Fox A, La Pointe P, Hermanson J, Öhman J, 2007. Statistical geological discrete fracture network model. Forsmark modelling stage 2.2. SKB R-07-46, Svensk Kärnbränslehantering AB.

Glamheden R, Hansen L M, Fredriksson A, Bergkvist L, Markström I, Elfström M, 2007. Mechanical modelling of the Singö deformation zone, Site descriptive modelling Forsmark stage 2.1. SKB R-07-06, Svensk Kärnbränslehantering AB.

Holmén J, Stigsson M, 2001. Modelling of future hydrogeological conditions at SFR. SKB R-01-02, Svensk Kärnbränslehantering AB.

Isaksson H, Mattsson H, Thunehed H, Keisu M, 2004. Forsmark site investigation. Petrophysical surface data. Stage 2 – 2003 (including 2002). SKB P-04-155, Svensk Kärnbränslehantering AB.

Isaksson H, Pitkänen T, Thunehed H, 2006a. Forsmark site investigation. Ground magnetic survey and lineament interpretation in an area northwest of Bolundsfjärden. Forsmark site investigation. SKB P-06-85, Svensk Kärnbränslehantering AB.

Isaksson H, Thunehed H, Pitkänen T, Keisu M, 2006b. Forsmark site investigation. Detailed ground and marine magnetic survey and lineament interpretation in the Forsmark area – 2006. SKB P-06-261, Svensk Kärnbränslehantering AB.

Isaksson H, Stephens M B, 2007. Forsmark site investigation. Assessment of the validity of the rock domain model, version 1.2, based on the modelling of gravity and petrophysical data. SKB R-07-217, Svensk Kärnbränslehantering AB.

Isaksson H, Thunehed H, Pitkänen T, Keisu M, 2007. Forsmark site investigation. Detailed ground magnetic survey and lineament interpretation in the Forsmark area, 2006-2007. SKB R-07-62, Svensk Kärnbränslehantering AB.

Juhlin C, Stephens M B, 2006. Gently dipping fracture zones in Paleoproterozoic metagranite, Sweden: Evidence from reflection seismic and cored borehole data and implications for the disposal of nuclear waste. Journal of Geophysical Research 111, B09302, 19 pp.

Lanaro F, 2005. Forsmark site investigation. Rock mechanics characterisation of borehole KFM03A. SKB P-05-114, Svensk Kärnbränslehantering AB.

Mattsson H, Thunehed H, Isaksson H, Kübler L, 2004. Forsmark site investigation. Interpretation of petrophysical data from the cored boreholes KFM01A, KFM02A, KFM03A and KFM03B. SKB P-04-107, Svensk Kärnbränslehantering AB.

Mattsson H, Thunehed H, Isaksson H, 2005. Forsmark site investigation. Interpretation of petrophysical data from the cored boreholes KFM04A, KFM05A, and KFM06A. SKB P-05-204, Svensk Kärnbränslehantering AB.

Munier R, Hökmark H, 2004. Respect distances. Rationale and means of computation. SKB R-04-17, Svensk Kärnbränslehantering AB.

Munier R, Stigsson S, 2007. Implementation of uncertainties in borehole geometries and geological orientation data in Sicada. SKB R-07-19, Svensk Kärnbränslehantering AB.

Nordgulen Ø, Saintot A, 2006. Forsmark site investigation. The character and kinematics of deformation zones (ductile shear zones, fault zones and fracture zones) at Forsmark – report from phase 1. SKB P-06-212, Svensk Kärnbränslehantering AB.

Nordgulen Ø, Saintot A, 2008. Forsmark site investigation. The character and kinematics of deformation zones (ductile shear zones, fault zones and fracture zones) at Forsmark – report from phase 3. SKB P-07-111, Svensk Kärnbränslehantering AB.

Olofsson I, Simeonov A, Stephens M, Follin S, Nilsson A-C, Röshoff K, Lindberg U, Lanaro F, Fredriksson A, Persson L, 2007. Site descriptive modelling Forsmark, stage 2.2. A fracture domain concept as a basis for the statistical modelling of fractures and minor deformation zones, and interdisciplinary coordination, Site descriptive modelling Forsmark, stage 2.2. SKB R-07-15, Svensk Kärnbränslehantering AB.

Petersson J, Andersson U B, Berglund J, 2007. Scan line fracture mapping and magnetic susceptibility measurements across two low magnetic lineaments with NNE and NE trend, Forsmark. In Stephens M B and Skagius K (edits.), Geology − Background complementary studies. Forsmark modelling stage 2.2. SKB R-07-56, Svensk Kärnbränslehantering AB.

Saintot A, Nordgulen Ø, 2007. Forsmark site investigation. The character and kinematics of deformation zones (ductile shear zones, fault zones and fracture zones) at Forsmark – report from phase 2. SKB P-07-101, Svensk Kärnbränslehantering AB.

Sandström B, Tullborg E-L, Smellie J, MacKenzie A B, Suksi J, 2008a. Fracture mineralogy of the Forsmark site. SDM-Site Forsmark. SKB R-08-102, Svensk Kärnbränslehantering AB.

Sandström B, Page L, Tullborg E-L, 2008b. Forsmark site investigation. Fracture mineralogy and $^{40}Ar/^{39}Ar$ ages of adularia in fracture filling and K-feldspar in breccia. Data from drill cores KFM01C, KFM01D, KFM02B, KFM04A, KFM06A, KFM06B, KFM07A, KFM08A, KFM08B, KFM08C, KFM08D, KFM09A, KFM09B, KFM10A and KFM11A. SKB P-08-14, Svensk Kärnbränslehantering AB.

SKB, 2002. Forsmark – site descriptive model version 0. SKB R-02-32, Svensk Kärnbränslehantering AB.

SKB, 2005. Preliminary site description Forsmark area – version 1.2. SKB R-05-18, Svensk Kärnbränslehantering AB.

SKB, 2006. Site descriptive modeling Forsmark stage 2.1. Feedback for completion of the site investigation including input from safety assessment and repository engineering. SKB R-06-38, Svensk Kärnbränslehantering AB.

Stephens M B, Lundqvist S, Ekström M, Bergman T, Andersson J, 2003. Forsmark site investigation. Bedrock mapping. Rock types, their petrographic and geochemical characteristics, and a structural analysis of the bedrock based on stage 1 (2002) surface data. SKB P-03-75, Svensk Kärnbränslehantering AB.

Stephens M B, Skagius K (edits.), 2007. Geology − background complementary studies. Forsmark modelling stage 2.2. SKB R-07-56, Svensk Kärnbränslehantering AB.

Stephens M B, Fox A, La Pointe P, Simeonov A, Isaksson H, Hermanson J, Öhman J, 2007. Geology Forsmark. Site descriptive modelling, Forsmark stage 2.2. SKB R-07-45. Svensk Kärnbränslehantering AB.

Söderbäck B (ed.), 2008. Geological evolution, palaeoclimate and historical development of the Forsmark and Laxemar-Simpevarp areas. Site descriptive modelling SDM-Site. SKB R-08-19, Svensk Kärnbränslehantering AB.

Appendix

Base information used in the evaluations carried out in chapter 2 (Table A-1, Table A-2 and Table A-3) and chapter 8 (Table A-4, Table A-5 and Table A-6).

Table A-1. Result of comparison between the vertical and steeply dipping, deterministic deformation zones, stage 2.2 in Forsmark and magnetic linked lineaments from /Isaksson et al. 2007/.

Table A-2. Result of comparison between vertical and steeply dipping, deterministic minor deformation zones, stage 2.2 in Forsmark and magnetic linked lineaments from /Isaksson et al. 2007/.

Table A-3. Potential vertical or steeply dipping deformation zones. Magnetic linked lineaments from /Isaksson et al. 2007/, longer than 1,000 m, intersecting the local model area and presently not included as deterministic deformation zones in model stage 2.2 at Forsmark.

Table A-4. Character of the fault core along possible deformation zones (DZ) identified with high confidence in the single-hole interpretation (SHI) of drill cores, based on /Nordgulen and Saintot 2006, 2008, Saintot and Nordgulen 2007/. Data acquired during stage 2.3 are marked with a grey tone. Modelled deformation zones identified as ZFM with two to four letters or digits are gently dipping zones whereas zones identified as ZFM with six to eight letters or digits are steeply dipping. The letters WNW, NW, EW, NNW, ENE, NE and NNE in the steeply dipping zones only provide a general indication of their strike and do not make use of the right-hand-rule method to report true strike (see section 2.4 in /Stephens et al 2007/). The motivations for the correlation of possible deformation zones in boreholes KFM02B, KFM08D, KFM11A and KFM12A (stage 2.3) with modelled zones (stage 2.2) are presented in chapters 3, 4, 5 and 6, respectively.

Table A-5. Summary of kinematic data from possible deformation zones (DZ) identified with high confidence in the single-hole interpretation (SHI) of drill cores based on /Nordgulen and Saintot 2006, 2008, Saintot and Nordgulen 2007/. Data presented on a deformation zone basis as modelled in /Stephens et al. 2007/. Data acquired during stage 2.3 are marked with a grey tone. The orientation of steeply dipping shear fractures that are minor faults is recorded as a strike direction in accordance with the right-hand-rule method (e.g. NNW steep in column 4 indicates that kinematic data have been acquired along fractures that strike NNW and dip steeply to the ENE). Modelled deformation zones identified as ZFM with two to four letters or digits are gently dipping zones whereas zones identified as ZFM with six to eight letters or digits are steeply dipping. The letters WNW, NW, EW, NNW, ENE, NE and NNE in the steeply dipping zones only provide a general indication of their strike and do not make use of the right-hand-rule method to report true strike (see section 2.4 in /Stephens et al 2007/). The motivations for the correlation of possible deformation zones in boreholes KFM02B, KFM08D, KFM11A and KFM12A (stage 2.3) with modelled zones (stage 2.2) are presented in sections 3, 4, 5 and 6, respectively.

Table A-6. Summary of kinematic data from possible deformation zones (DZ) identified with high confidence in the single-hole interpretation (SHI) of drill cores, based on /Nordgulen and Saintot 2006, 2008, Saintot and Nordgulen 2007/. Data presented firstly on a fracture orientation and secondly on a deformation zone basis. The identification of deformation zones is after /Stephens et al. 2007/: Green = steep WNW-NW set of zones, dark blue = steep NNW set, brown = ENE (NE) sub-set, orange = NNE sub-set, pale blue = gentle set, unshaded = possible deformation zone not modelled in a deterministic manner (PDZ).

Table A-1. Result of comparison between the vertical and steeply dipping, deterministic deformation zones, stage 2.2 in Forsmark and magnetic linked lineaments from /Isaksson et al. 2007/.

Zone ID code	DZ block model	DZ orientation group	Evaluation	Length in model stage 2.2 [m]	Proposed revised length [m]	Change of length [m]	Implication index
ZFMENE0061	Local	Vertical and steeply dipping. ENE-NNE-(NE)	Change of route; WSW extension deviates to the SW and terminates at ZFMNW0017. 350 m longer. Terminates at ZFMNW0017.	2,081	2,433	352	3
ZFMENE0103	Local	Vertical and steeply dipping. ENE-NNE-(NE)	Extended towards SW 130 m and NE 360 m.	1,399	1,894	495	3
ZFMENE0159A	Local	Vertical and steeply dipping. ENE-NNE-(NE)	No significant change. Small changes in route in the SW parts.			0	1
ZFMENE0159B	Local	Vertical and steeply dipping. ENE-NNE-(NE)	No significant change (corresponds to MFM2326G0).			0	1
ZFMENE0169	Local	Vertical and steeply dipping. ENE-NNE-(NE)	NE extension slightly more towards ENE and 220 m longer.	1,069	1,293	224	3
ZFMENE0401A	Local	Vertical and steeply dipping. ENE-NNE-(NE)	Extended towards SW 350 m and NE 610 m. Now close to 3 km in length. SW termination at ZFMNW0003.	1,961	2,918	957	3
ZFMENE0401B	Local	Vertical and steeply dipping. ENE-NNE-(NE)	No new data => no change			0	1
ZFMENE0810	Local	Vertical and steeply dipping. ENE-NNE-(NE)	No new data => no change			0	1
ZFMENE1061A	Local	Vertical and steeply dipping. ENE-NNE-(NE)	No new data => no change			0	1
ZFMENE1061B	Local	Vertical and steeply dipping. ENE-NNE-(NE)	No new data => no change			0	1
ZFMENE1192	Local	Vertical and steeply dipping. ENE-NNE-(NE)	Identity 1,192 dropped as lineament. Replaced by MFM2253G0. MFM2253G1 continuous after a minor displacement, 758 m further towards SE. Terminated at ZFMNW0017.	1,090	1,163	73	3
ZFMENE1208A	Local	Vertical and steeply dipping. ENE-NNE-(NE)	No significant change. New data partly indicate one lineament MFM3033G in the same area and direction. Otherwise no new data or data disturbed.			0	1
ZFMENE1208B	Local	Vertical and steeply dipping. ENE-NNE-(NE)	No significant change. New data partly indicate one lineament MFM3033G in the same area and direction. Otherwise no new data or data disturbed.			0	1

Zone ID code	DZ block model	DZ orientation group	Evaluation	Length in model stage 2.2 [m]	Proposed revised length [m]	Change of length [m]	Implication index
ZFMENE2248	Local	Vertical and steeply dipping. ENE-NNE-(NE)	No new data => no change			0	1
ZFMENE2254	Local	Vertical and steeply dipping. ENE-NNE-(NE)	No significant change. Terminates in DS1 area. Disturbed area.			0	1
ZFMENE2320	Local	Vertical and steeply dipping. ENE-NNE-(NE)	Significant change of route; WSW extension deviates to the SW and terminates at ZFMNW0017. Uncertainty due to disturbed area. 620 m longer.	1,251	1,870	619	3
ZFMENE2332	Local	Vertical and steeply dipping. ENE-NNE-(NE)	Extended 250 m towards SW and terminates at ZFMNW1200. Shortened with 190 m in NE and change of termination.	1,458	1,525	67	3
ZFMENE2383	Local	Vertical and steeply dipping. ENE-NNE-(NE)	No new data => no change			0	1
ZFMNNE0725	Local	Vertical and steeply dipping. ENE-NNE-(NE)	Extended 520 m towards NNE. Terminates in the Singö deformation zone area.	1,274	1,797	523	3
ZFMNNE0869	Local	Vertical and steeply dipping. ENE-NNE-(NE)	No clear sign of this zone in the new magnetic data. MFM3143G is coincident with the central part of the zone. The magnetic lineament is fully outside the local model area and shorter than 1,000 m. Partly disturbed and low magnetic area.	1,065	507	–558	3
ZFMNNE2280	Local	Vertical and steeply dipping. ENE-NNE-(NE)	No new data => no change			0	1
ZFMNNE2293	Local	Vertical and steeply dipping. ENE-NNE-(NE)	No new data => no change			0	1
ZFMNNE2308	Local	Vertical and steeply dipping. ENE-NNE-(NE)	No new data => no change			0	1
ZFMNNW0100	Local	Vertical and steeply dipping. NNW	No significant change, no new data in NNW. No clear sign in new data in SSE. However, extends close to a disturbed area and in an area with diffuse pattern and partly low magnetic intensity and relief.			0	2
ZFMNNW0101	Local	Vertical and steeply dipping. NNW	Partly shows a new route and terminates differently in the N part. MFM 2469G partly takes over the northern end.	1,726	1,073	–653	3
ZFMNNW0404	Local	Vertical and steeply dipping. NNW	Identity 404 dropped as lineament. SSE end partly replaced by MFM1196G, which is reduced in length in the NW.	947	533	–414	3
ZFMWNW0813	Local	Vertical and steeply dipping. WNW-(NW)	Slightly different route, parallel to the previous location c. 50 m apart (following MFM3259). Extends both towards NW (400 m) and ESE (700 m), terminating against ZFMNW0001 (equal to MFM0803) in both ends (branching). Closer to 3 km in length.	1,609	2,709	1,100	3

Zone ID code	DZ block model	DZ orientation group	Evaluation	Length in model stage 2.2 [m]	Proposed revised length [m]	Change of length [m]	Implication index
ZFMWNW1053	Local	Vertical and steeply dipping. WNW-(NW)	Identity 1,053 dropped as lineament. Replaced by MFM1094G. Terminated at ZFMNW0809A. Otherwise, no significant change in route or length.			0	1
ZFMWNW1056	Local	Vertical and steeply dipping. WNW-(NW)	ZFMWNW1056 in the present version makes a major step over, from lineament MFM1056 to lineament MFM2496. Closer to 3 km in length.	1,557	2,758	1,201	3
ZFMWNW1068	Local	Vertical and steeply dipping. WNW-(NW)	No new data or data disturbed. No significant change.			0	1
ZFMWNW2225	Local	Vertical and steeply dipping. WNW-(NW)	No new data => no change			0	1
ZFMENE0060A	Regional and local	Vertical and steeply dipping. ENE-NNE-(NE)	No significant change in the NE part. New data indicate a straighter route in the SW part. ZFMENE60A makes a step over to the lineament MFM0060G2 for about 400–500 m in length.	3,120	3,110	–10	3
ZFMENE0060B	Regional and local	Vertical and steeply dipping. ENE-NNE-(NE)	No new data => no change			0	1
ZFMENE0060C	Regional and local	Vertical and steeply dipping. ENE-NNE-(NE)	Change of route and no longer a branch of ZFMENE60A. Instead it forms a splay and follows the lineament MFM2281G. Terminates at ZMFNW0017.	1,161	1,556	395	3
ZFMENE0062A	Regional and local	Vertical and steeply dipping. ENE-NNE-(NE)	Extended towards SW with 1,000 m. Terminates at ZMFNW0003 and not at ZMFNW0017. Small change of route in a central segment. Somewhat shortened, 100 m, in NE.	3,543	4,458	915	3
ZFMENE0062B	Regional and local	Vertical and steeply dipping. ENE-NNE-(NE)	Insignificant change at NE termination.	616	555	–61	1
ZFMENE0062C	Regional and local	Vertical and steeply dipping. ENE-NNE-(NE)	No new data => no change			0	1
ZFMEW0137	Regional and local	Vertical. EW	No new data => no change. A possible extension with 1,294 m towards ENE with lineament MFM0137B.			0	1
ZFMNE0808C	Regional and local	Vertical and steeply dipping. ENE-NNE-(NE)	Extended 80 m towards SW. Terminates at MFM2193G and not at ZFMWNW0044. Insignificant change of NE termination at MFM0803 (ZFMNW0001).	1,156	1,265	109	3
ZFMNW0002	Regional and local	Vertical and steeply dipping. WNW-(NW)	The southeast part of ZFMNW0002 can be redrawn to follow MFM0804G. Partly forms a new representation of the Singö deformation zone, see ZFMNW0001.	18,000	19,135	1,135	3

Zone ID code	DZ block model	DZ orientation group	Evaluation	Length in model stage 2.2 [m]	Proposed revised length [m]	Change of length [m]	Implication index
ZFMNW0017	Regional and local	Vertical and steeply dipping. WNW-(NW)	Insignificant change of route in the central sections, where new data exist.			0	1
ZFMNW1200	Regional and local	Vertical and steeply dipping. WNW-(NW)	Different route, mainly 50–70 m to the SW and parallel to the previous location. Not terminated in NW at new data boundary. Would mean an extra 1,500 m towards NW.	3,121	7,325	4,204	3
ZFMWNW0001	Regional and local	Vertical and steeply dipping. WNW-(NW)	The representation of the NW-trending Singö deformation zone area has been changed in the last lineament interpretation. Lineament MFM1127 corresponding to ZFMNW1127 has been dropped and the deformation area is now represented by MFM0803, MFM0813 and MFM0804 with interstitial areas of low magnetic intensity and relief. See also ZFMNW1127, ZFMNW0813 and ZFMNW0002. MFM0803 has a slightly different route compared with ZFMNW0001. Equal in length.			0	3
ZFMWNW0123	Regional and local	Vertical and steeply dipping. WNW-(NW)	Similar route in the SE part. Towards NW the lineament MFM0123G is not terminated at ZFMENE0060A and continues an additional 480 m.	5,086	5,569	483	3
ZFMWNW0809A	Regional and local	Vertical and steeply dipping. WNW-(NW)	ZFMWNW0809A now follows lineament MFM2215G, which is parallel and runs c. 50 m to the SW of MFM0809G. The NW termination is difficult to determine. In the SE, no new data => no change. Will continue with ZFMNW0809B.	3,347	4,100	753	3
ZFMWNW0809B	Regional and local	Vertical and steeply dipping. WNW-(NW)	Significant change in route and direction. Now forms a continuation of ZFMNW0809A (MFM0809) towards SE and terminates at ZFMNE0065. For length see ZFMNW0809A.			0	3
ZFMWNW0835B	Regional and local	Vertical and steeply dipping. WNW-(NW)	No confirmation of this zone at this location in the new data. A more north-westerly trend is suggested giving a shortening. No longer intersecting the local model area.	1,532	1,068	–464	3
ZFMWNW1127	Regional and local	Vertical and steeply dipping. WNW-(NW)	The representation of the NW-trending Singö deformation zone area has been changed in the last lineament interpretation. Lineament MFM1127 corresponding to ZFMNW1127 has been dropped and the deformation area is now represented by MFM0803, MFM0813 and MFM0804 with interstitial areas of low magnetic intensity and relief. See also ZFMNW0001, ZFMNW0813 and ZFMNW0002. In the SE, part of ZFMNW1127 is partly taken over by MFM0803G1. In the NW the SE part of MFM0804 will correspond to the remains of ZFMNW1127. Now shorter than 3,000 m.	5,394	2,500	–2,894	3

Zone ID code	DZ block model	DZ orientation group	Evaluation	Length in model stage 2.2 [m]	Proposed revised length [m]	Change of length [m]	Implication index
ZFMEW1156	Regional	Vertical. EW	No new data => no change			0	1
ZFMNE0065	Regional	Vertical and steeply dipping. ENE-NNE-(NE)	No new data => no change			0	1
ZFMNE0808A	Regional	Vertical and steeply dipping. ENE-NNE-(NE)	No new data => no change			0	1
ZFMNE0808B	Regional	Vertical and steeply dipping. ENE-NNE-(NE)	No new data => no change. Insignificant change of termination at MFM0803 (ZFMNW0001).			0	1
ZFMNNE0828	Regional	Vertical and steeply dipping. ENE-NNE-(NE)	No new data => no change			0	1
ZFMNNE0842	Regional	Vertical and steeply dipping. ENE-NNE-(NE)	No new data => no change			0	1
ZFMNNE0860	Regional	Vertical and steeply dipping. ENE-NNE-(NE)	No new data => no change			0	1
ZFMNNE0929	Regional	Vertical and steeply dipping. ENE-NNE-(NE)	No new data => no change			0	1
ZFMNNE1132	Regional	Vertical and steeply dipping. ENE-NNE-(NE)	No new data => no change			0	1
ZFMNNE1133	Regional	Vertical and steeply dipping. ENE-NNE-(NE)	No new data => no change			0	1
ZFMNNE1134	Regional	Vertical and steeply dipping. ENE-NNE-(NE)	No new data => no change			0	1
ZFMNNE1135	Regional	Vertical and steeply dipping. ENE-NNE-(NE)	No new data => no change			0	1
ZFMNNW0823	Regional	Vertical and steeply dipping. NNW	No new data => no change			0	1
ZFMNW0003	Regional	Vertical and steeply dipping. WNW-(NW)	No new data => no change			0	1
ZFMNW0029	Regional	Vertical and steeply dipping. WNW-(NW)	No new data => no change			0	1

Zone ID code	DZ block model	DZ orientation group	Evaluation	Length in model stage 2.2 [m]	Proposed revised length [m]	Change of length [m]	Implication index
ZFMNW0805	Regional	Vertical and steeply dipping. WNW-(NW)	Slightly different route for MFM0805G0 in the new data area. Different termination in the SE, at MFM0803G1. New branch MFM0805G1 in the central part of the zone, close to the SFR underground facility.			0	3
ZFMNW0806	Regional	Vertical and steeply dipping. WNW-(NW)	No new data => no change			0	1
ZFMNW0854	Regional	Vertical and steeply dipping. WNW-(NW)	No new data => no change			0	1
ZFMWNW0004	Regional	Vertical and steeply dipping. WNW-(NW)	No new data => no change			0	1
ZFMWNW0016	Regional	Vertical and steeply dipping. WNW-(NW)	No new data => no change			0	1
ZFMWNW0019	Regional	Vertical and steeply dipping. WNW-(NW)	No new data => no change			0	1
ZFMWNW0023	Regional	Vertical and steeply dipping. WNW-(NW)	No new data => no change			0	1
ZFMWNW0024	Regional	Vertical and steeply dipping. WNW-(NW)	No new data => no change			0	1
ZFMWNW0035	Regional	Vertical and steeply dipping. WNW-(NW)	No new data => no change			0	1
ZFMWNW0036	Regional	Vertical and steeply dipping. WNW-(NW)	No new data => no change			0	1
ZFMWNW0835A	Regional	Vertical and steeply dipping. WNW-(NW)	No new data => no change			0	1
ZFMWNW0836	Regional	Vertical and steeply dipping. WNW-(NW)	No significant change, little new data at the NW end.			0	1
ZFMWNW0851	Regional	Vertical and steeply dipping. WNW-(NW)	No new data => no change			0	1
ZFMWNW0853	Regional	Vertical and steeply dipping. WNW-(NW)	No new data => no change			0	1
ZFMWNW0974	Regional	Vertical and steeply dipping. WNW-(NW)	No new data => no change			0	1
ZFMWNW1173	Regional	Vertical and steeply dipping. WNW-(NW)	No new data => no change			0	1

Table A-2. Result of comparison between vertical and steeply dipping, deterministic minor deformation zones, stage 2.2 in Forsmark and magnetic linked lineaments from /Isaksson et al. 2007/.

Zone ID code	DZ block model	DZ orientation group	Evaluation	Length in model stage 2.2 [m]	Proposed revised length [m]	Change of length [m]	Implication index
ZFMWNW0044	Local	Vertical and steeply dipping. WNW-(NW)	Extended with 320 m towards NW. Different route and direction at SE. Longer than 1,000 m.	834	1,186	352	3
ZFMNNW1204	Local	Vertical and steeply dipping. NNW	No new data => no change			0	1
ZFMNNW1205	Local	Vertical and steeply dipping. NNW	No new data => no change			0	1
ZFMNNW1209	Local	Vertical and steeply dipping. NNW	Slightly different in location. Shortened.	352	230	–122	1
ZFMEW2311	Local	Vertical. EW	No new data => no change			0	1
ZFMNNE0130	Local	Vertical and steeply dipping. ENE-NNE-(NE)	Extended towards SSW with 160 m.	657	801	144	3
ZFMENE0168	Local	Vertical and steeply dipping. ENE-NNE-(NE)	No new data => no change			0	1
ZFMNE0811	Local	Vertical and steeply dipping. ENE-NNE-(NE)	No new data => no change. Can possibly be extended towards NE with 54 m, terminating at MFM0809G (ZFMWNW809A).	522	576	54	1
ZFMNE0870	Local	Vertical and steeply dipping. ENE-NNE-(NE)	No clear sign of this zone in the new data. Some smaller lineaments are partly coincident with the SW part of the zone. Partly disturbed area. MFM3266G can possibly form a north-easterly extension and if so the length is increased with c. 1,000 m.	854	1,869	1,015	2
ZFMENE1057	Local	Vertical and steeply dipping. ENE-NNE-(NE)	No clear sign of this zone in the new data. To a large extent, low magnetic area.			0	2
ZFMNE1188	Local	Vertical and steeply dipping. ENE-NNE-(NE)	Identity 1,188 dropped as lineament. Replaced by MFM3013G. Shortened both in the SSW and NNE end.	606	342	–264	3
ZFMNNE2008	Local	Vertical and steeply dipping. ENE-NNE-(NE)	No new data => no change			0	1
ZFMENE2120	Local	Vertical and steeply dipping. ENE-NNE-(NE)	No new data => no change			0	1
ZFMNNE2255	Local	Vertical and steeply dipping. ENE-NNE-(NE)	No new data => no change			0	1

Zone ID code	DZ block model	DZ orientation group	Evaluation	Length in model stage 2.2 [m]	Proposed revised length [m]	Change of length [m]	Implication index
ZFMNNE2263	Local	Vertical and steeply dipping. ENE-NNE-(NE)	No new data => no change			0	1
ZFMNNE2273	Local	Vertical and steeply dipping. ENE-NNE-(NE)	No new data => no change			0	1
ZFMNE2282	Local	Vertical and steeply dipping. ENE-NNE-(NE)	Extended 150 m towards SW. Terminated at the intersection of MFM0401G0 (ZFMNE401A) and MFM0123G0 (ZFMNW0123). Close to 1,000 m in length.	842	996	154	3
ZFMENE2283	Local	Vertical and steeply dipping. ENE-NNE-(NE)	No new data => no change			0	1
ZFMNNE2298	Local	Vertical and steeply dipping. ENE-NNE-(NE)	No new data => no change			0	1
ZFMNNE2299	Local	Vertical and steeply dipping. ENE-NNE-(NE)	Extended towards NE with 66 m, terminating at MFM0809G (ZFMWNW809A). Close to 1,000 m in length.	849	915	66	1
ZFMNNE2300	Local	Vertical and steeply dipping. ENE-NNE-(NE)	Extended towards NE with 46 m, terminating at MFM0809G (ZFMWNW809A). Close to 1,000 m.	946	992	46	1
ZFMNNE2309	Local	Vertical and steeply dipping. ENE-NNE-(NE)	No new data => no change			0	1
ZFMNNE2312	Local	Vertical and steeply dipping. ENE-NNE-(NE)	No new data => no change			0	1
ZFMENE2325A	Local	Vertical and steeply dipping. ENE-NNE-(NE)	Significant change of route; WSW extension deviates to the SW and terminates at MFM2074G. Uncertainty due to disturbed area. 450 m longer and now longer than 1,000 m.	963	1,412	449	3
ZFMENE2325B	Local	Vertical and steeply dipping. ENE-NNE-(NE)	No clear sign of this zone in the new data. However, very close to ZFMENE2325A. Revised together with A?			0	1
ZFMNE2374	Local	Vertical and steeply dipping. ENE-NNE-(NE)	Extended towards NE with 134 m.	764	898	134	3
ZFMNE2384	Local	Vertical and steeply dipping. ENE-NNE-(NE)	No new data => no change			0	1
ZFMENE2403	Local	Vertical and steeply dipping. ENE-NNE-(NE)	Extended 140 m towards SW. Now longer than 1,000 m.	958	1,099	141	3

Table A-3. Potential vertical or steeply dipping deformation zones. Magnetic linked lineaments from /Isaksson et al. 2007/, longer than 1,000 m, intersecting the local model area and presently not included as deterministic deformation zones in model stage 2.2 at Forsmark.

Lineament ID code	DZ block model	DZ orientation group	Evaluation	Length [m]	Length in model stage 2.2 [m]	Change of length [m]	Implication index
MFM2074G	Local	Probably vertical or steeply dipping. ENE-NNE-(NE)	The change of route for ZFMENE0061 means that this discordant lineament will have to be considered as a parallel deformation zone. Ranks with high uncertainty.	1,215	0	1,215	3
MFM0063G0	Local	Probably vertical or steeply dipping. ENE-NNE-(NE)	Discordant lineament that precisely intersect the local model area in the south corner. Will not have any significant impact on the present model. Passes SE of DS2. Ranks with low uncertainty.	1,974	0	1,974	3
MFM0126G0	Local	Probably vertical or steeply dipping. ENE-NNE-(NE)	Discordant lineament in a close to a south-north trend. Passes east of DS2. Ranks with low-medium uncertainty.	1,519	0	1,519	3
MFM0137BG	Local	Probably vertical or steeply dipping. ENE-NNE-(NE)	Discordant lineament, a possible continuation of ZFMEW0137, northeast of the Singö deformation zone. Ranks with medium uncertainty.	1,294	0	1,294	3
MFM3148G	Local	Probably vertical or steeply dipping. WNW-(NW)	Discordant lineament in NW direction located northeast of the Singö deformation zone and precisely intersects the local model area. Ranks with medium uncertainty.	1,130	0	1,130	3
MFM2496G	Local	Probably vertical or steeply dipping. WNW-(NW)	Concordant lineament in WNW direction, located in the Singö deformation zone area. Currently part of ZFMWNW1056. Ranks with low uncertainty.	2,012	0	2,012	3

Table A-4. Character of the fault core along possible deformation zones (DZ) identified with high confidence in the single hole interpretations (SHI), based on /Nordgulen and Saintot 2006, 2008, Saintot and Nordgulen 2007/. Data acquired during stage 2.3 are marked with a grey tone. Modelled deformation zones identified as ZFM with two to four letters or digits are gently dipping zones whereas zones identified as ZFM with six to eight letters or digits are steeply dipping. The letters WNW, NW, EW, NNW, ENE, NE and NNE in the steeply dipping zones only provide a general indication of their strike and do not make use of the right-hand-rule method to report true strike (see section 2.4 in /Stephens et al 2007/). The motivations for the correlation of possible deformation zones in boreholes KFM02B, KFM08D, KFM11A and KFM12A (stage 2.3) with modelled zones (stage 2.2) are presented in sections 3, 4, 5 and 6, respectively.

Borehole	Borehole length	DZ (SHI) / DZ (model stage 2.2)	Character of fault core within DZ
KFM01A	639 – 684 m	DZ3 / ZFMENE2254	Fault core intervals with elevated fracture frequency, including local sealed fracture networks
KFM01B	16 – 53 m	DZ1 / ZFMA2	Two fault core intervals with elevated fracture frequency. Clay mineral coating
KFM01B	107 – 135 m	DZ2 / DZ not modelled	Fault core intervals with elevated fracture frequency and sporadic sealed fracture networks
KFM01B	415 – 454 m	DZ3 / ZFMNNW0404	Two fault core intervals with sealed fracture networks. Brecciated cataclasite also present along the zone
KFM01C	23 – 48 m	DZ1 / ZFMA2 and ZFMENE1192	Three fault core intervals with crush zones
KFM01C	62 – 99 m	DZ2 / ZFMA2	Fault core interval with elevated frequency of open/partly open fractures and crush zone. Partial core loss
KFM01C	235 – 450 m	DZ3 / ZFMENE0060A and ZFMENE0060C	Several fault core intervals with sealed fracture networks, cohesive breccias and, locally, cataclasite
KFM01D	176 – 184 m	DZ1 / DZ not modelled	No fault core recognised
KFM01D	411 – 421 m	DZ2 / DZ not modelled	No fault core recognised
KFM01D	488 – 496 m	DZ3 / DZ not modelled	No fault core recognised
KFM01D	670 – 700 m	DZ4 / ZFMENE0061	Fault core interval with sealed fracture network
KFM01D	771 – 774 m	DZ5 / DZ not modelled	No fault core recognised
KFM02A	110 – 122 m	DZ2 / ZFM866	Two fault core intervals with elevated fracture frequency
KFM02A	160 – 184 m	DZ3 / ZFMA3	Three fault core intervals with altered vuggy rock
KFM02A	415 – 520 m	DZ6 / ZFMA2 and ZFMF1	Four fault core intervals with elevated fracture frequency and cohesive breccia/cataclasite
KFM02A	893 – 905 m	DZ8 / ZFMB4	No fault core recognised
KFM02A	922 – 925 m	DZ9 / DZ not modelled. Possibly related to ZFMB4	No fault core recognised
KFM02B	98 – 115 m	DZ1 / correlated with ZFM866	No fault core recognised. Two minor crush zones occur in the lower part of the zone
KFM02B	145 – 204 m	DZ2 / correlated with ZFMA3	No fault core recognised. Altered vuggy metagranite is present in the middle part of the zone and sealed fracture networks in occurrences of pegmatite are present in the lower part
KFM02B	411 – 431 m	DZ3 / correlated with ZFMA2	No fault core recognised
KFM02B	447 – 451 m	DZ4	No fault core recognised. Crush zone present at top of amphibolite. Elevated fracture frequency along DZ4 related to occurrence of amphibolite

Borehole	Borehole length	DZ (SHI) / DZ (model stage 2.2)	Character of fault core within DZ
KFM02B	462 – 473 m	DZ5 / correlated with ZFMF1	No fault core recognised. Sealed fracture networks in upper part of zone and crush zone in lower part
KFM02B	485 – 512 m	DZ6 / correlated with ZFMF1	No fault core recognised. Sealed fracture networks in amphibolite in upper part of zone. Also present, together with crush zone, in lower part of zone
KFM03A	356 – 399 m	DZ1 / ZFMA4	Two fault core intervals with elevated fracture frequency and crush zone
KFM03A	448 – 455 m	DZ2 / ZFMA7	Fault core interval with sealed fracture network
KFM03A	638 – 646 m	DZ3 / ZFMB1	No fault core recognised
KFM03A	803 – 816 m	DZ4 / ZFMA3	Fault core interval with elevated fracture frequency
KFM03A	942 – 949 m	DZ5 / DZ not modelled	Fault core interval with elevated fracture frequency
KFM03B	62 – 67 m	DZ2 / DZ not modelled. Possibly related to ZFMA5	Fault core interval with elevated fracture frequency, including crush zone
KFM04A	202 – 213 m	DZ2 / ZFMA2	Fault core interval with cataclasite and cohesive breccia
KFM04A	232 – 242 m	DZ3 / ZFMA2	Fault core interval with sealed fracture network, cohesive breccia and cataclasite
KFM04A	412 – 462 m	DZ4 / ZFMNE1188	Three fault core intervals with elevated fracture frequency including sealed fracture networks. Cohesive breccia and cataclasite also present along the zone, which is sub-parallel to the drill core
KFM05A	102 – 114 m	DZ1 / ZFMA2	Fault core intervals with narrow crush zones
KFM05A	416 – 436 m	DZ2 / ZFMNE2282	No fault core recognised. However, sealed fracture networks, cohesive breccia and cataclasite occur in a few places along the zone
KFM05A	606 – 619 m	Part of DZ3 / ZFMENE0401B	Three fault core intervals with elevated fracture frequency, including sealed fracture networks, cohesive breccia and cataclasite
KFM05A	712 – 720 m	Part of DZ3 / ZFMENE0401A	Fault core interval with elevated fracture frequency, including sealed fracture networks, and cohesive breccia
KFM06A	126 – 148 m	DZ1 / DZ not modelled	No fault core recognised
KFM06A	195 – 245 m	DZ2 / ZFMENE0060B	Two fault core intervals with elevated fracture frequency including sealed fracture networks
KFM06A	260 – 278 m	DZ3 / ZFMENE0060B	Three fault core intervals with sealed fracture network and local crush zone
KFM06A	318 – 358 m	DZ4 / ZFMENE0060A and ZFMB7	Fault core interval with sealed fracture network. Cataclasite and altered vuggy also present along the zone
KFM06A	740 – 775 m	DZ7 / ZFMNNE0725	Two fault core intervals with elevated fracture frequency, including sealed fracture networks, and cohesive breccia
KFM06A	788 – 810 m	DZ8 / ZFMENE0061	Fault core interval with sealed fracture network, cohesive breccia and cataclasite
KFM06A	882 – 905 m	DZ9 / DZ not modelled	Three fault core intervals with elevated fracture frequency including sealed fracture networks
KFM06A	925 – 933 m	DZ10 / DZ not modelled	Three fault core intervals with elevated fracture frequency, including sealed fracture networks, and cataclasite
KFM06A	950 – 990 m	DZ11 / ZFMNNE2280	Two fault core intervals with elevated fracture frequency, including sealed fracture networks, and cataclasite
KFM06B	55 – 93 m	DZ1 / ZFMA8	No fault core recognised. Sealed fracture network, abundant open fractures and core loss are conspicuous at top of zone
KFM06C	102 – 169 m	DZ1 / DZ not modelled	No fault core recognised. Sealed fracture networks are conspicuous in the upper part of the zone, where also subordinate rock types in the metagranite are present

Borehole	Borehole length	DZ (SHI) / DZ (model stage 2.2)	Character of fault core within DZ
KFM06C	359 – 400 m	DZ2 / ZFMB7	No fault core recognised. Sealed fracture networks and a crush zone are conspicuous in the lower part of the zone
KFM06C	415 – 489 m	DZ3 / ZFMNNE2263	No fault core recognised. Sealed fracture networks are common along the zone. Breccia and cataclasite locally present
KFM06C	502 – 555 m	DZ4 / ZFMWNW0044	Fault core with elevated frequency of both sealed fractures in network and open fractures including crush zone
KFM07A	108 – 183 m	DZ1 / ZFM1203 and ZFMNNW0404	Three fault core intervals with elevated fracture frequency, including sealed fracture network, and locally cataclasite. Crush zones also present in the upper part of the zone
KFM07A	196 – 205 m	DZ2 / DZ not modelled	Fault core with elevated fracture frequency including sealed fracture networks
KFM07A	417 – 422 m	DZ3 / ZFMENE0159A	No fault core recognised. Sealed fracture network at 419–420 m borehole length
KFM07A	803 – 999 m divided into three sections, 803–843 m, 857–900 m and 920–999 m	DZ4 / ZFMENE1208B (upper section), ZFMENE1208A (middle section), and ZFMNNW0100 (lower section)	*Section 803–843 m:* Fault core with elevated fracture frequency in sealed fracture network and marked grain-size reduction. Cohesive breccia and cataclasite also observed along the zone. *Section 857–900 m:* Fault core with elevated fracture frequency in sealed fracture network, cohesive breccia and cataclasite *Section 920–999 m:* Five fault cores with elevated fracture frequency including sealed fracture networks, cohesive breccia and cataclasite
KFM07B	51 – 58 m	DZ1 / DZ not modelled	No fault core recognised. Sealed fracture network and crush zone in amphibolite are present
KFM07B	93 – 102 m	DZ2 ZFM1203	No fault core recognised
KFM07B	225 – 245 m	DZ4 / ZFMENE2320	Fault core with elevated fracture frequency, including sealed fracture networks, and cataclasite
KFM07C	92 – 103 m	DZ1 ZFM1203	No fault core recognised
KFM07C	308 – 388 m	DZ2 / ZFMENE2320	Two fault cores with sealed fracture networks, fault breccia or proto-breccia and cataclasite
KFM07C	429 – 439 m	DZ3 / ZFMENE2320	No fault core recognised
KFM08A	172 – 342 m	DZ1 / ZFMENE1061A	Sections of fault core along an interval with elevated fracture frequency, including sealed fracture networks, and cataclasite
KFM08A	479 – 496 m	DZ2 / ZFMNNW1204	No fault core recognised. Sealed fracture networks in the upper and lower parts of the zone
KFM08A	672 – 693 m	DZ4 / DZ not modelled	Fault core with elevated fracture frequency in sealed fracture networks.
KFM08A	915 – 946 m	DZ6 / DZ not modelled	Two fault cores with elevated fracture frequency including sealed fracture networks and a crush zone
KFM08B	167 – 185 m	DZ2 / ZFMNNW1205	No fault core recognised. Sealed fracture networks and brecciated cataclasite occur in the lower part of the zone
KFM08C	161 – 191 m	DZ1 / DZ not modelled	No fault core recognised. Minor crush zones are present in the lower half of the zone
KFM08C	419 – 542 m	DZ2 / ZFMNNE2312	No fault core recognised. Altered vuggy rock without elevated fracture frequency and minor crush zones are present at several intervals
KFM08C	673 – 705 m	DZ3 / ZFMWNW2225	Fault core with elevated fracture frequency in sealed fracture network
KFM08C	829 – 832 m	DZ4 / ZFMENE1061A and ZFMENE1061B	Fault core with elevated fracture frequency including crush zone
KFM08D	371 – 396 m	DZ3 / correlated with ZFMENE0159B	No fault core recognised
KFM08D	546 – 571 m	DZ5 / correlated with ZFMNNE2309	No fault core recognised. Sealed fracture networks in lower part

Borehole	Borehole length	DZ (SHI) / DZ (model stage 2.2)	Character of fault core within DZ
KFM08D	621 – 634 m	DZ7 / correlated with ZFMENE2320	No fault core recognised. Sealed fracture networks in lower part
KFM08D	903 – 934 m	DZ12 / correlated with ZFMNNE2300	Fault core with crush zone. High frequency of sealed fractures, including sealed fracture networks, in rock adjacent to fault core
KFM09A	15 – 40 m	DZ1 / ZFMENE1208A	No fault core recognised. Elevated fracture frequency with sealed fracture networks at two intervals. Cohesive breccia, cataclasite and proto-cataclasite close to lower occurrence. Crush zones at two intervals, both above and beneath the elevated sealed fracture intervals
KFM09A	86 – 116 m	DZ2 / ZFMENE1208B	No fault core recognised. Elevated frequency of sealed fractures, mainly as sealed fracture networks at two intervals. Cohesive breccia present in upper interval
KFM09A	217 – 280 m	DZ3 / ZFMENE0159 A and ZFMNNW0100	Two fault cores with elevated fracture frequency defined by sealed fracture networks and cohesive breccia. Crush zone also present in lower part of zone
KFM09A	723 – 754 m	DZ4 / ZFMNW1200	No fault core recognised. Elevated frequency of sealed fractures, mainly as sealed fracture networks, in lower part
KFM09A	770 – 790 m	DZ5 / ZFMNW1200	No fault core recognised
KFM09B	9 – 132 m	DZ1 / ZFMENE1208A (upper section), ZFMENE1208B (middle section), and ZFMENE0159A (lower section)	*Section 9–43 m:* Fault core with elevated fracture frequency in sealed fracture network and crush zone. Elevated fracture frequency in sealed networks and cohesive breccia also present in middle and upper parts *Section 59–78 m:* No fault core recognised *Section 106–132 m:* Fault core with sealed fracture network, cohesive breccia and cataclasite
KFM09B	363 – 413 m	DZ3 / ZFMENE2320	Two fault core intervals. Elevated fracture frequency in sealed fracture network, cohesive breccia and cataclasite in middle part of zone; cataclasite and ultra-cataclasite in amphibolite in lower part of zone
KFM09B	520 – 550 m	DZ4 / ZFMENE2325A	Fault core with elevated fracture frequency in sealed fracture network and cohesive breccia
KFM09B	561 – 574 m	DZ5 / ZFMENE2325B	No fault core recognised. Altered vuggy rock in lower part of zone with relatively few fractures
KFM10A	63 – 145 m	DZ1 / ZFMWNW 0123	No fault core recognised. Sealed fracture networks and crush zones present at several intervals. In particular, note the high frequency of sealed fractures and the occurrences of crush zone and altered vuggy rock in the central part of the zone
KFM10A	430 – 449 m	DZ2 / ZFMA2	No fault core recognised. Elevated frequency of sealed fractures, mainly as sealed fracture networks, in upper part
KFM10A	478 – 490 m	DZ3 / ZFMA2	No fault core recognised. Elevated frequency of sealed fractures as sealed fracture network and altered vuggy rock in lower part
KFM11A	498 – 630 m	Part of DZ1 / ZFMWNW0001 (Singö deformation zone)	Two fault core intervals identified in this part of DZ1 (KFM11A). Elevated fracture frequency particularly in the form of sealed fracture networks and crush zones, strong alteration and several short intervals of cohesive breccia and cataclasite
KFM12A	125 – 158 m	DZ1	No fault core recognised. Elevated frequency of sealed fractures as sealed fracture networks in upper and lower parts. Minor crush zone in uppermost part
KFM12A	170 – 402 m	DZ2	Four fault core intervals with most conspicuous interval at 312 to 338 m. This interval contains nearly 100% cataclasite, fault breccia and minor ultra-cataclasite, with highly elevated frequency of sealed fractures
KFM12A	513 – 523 m	DZ3	No fault core recognised. Elevated fracture frequency in the form of sealed fracture network and crush zone in the upper part

Table A-5. Summary of kinematic data from possible deformation zones (DZ) identified with high confidence in the single hole interpretation (SHI) of drill cores, based on /Nordgulen and Saintot 2006, 2008, Saintot and Nordgulen 2007/. Data presented on a deformation zone basis as modelled in /Stephens et al. 2007/. Data acquired during stage 2.3 are marked with a grey tone. The orientation of steeply dipping fractures that are minor faults is recorded as a strike direction in accordance with the right-hand-rule method (e.g. NNW steep in column 4 indicates that kinematic data have been acquired along fractures that strike NNW and dip steeply to the ENE). Modelled deformation zones identified as ZFM with two to four letters or digits are gently dipping zones whereas zones identified as ZFM with six to eight letters or digits are steeply dipping. The letters WNW, NW, EW, NNW, ENE, NE and NNE in the steeply dipping zones only provide a general indication of their strike and do not make use of the right-hand-rule method to report true strike (see section 2.4 in /Stephens et al 2007/). The motivations for the correlation of possible deformation zones in boreholes KFM02B, KFM08D, KFM11A and KFM12A (stage 2.3) with modelled zones (stage 2.2) are presented in sections 3, 4, 5 and 6, respectively.

Zone ID code	DZ in SHI	Borehole	Orientation of fractures with shear striae / steps (minor faults)	Mineral along shear striae / steps	Sense of movement	Number of fractures with shear striae / steps (minor faults)
Vertical and steeply dipping deformation zones with sub-sets referred to as WNW and NW						
ZFMWNW0001 (Singö deformation zone)	Part of DZ1 (498–630 m)	KFM11A	SE, ESE, NW, WNW steep	Chlorite, hematite, laumontite, calcite, some clay minerals	Dextral strike-slip, oblique-slip with a reverse dip-slip component, sinistral strike-slip or normal dip-slip (19). Remainder strike-slip or oblique slip (13)	32 fractures
ZFMWNW0001 (Singö deformation zone)	Part of DZ1 (498–630 m)	KFM11A	NE, ENE, SW and WSW steep	Chlorite, hematite, laumontite, calcite, some clay minerals	Strike-slip, oblique-slip with dominant strike-slip component in part dextral, oblique-slip with dominant reverse dip-slip component or normal dip-slip	9 fractures
ZFMWNW0001 (Singö deformation zone)	Part of DZ1 (498–630 m)	KFM11A	Gentle (dip to E)	Chlorite, hematite, laumontite, calcite, some clay minerals	Dextral strike-slip, oblique-slip with dominant dextral strike-slip component or reverse dip-slip	4 fractures
ZFMWNW0001 (Singö deformation zone)	Part of DZ1 (498–630 m)	KFM11A	NNW steep	Chlorite, hematite, laumontite, calcite, some clay minerals	Sinistral strike-slip	1 fracture
ZFMWNW0004 (Forsmark deformation zone)	DZ1	KFM12A	SE, ESE and NW steep	Chlorite, hematite, laumontite, calcite, some clay minerals	Strike-slip including both sinistral and dextral strike-slip	6 fractures
ZFMWNW0004 (Forsmark deformation zone)	DZ1	KFM12A	Gentle	Chlorite, hematite, laumontite, calcite, some clay minerals	Sinistral strike-slip, dextral strike-slip or reverse dip-slip	3 fractures
ZFMWNW0004 (Forsmark deformation zone)	DZ1	KFM12A	ENE steep	Chlorite, hematite, laumontite, calcite, some clay minerals	Sinistral strike-slip	1 fracture
ZFMWNW0004 (Forsmark deformation zone)	DZ2	KFM12A	SE, ESE, NW and WNW steep	Chlorite, hematite, laumontite, calcite, some clay minerals	Oblique-slip including dominant sinistral or dextral strike-slip component, dextral strike-slip, sinistral strike-slip, reverse dip-slip or normal dip-slip displacement	22 fractures

Zone ID code	DZ in SHI	Borehole	Orientation of fractures with shear striae / steps (minor faults)	Mineral along shear striae / steps	Sense of movement	Number of fractures with shear striae / steps (minor faults)
ZFMWNW0004 (Forsmark deformation zone)	DZ2	KFM12A	NE, ENE, SW and WSW steep	Chlorite, hematite, laumontite, calcite, some clay minerals	Strike-slip including two fractures with sinistral strike-slip displacement, dip-slip or oblique-slip	6 fractures
ZFMWNW0004 (Forsmark deformation zone)	DZ2	KFM12A	NNE and SSW steep	Chlorite, hematite, laumontite, calcite, some clay minerals	Reverse dip-slip or oblique-slip with dominant strike-slip component	3 fractures
ZFMWNW0004 (Forsmark deformation zone)	DZ2	KFM12A	Gentle (dip to E)	Chlorite, hematite, laumontite, calcite, some clay minerals	Reverse dip-slip or oblique-slip	2 fractures
ZFMWNW0044	DZ4	KFM06C	N, SSW and NNE steep	Chlorite, hematite, clay minerals	Strike-slip. One fracture shows sinistral strike-slip displacement	5 fractures
ZFMWNW0044	DZ4	KFM06C	E moderate	Chlorite, hematite, clay minerals	Oblique-slip with dominant dip-slip component	1 fracture
ZFMWNW0123	DZ1	KFM10A	SE, ESE and WNW steep	Chlorite, calcite, clay minerals	Strike-slip. Eight fractures show sinistral strike-slip displacement	34 fractures
ZFMWNW0123	DZ1	KFM10A	SSE steep	Chlorite	Strike-slip	1 fracture
ZFMWNW0123	DZ1	KFM10A	Gentle	Chlorite, calcite, clay minerals	Oblique slip with dominant reverse dip-slip component or dip-slip	2 fractures
ZFMWNW2225	DZ3	KFM08C	WNW-ESE vertical	Calcite, quartz	Sinistral strike-slip	1 fracture
ZFMWNW2225	DZ3	KFM08C	Gentle	Chlorite, calcite	Dextral strike-slip	1 fracture
ZFMNW1200	DZ4	KFM09A	NW and SE steep	Chlorite, quartz, calcite, some laumontite	Sinistral strike-slip (7), reverse dip-slip (1) or oblique-slip with dominant dextral strike-slip component (1)	9 fractures
ZFMNW1200	DZ4	KFM09A	WSW steep	Calcite	Dextral strike-slip	1 fracture
ZFMNW1200	DZ5	KFM09A	NW and SE steep	Chlorite, calcite, clay minerals	Sinistral strike-slip	4 fractures
Vertical and steeply dipping fracture zones referred to as NNW						
ZFMNNW0100. ZFMB8 also close to DZ4 in KFM07A	920–999 m along DZ4	KFM07A	NW, NNW, SSE and NNE steep	Chlorite, calcite, hematite, some adularia and clay minerals	Strike-slip dominates with both dextral and sinistral displacement. Oblique-slip or dip-slip displacement also present	26 fractures
ZFMNNW0100. ZFMB8 also close to DZ4 in KFM07A	920–999 m along DZ4	KFM07A	ENE, WSW and E steep	Chlorite, some calcite, laumontite, hematite, clay minerals	Strike-slip, oblique-slip or normal dip-slip	5 fractures

Zone ID code	DZ in SHI	Borehole	Orientation of fractures with shear striae / steps (minor faults)	Mineral along shear striae / steps	Sense of movement	Number of fractures with shear striae / steps (minor faults)
ZFMNNW0100. ZFMB8 also close to DZ4 in KFM07A	920–999 m along DZ4	KFM07A	Gentle	Chlorite, calcite, some hematite and adularia	Strike-slip or oblique-slip, including dextral strike-slip and dextral reverse displacement	7 fractures
ZFMNNW0100/ ZFMENE0159A	DZ3	KFM09A	NNW and SSE steep (24), SE steep (1)	Chlorite, calcite, some clay minerals and hematite	Strike-slip or oblique-slip. Two fractures show sinistral strike-slip displacement. One fracture shows oblique-slip with dominant normal dip-slip displacement	25 fractures
ZFMNNW0100/ ZFMENE0159A	DZ3	KFM09A	Moderate	Chlorite, calcite	Oblique-slip with dominant dextral strike-slip component	1 fracture
ZFMNNW0404	DZ3	KFM01B	NNW steep	Chlorite, some epidote	Sinistral strike-slip	1 fracture
ZFMNNW0404	DZ3	KFM01B	NNW steep	Chlorite, some calcite	Normal or reverse dip-slip	3 fractures
ZFMNNW1204	DZ2	KFM08A	NNW steep	Chlorite, clay minerals	Strike-slip	1 fracture
ZFMNNW1204	DZ2	KFM08A	SW steep	Chlorite, calcite	Strike-slip. One fracture shows sinistral strike-slip	2 fractures
ZFMNNW1205	DZ2	KFM08B	SSE steep	Chlorite, calcite	Strike-slip. Three fractures show sinistral strike-slip displacement	5 fractures
ZFMNNW1205	DZ2	KFM08B	Gentle	Chlorite, corrensite	Reverse dip-slip	1 fracture
Vertical and steeply dipping fracture zones referred to as ENE (NE)						
ZFMENE0060A/ ZFMB7	DZ4	KFM06A	SW steep	Chlorite, some calcite	Oblique-slip with dominant strike-slip component	2 fractures
ZFMENE0060A/ ZFMB7	DZ4	KFM06A	Gentle	Chlorite, some calcite	Dip-slip	1 fracture
ZFMENE0060A/ ZFMENE0060C	DZ3	KFM01C	NE and SW steep	Chlorite, hematite, clay minerals	Strike-slip, dip-slip or oblique-slip. One fracture shows dextral strike-slip displacement	11 fractures
ZFMENE0060A/ ZFMENE0060C	DZ3	KFM01C	W moderate	Chlorite, hematite, calcite	Reverse dip-slip	1 fracture
ZFMENE0060A/ ZFMENE0060C	DZ3	KFM01C	E steep	Chlorite, hematite, clay minerals	Dip-slip or dextral strike-slip	2 fractures
ZFMENE0060A/ ZFMENE0060C	DZ3	KFM01C	NNW steep	Chlorite, hematite, clay minerals	Reverse dip-slip or oblique slip	2 fractures
ZFMENE0060B	DZ2	KFM06A	WSW steep	Chlorite, some calcite	Strike-slip	1 fracture
ZFMENE0060B	DZ2	KFM06A	ESE steep	Chlorite, some calcite	Strike-slip or oblique-slip with reverse sinistral displacement	2 fractures
ZFMENE0060B	DZ3	KFM06A	SSW steep	Calcite	Reverse dip-slip	1 fracture

Zone ID code	DZ in SHI	Borehole	Orientation of fractures with shear striae / steps (minor faults)	Mineral along shear striae / steps	Sense of movement	Number of fractures with shear striae / steps (minor faults)
ZFMENE0060B	DZ3	KFM06A	Gentle	Chlorite, some calcite	Normal dip-slip	1 fracture
ZFMENE0061	DZ4	KFM01D				No fault-slip data observed
ZFMENE0061	DZ8	KFM06A	WSW, ESE and SW steep	Chlorite, some calcite	Strike-slip	5 fractures
ZFMENE0061	DZ8	KFM06A	NNW steep	Chlorite	Dip-slip	1 fracture
ZFMENE0159A	DZ3	KFM07A	NNW and SSE steep	Chlorite, hematite	Strike-slip	2 fractures
Correlated with ZFMENE0159B	DZ3	KFM08D	ENE steep	Chlorite, hematite	Dextral strike-slip	1 fracture
ZFMENE0401A	712–720 m along DZ3	KFM05A	SW steep	Chlorite	Strike-slip	1 fracture
ZFMENE0401B	609–616 m along DZ3	KFM05A	S steep	Chlorite	Strike-slip	1 fracture
ZFMENE1061A	DZ1	KFM08A	NNW steep	Chlorite, some calcite and laumontite	Strike-slip, in part sinistral strike-slip	6 fractures
ZFMENE1061A	DZ1	KFM08A	SSW steep	Calcite	Sinistral strike-slip	1 fracture
ZFMENE1061A	DZ1	KFM08A	Gentle	Chlorite, calcite	Reverse dip-slip or dextral strike-slip	2 fractures
ZFMENE1061A/ ZFMENE1061B	DZ4	KFM08C	ENE steep	Chlorite, hematite, calcite	Oblique-slip	1 fracture
ZFMENE1208A	857–900 m along DZ4	KFM07A	SSE steep	Chlorite, some calcite, laumontite, adularia, clay minerals	Strike-slip. Nine fractures show sinistral or dextral strike-slip displacement	17 fractures
ZFMENE1208A	857–900 m along DZ4	KFM07A	ENE steep	Chlorite	Strike-slip	1 fracture
ZFMENE1208A	DZ1	KFM09A	NNW and SSE steep	Chlorite, calcite, hematite	Strike-slip	3 fractures
ZFMENE1208A	DZ1	KFM09A	ENE steep	Chlorite, calcite, hematite	Strike-slip	1 fracture
ZFMENE1208A/ ZFMENE1208B/ ZFMENE0159A	DZ1	KFM09B	NNW and SSE steep	Chlorite, hematite, calcite, clay minerals	Strike-slip. Two fractures show dextral strike-slip and one fracture shows sinistral strike-slip displacement	5 fractures
ZFMENE1208B	803–843 m along DZ4	KFM07A	NNW and SSE steep	Chlorite, calcite, laumontite, hematite, some clay minerals	Strike-slip. One fracture shows sinistral strike-slip displacement	3 fractures
ZFMENE1208B	803–843 m along DZ4	KFM07A	NNE steep	Chlorite, calcite, hematite	Oblique-slip with sinistral strike-slip and normal dip-slip displacement	1 fracture

Zone ID code	DZ in SHI	Borehole	Orientation of fractures with shear striae / steps (minor faults)	Mineral along shear striae / steps	Sense of movement	Number of fractures with shear striae / steps (minor faults)
ZFMENE1208B	DZ2	KFM09A	W steep	Chlorite, calcite, hematite	Dextral strike-slip	1 fracture
ZFMENE1208B	DZ2	KFM09A	NNW steep	Hematite	Strike-slip	1 fracture
ZFMENE2254	DZ3	KFM01A	NE steep	Chlorite, laumontite	Oblique-slip. One fracture shows normal dip-slip and dextral strike-slip displacement	2 fractures
ZFMENE2320	DZ4	KFM07B				No fault-slip data observed
ZFMENE2320	DZ2	KFM07C	WSW steep	Chlorite, calcite	Strike-slip	1 fracture
ZFMENE2320	DZ2	KFM07C	SE steep to NNW and SSE steep	Chlorite, hematite, calcite	Strike-slip, including three fractures with sinistral strike-slip, or oblique-slip with dominant strike-slip component	6 fractures
ZFMENE2320	DZ2	KFM07C	ESE steep	Chlorite, hematite	Dextral strike-slip	1 fracture
ZFMENE2320	DZ2	KFM07C	Gentle	Calcite	Dip-slip or oblique-slip with dominant strike-slip component	2 fractures
ZFMENE2320	DZ3	KFM07C				No fault-slip data observed
ZFMENE2320	DZ7	KFM08D	WSW steep	Chlorite, calcite	Dextral strike-slip	1 fracture
ZFMENE2320	DZ3	KFM09B	ENE steep	Chlorite, hematite, calcite	Strike-slip	2 fractures
ZFMENE2320	DZ3	KFM09B	NNW steep	Chlorite, hematite, calcite	Sinistral strike-slip	1 fracture
ZFMENE2320	DZ3	KFM09B	Gentle	Chlorite, hematite, calcite	Oblique-slip with dominant dextral strike-slip displacement	1 fracture
ZFMENE2325A	DZ4	KFM09B	SSE steep	Chlorite, hematite, calcite	Sinistral strike-slip (1), oblique-slip (2) with both normal dextral and reverse sinistral displacements, dip-slip (1)	4 fractures
ZFMENE2325B	DZ5	KFM09B	ENE and WSW steep	Chlorite, calcite	Strike-slip. One fracture shows dextral strike-slip	2 fractures
ZFMNE1188	DZ4	KFM04A	SE to ESE, W, SW and NE steep to moderate. Gentle	Chlorite. Some calcite, laumontite and hematite	Strike-slip or dip-slip. One SE fracture shows sinistral strike-slip displacement	22 fractures
ZFMNE2282	DZ2	KFM05A	SW steep	Chlorite, hematite, calcite	Strike-slip	1 fracture
ZFMNE2282	DZ2	KFM05A	SE steep	Chlorite, hematite	Oblique-slip	1 fracture
Vertical and steeply dipping fracture zones referred to as NNE						
ZFMNNE0725	DZ7	KFM06A	ENE and WSW steep	Chlorite, calcite	Strike-slip or oblique-slip with dominant strike-slip component. One fracture shows sinistral strike-slip displacement	4 fractures
ZFMNNE0725	DZ7	KFM06A	ESE steep	Chlorite	Strike-slip or oblique-slip with dominant dip-slip component	3 fractures
ZFMNNE0725	DZ7	KFM06A	NW steep	Chlorite, calcite	Dextral strike-slip	1 fracture

Zone ID code	DZ in SHI	Borehole	Orientation of fractures with shear striae / steps (minor faults)	Mineral along shear striae / steps	Sense of movement	Number of fractures with shear striae / steps (minor faults)
ZFMNNE0725	DZ7	KFM06A	NNE, steep	Chlorite, laumontite	Dextral strike-slip	1 fracture
ZFMNNE0725	DZ7	KFM06A	Gentle	Chlorite	Dip-slip	1 fracture
ZFMNNE2263	DZ3	KFM06C	NW steep	Chlorite, clay minerals	Oblique-slip	1 fracture
ZFMNNE2263	DZ3	KFM06C	E steep	Chlorite, hematite	Strike-slip	1 fracture
ZFMNNE2263	DZ3	KFM06C	Gentle	Chlorite, clay minerals	Reverse dip-slip	1 fracture
ZFMNNE2280	DZ11	KFM06A	NNE steep	Chlorite, laumontite	Oblique-slip with dominant strike-slip component	1 fracture
ZFMNNE2280	DZ11	KFM06A	SW steep	Hematite	Oblique-slip with dominant normal dip-slip component	1 fracture
ZFMNNE2280	DZ11	KFM06A	Gentle	Chlorite, laumontite, hematite	Strike-slip or oblique-slip with dominant dextral strike-slip and subordinate normal dip-slip in two fractures	3 fractures
Correlated with ZFMNNE2300	DZ12	KFM08D	SSW steep	Chlorite	Strike-slip	1 fracture
Correlated with ZFMNNE2300	DZ12	KFM08D	Gentle to moderate	Chlorite	Reverse dip-slip or oblique-slip with reverse dip-slip and sinistral strike-slip components	2 fractures
Correlated with ZFMNNE2309	DZ5	KFM08D				No fault-slip data observed
ZFMNNE2312	DZ2	KFM08C	SSW steep	Chlorite, hematite, calcite	Strike-slip. Two fractures show sinistral strike-slip displacement	4 fractures
ZFMNNE2312	DZ2	KFM08C	NNW steep	Chlorite, hematite, calcite	Sinistral strike-slip	2 fractures
ZFMNNE2312	DZ2	KFM08C	NE steep	Hematite	Normal dip-slip	1 fracture
ZFMNNE2312	DZ2	KFM08C	Gentle	Calcite	Oblique-slip with reverse dip-slip and dextral strike-slip components	1 fracture
Gently-dipping fracture zones						
ZFMA2	DZ1	KFM01B	NNW steep	Chlorite, some hematite	Strike-slip	2 fractures
ZFMA2/ ZFMENE1192	DZ1	KFM01C	Gentle	Clay minerals and hematite/clay minerals and calcite	Reverse dip-slip or oblique-slip	2 fractures
ZFMA2/ ZFMENE1192	DZ1	KFM01C	WSW steep	Calcite/clay minerals and hematite	Strike-slip or dip-slip	2 fractures
ZFMA2	DZ2	KFM01C	Gentle	Hematite and/or chlorite and/or clay minerals	Dip-slip (3) or strike-slip (2) displacement	5 fractures
ZFMA2	DZ2	KFM01C	NNW and SSE steep	Hematite and/or chlorite and/or clay minerals	Strike-slip. One fracture shows sinistral strike-slip displacement	5 fractures

Zone ID code	DZ in SHI	Borehole	Orientation of fractures with shear striae / steps (minor faults)	Mineral along shear striae / steps	Sense of movement	Number of fractures with shear striae / steps (minor faults)
ZFMA2	DZ2	KFM01C	SW steep	Hematite, chlorite, calcite	Oblique-slip with dominant dip-slip displacement	1 fracture
ZFMA2	DZ2	KFM01C	ESE steep	Hematite, chlorite, calcite	Strike-slip	1 fracture
ZFMA2/ZFMF1	DZ6	KFM02A	Gentle	Chlorite	Dip-slip or strike-slip. Reverse dip-slip and both dextral and sinistral strike-slip displacements defined	15 fractures
ZFMA2/ZFMF1	DZ6	KFM02A	WNW steep	Chlorite, calcite	Dip-slip or oblique-slip	3 fractures
Correlated with ZFMA2	DZ3	KFM02B				No fault-slip data observed
Correlated with ZFMF1	DZ5	KFM02B	Gentle	Chlorite, calcite	Dip-slip or oblique-slip with significant reverse dip-slip component	2 fractures
Correlated with ZFMF1	DZ5	KFM02B	WSW steep	Chlorite, clay minerals	Oblique-slip with dextral normal displacement	1 fracture
Correlated with ZFMF1	DZ6	KFM02B	ENE and SW steep	Epidote, chlorite	Strike-slip. The steep ENE fracture shows sinistral strike-slip displacement	2 fractures
ZFMA2	DZ2	KFM04A	Gentle	Chlorite, hematite, calcite	Strike-slip	1 fracture
ZFMA2	DZ2	KFM04A	WSW steep	Chlorite, hematite, calcite	Oblique-slip with dominant dip-slip component	1 fracture
ZFMA2	DZ2	KFM04A	SE steep	Chlorite, hematite, calcite	Dip-slip	1 fracture
ZFMA2	DZ3	KFM04A	Gentle	Chlorite, hematite	Oblique-slip with dominant strike-slip component	1 fracture
ZFMA2	DZ3	KFM04A	SW and WSW steep	Chlorite, hematite	Strike-slip or dip-slip	3 fractures
ZFMA2	DZ1	KFM05A				No fault-slip data observed
ZFMA2	DZ2	KFM10A	Gentle	Chlorite, calcite	Oblique-slip with dominant sinistral strike-slip and subordinate reverse dip-slip displacement	2 fractures
ZFMA2	DZ3	KFM10A	Gentle	Chlorite, prehnite	Dip-slip	1 fracture
ZFMA3	DZ3	KFM02A	Gentle	Chlorite, some calcite and hematite	Dip-slip reverse or oblique- to strike-slip. Conjugate system of reverse minor faults with dip to NNW and SE inferred to be present along DZ3	14 fractures
ZFMA3	DZ3	KFM02A	NW steep	Chlorite, some calcite and hematite	Normal dip-slip	1 fracture
ZFMA3	DZ3	KFM02A	SSW steep	Chlorite, some calcite and hematite	Sinistral strike-slip	1 fracture
Correlated with ZFMA3	DZ2	KFM02B	Gentle	Calcite	Dip-slip	2 fractures
ZFMA3	DZ4	KFM03A				No fault-slip data observed

Zone ID code	DZ in SHI	Borehole	Orientation of fractures with shear striae / steps (minor faults)	Mineral along shear striae / steps	Sense of movement	Number of fractures with shear striae / steps (minor faults)
ZFMA4	DZ1	KFM03A	Gentle	Chlorite	Dip-slip	1 fracture
ZFMA4	DZ1	KFM03A	NNE steep	Chlorite	Strike-slip	1 fracture
Zone possibly related to ZFMA5	DZ2	KFM03B				No fault-slip data observed
ZFMA7	DZ2	KFM03A	WSW steep	Chlorite, calcite	Strike-slip	1 fracture
ZFMA8	DZ1	KFM06B	Gentle	Chlorite	Reverse dip-slip	1 fracture
ZFMA8	DZ1	KFM06B	SSE steep	Chlorite	Strike-slip	1 fracture
ZFMB1	DZ3	KFM03A				No fault-slip data observed
ZFMB4	DZ8	KFM02A	Gentle	Chlorite	Dip-slip or oblique-slip. One fracture with reverse dip-slip	4 fractures
ZFMB4	DZ8	KFM02A	SE steep	Chlorite	Oblique-slip with dominant strike-slip component	1 fracture
Zone possibly related to ZFMB4	DZ9	KFM02A	Gentle	Calcite, laumontite	Dip-slip. One fracture with reverse dip-slip	4 fractures
ZFMB7	DZ2	KFM06C	Gentle	Chlorite	Dip-slip or oblique-slip with a reverse component of displacement	2 fractures
ZFMB7	DZ2	KFM06C	NW steep	Chlorite	Dextral strike-slip	1 fracture
ZFM866	DZ2	KFM02A	Gentle	Chlorite	Reverse dip-slip or oblique-slip with dominant reverse dip-slip, dextral strike-slip, normal dip-slip or dip-slip displacement	5 fractures
ZFM866	DZ2	KFM02A	SSW steep	Chlorite	Dip-slip	1 fracture
Correlated with ZFM866	DZ1	KFM02B				No fault-slip data observed
ZFM1203/ ZFMNNW0404	DZ1	KFM07A	Gentle	Chlorite, calcite	Reverse dip-slip (2) or oblique-slip with dominant strike-slip component (4). One oblique-slip fracture shows sinistral strike-slip and reverse components	6 fractures
ZFM1203/ ZFMNNW0404	DZ1	KFM07A	ENE and WSW steep	Chlorite, calcite	Dextral or sinistral strike-slip	2 fractures
ZFM1203/ ZFMNNW0404	DZ1	KFM07A	NNW steep	Chlorite, calcite	Dextral strike-slip	1 fracture
ZFM1203	DZ2	KFM07B				No fault-slip data observed
ZFM1203	DZ1	KFM07C				No fault-slip data observed

Zone ID code	DZ in SHI	Borehole	Orientation of fractures with shear striae / steps (minor faults)	Mineral along shear striae / steps	Sense of movement	Number of fractures with shear striae / steps (minor faults)
Possible deformation zones in SHI that have not been modelled deterministically (PDZ)						
PDZ	DZ1	KFM01D	SSE steep	Chlorite, hematite	Dip-slip	1 fracture
PDZ	DZ3	KFM01D	SE steep	Chlorite, hematite	Oblique-slip	1 fracture
PDZ	DZ5	KFM01D	WSW steep	Chlorite, calcite	Dextral strike-slip	1 fracture
PDZ	DZ4	KFM02B	SSW steep	Epidote, prehnite(?)	Sinistral strike-slip	1 fracture
PDZ	DZ4	KFM02B	N steep	Chlorite, prehnite	Oblique-slip with dominant reverse dip-slip component	1 fracture
PDZ	DZ5	KFM03A				No fault-slip data observed
PDZ	DZ1	KFM06A	NNE steep	Chlorite	Oblique-slip	1 fracture
PDZ	DZ9	KFM06A	WSW steep	Laumontite, calcite and chlorite	Strike-slip or dip-slip	8 fractures
PDZ	DZ9	KFM06A	SSW steep	Chlorite, hematite, laumontite	Oblique-slip with dominant dip-slip component	1 fracture
PDZ	DZ10	KFM06A	WSW steep	Chlorite	Strike-slip	2 fractures
PDZ	DZ1	KFM06C	SE moderate	Chlorite	Reverse dip-slip	1 fracture
PDZ	DZ1	KFM06C	N and S steep	Chlorite	Strike-slip. One fracture shows sinistral strike-slip displacement	2 fractures
PDZ	DZ2	KFM07A	WSW steep	Laumontite, chlorite	Strike-slip	1 fracture
PDZ	DZ1	KFM07B	Gentle	Chlorite	Dip-slip	1 fracture
PDZ	DZ4	KFM08A	Gentle (N or S strike)	Chlorite, hematite, some calcite	Reverse dip-slip or strike-slip	2 fractures
PDZ	DZ4	KFM08A	Gentle (ENE strike)	Laumontite, calcite	Normal dip-slip	1 fracture
PDZ	DZ4	KFM08A	Gentle (ENE strike)	Chlorite, calcite, clay minerals	Reverse dip-slip	1 fracture
PDZ	DZ4	KFM08A	ENE-WSW vertical	Laumontite	Oblique-slip with south-side-down and sinistral strike-slip components	1 fracture
PDZ	DZ6	KFM08A	ENE steep	Chlorite, laumontite, calcite	Reverse dip-slip or oblique-slip.	2 fractures
PDZ	DZ6	KFM08A	ESE steep	Chlorite, calcite	Oblique-slip with normal dip-slip and dextral strike-slip components	1 fracture
PDZ	DZ1	KFM08C	N steep	Chlorite, hematite, calcite	Sinistral strike-slip	1 fracture

Table A-6. Summary of kinematic data from possible deformation zones (DZ) identified with high confidence in the single hole interpretation (SHI) of drill cores, based on /Nordgulen and Saintot 2006, 2008, Saintot and Nordgulen 2007/. Data presented firstly on a fracture orientation and secondly on a deformation zone basis. The identification of deformation zones is after /Stephens et al. 2007/: Green = steep WNW-NW set of zones, dark blue = steep NNW set, brown = ENE (NE) sub-set, orange = NNE sub-set, pale blue = gentle set, unshaded = possible deformation zone not modelled in a deterministic manner (PDZ).

Zone ID code (DZ in SHI, borehole)	Strike-slip			Dip-slip			Oblique-slip	
	Dextral	Sinistral	Not specified	Reverse	Normal	Not specified	Strike-slip dominant	Dip-slip dominant
Steep fractures with WNW-ESE and NW-SE strike (some steep fractures with E-W strike included here)								
ZFMWNW0001 (498-630 m in DZ1, KFM11A)	5	4	9	2	2	1	6 (in part both dextral and sinistral)	2 (reverse)
ZFMWNW0004 (DZ1, KFM12A)	1	3	2					
ZFMWNW0004 (DZ2, KFM12A)	4	3	2	1	1		4 (in part sinistral)	6 (in part normal)
ZFMWNW0123 (DZ1, KFM10A)		8	26					
ZFMWNW2225 (DZ3, KFM08C)		1						
ZFMNW1200 (DZ4, KFM09A)		7		1			1 (dextral)	
ZFMNW1200 (DZ5, KFM09A)		4						
ZFMNNW0100 (920-999 m along DZ4, KFM07A)	1		3					1 (normal)
ZFMNNW0100/ZFMENE0159A (DZ3, KFM09A)			1					
ZFMENE0060A/ZFMENE0060C (DZ3, KFM01C)	1					1		
ZFMENE0060B (DZ2, KFM06B)			1				1 (sinistral)	
ZFMENE0061 (DZ8, KFM06A)			2					
ZFMENE2320 (DZ2, KFM07C)	1							
ZFMNE1188 (DZ4, KFM04A)		1	6			5	2	3
ZFMNE2282 (DZ2, KFM05A)								1
ZFMNNE0725 (DZ7, KFM06A)	1		1					2
ZFMNNE2263 (DZ3, KFM06C)			1				1	
ZFMA2 (DZ2, KFM01C)			1					
ZFMA2/ZFMF1 (DZ6, KFM02A)		1				1	2	
ZFMA2 (DZ2, KFM04A)						1		
ZFMA3 (DZ3, KFM2A)					1			

Zone ID code (DZ in SHI, borehole)	Strike-slip			Dip-slip			Oblique-slip	
	Dextral	Sinistral	Not specified	Reverse	Normal	Not specified	Strike-slip dominant	Dip-slip dominant
ZFMB4 (DZ8, KFM02A)							1	
ZFMB7 (DZ2, KFM06C)	1							
PDZ (DZ1, KFM01D)							1	
PDZ (DZ1, KFM06C)				1				
PDZ (DZ6, KFM08A)							1 (dextral)	
Steep fractures with NNW-SSE strike								
ZFMWNW0001 (part of DZ1, KFM11A)		1						
ZFMWNW0044 (DZ4, KFM06C)								1
ZFMWNW0123 (DZ1, KFM10A)			1					
ZFMNNW0100 (920-999 m along DZ4, KFM07A)	2	2	13		1	1	1 (sinistral)	1
ZFMNNW0100/ZFMENE0159A (DZ3, KFM09A)		2	14				3	5 (in part normal)
ZFMNNW404 (DZ3, KFM01B)	1	1		1	2			
ZFMNNW1204 (DZ2, KFM08A)			1					
ZFMNNW1205 (DZ2, KFM08B)		3	2					
ZFMENE0060A/ZFMENE0060C (DZ3, KFM01C)				1			1	
ZFMENE0061 (DZ8, KFM06A)			2			1		
ZFMENE0159A (DZ3, KFM07A)			2					
ZFMENE0401B (609-616 m in DZ3, KFM05A)			1					
ZFMENE1061A (DZ1, KFM08A)		3	3					
ZFMENE1208A (857-900 m in DZ3, KFM07A)	2	6	7					
ZFMENE1208A (DZ1, KFM09A)			3					
ZFMENE1208A/ZFMENE1208B/ZFME-NE0159A (DZ1, KFM09B)	2	1	2					
ZFMENE1208B (803-843 m in DZ4, KFM07A)		1	2					
ZFMENE1208B (DZ2, KFM09A)			1					
ZFMENE2320 (DZ2, KFM07C)		3	2				1	

Zone ID code (DZ in SHI, borehole)	Strike-slip			Dip-slip			Oblique-slip	
	Dextral	Sinistral	Not specified	Reverse	Normal	Not specified	Strike-slip dominant	Dip-slip dominant
ZFMENE2320 (DZ3, KFM09B)		1						
ZFMENE2325A (DZ4, KFM09B)		1				1	2 (dextral and sinistral)	
ZFMNNE2312 (DZ2, KFM08C)		2						
ZFMA2 (DZ1, KFM01B)			2					
ZFMA2 (DZ2, KFM01C)		1	4					
ZFMA8 (DZ1, KFM06B)			1					
ZFM1203/ZFMNNW0404 (DZ1, KFM07A)	1							
PDZ (DZ1, KFM01D)						1		
Steep fractures with ENE-WSW and NE-SW strike (some steep fractures with E-W strike included here)								
ZFMWNW0001 (498-630 m in DZ1, KFM11A)			1	2	1	1	3 (in part both dextral and sinistral)	1 (reverse)
ZFMWNW0004 (DZ1, KFM12A)		1				1	1	1
ZFMWNW0004 (DZ2, KFM12A)		1	2			1		1
ZFMNW1200 (DZ4, KFM09A)	1							
ZFMNNW0100 (920-999 m in DZ4, KFM07A)			3		1		1	
ZFMNNW1204 (DZ2, KFM08A)		1	1					
ZFMENE0060A/ZFMB7 (DZ4, KFM06A)							2	
ZFMENE0060A/ZFMENE0060C (DZ3, KFM01C)	1		4			5		1
ZFMENE0060B (DZ2, KFM06B)			1					
ZFMENE0061 (DZ8, KFM06A)			3					
ZFMENE0159B (DZ3, KFM08D)	1							
ZFMENE0401A (712-720 m in DZ3, KFM05A)			1					
ZFMENE1061A (DZ1, KFM08A)		1						
ZFMENE1061A/ ZFMENE1061B (DZ4, KFM08C)								1
ZFMENE1208A (857-900 m, KFM07A)			1					
ZFMENE1208A (DZ1, KFM09A)			1					
ZFMENE1208B (DZ2, KFM09A)	1							
ZFMENE2254 (DZ3, KFM01A								2 (in part normal)

Zone ID code (DZ in SHI, borehole)	Strike-slip			Dip-slip			Oblique-slip	
	Dextral	Sinistral	Not specified	Reverse	Normal	Not specified	Strike-slip dominant	Dip-slip dominant
ZFMENE2320 (DZ2, KFM07C)			1					
ZFMENE2320 (DZ7, KFM08D)	1							
ZFMENE2320 (DZ3, KFM09B)			2					
ZFMENE2325B (DZ5, KFM09B)	1		1					
ZFMNE1188 (DZ4, KFM04A)			2			2		
ZFMNE2282 (DZ2, KFM05A)			1					
ZFMNNE0725 (DZ7, KFM06A)		1	1				2	
ZFMNNE2280 (DZ11, KFM06A)								1 (normal)
ZFMNNE2312 (DZ2, KFM08C)					1			
ZFMA2/ZFMENE1192 (DZ1, KFM01C)			1			1		
ZFMA2 (DZ2, KFM01C)								1
ZFMA2/ZFMF1 (DZ6, KFM02A)			1				1	
ZFMF1 (DZ5, KFM02B)							1 (dextral)	
ZFMF1 (DZ6, KFM02B)		1	1					
ZFMA2 (DZ2, KFM04A)								1
ZFMA2 (DZ3, KFM04A)			2			1		
ZFMA3 (DZ3, KFM02A)						1	1 (dextral)	
ZFMA7 (DZ2, KFM03A)			1					
ZFM1203/ZFMNNW0404 (DZ1, KFM07A)	1	1						
PDZ (DZ5, KFM01D)	1							
PDZ (DZ9, KFM06A)			6			2		
PDZ (DZ10, KFM06A)			2					
PDZ (DZ2, KFM07A)			1					
PDZ (DZ4, KFM08A)								1 (normal)
PDZ (DZ6, KFM08A)				1				1
Steeply dipping fractures with NNE-SSW strike								
ZFMWNW0004 (DZ2, KFM12A)			1	1			1	
ZFMWNW0044 (DZ4, KFM06C)		1	4					
ZFMENE0060B (DZ3, KFM06B)				1				

Zone ID code (DZ in SHI, borehole)	Strike-slip			Dip-slip			Oblique-slip	
	Dextral	Sinistral	Not specified	Reverse	Normal	Not specified	Strike-slip dominant	Dip-slip dominant
ZFMENE1208A/ (857-900 m in DZ4, KFM07A)		1	1					
ZFMENE1208B/ (803-843 m in DZ4, KFM07A)							1 (sinistral)	
ZFMNNE0725 (DZ7, KFM06A)	1							
ZFMNNE2280 (DZ11, KFM06A)							1	
ZFMNNE2300 (DZ12, KFM08D)			1					
ZFMNNE2312 (DZ2, KFM08C)		2	2					
ZFMA2/ZFMF1 (DZ6, KFM02A)						1		
ZFMA3 (DZ3, KFM02A)		1						
ZFMA4 (DZ1, KFM03A)			1					
ZFM866 (DZ2, KFM02A)						1		
PDZ (DZ4, KFM02B)		1						
PDZ (DZ4, KFM02B)								1 (reverse)
PDZ (DZ1, KFM06A)								1
PDZ (DZ9, KFM06A)								1
PDZ (DZ1, KFM06C)		1	1					1
PDZ (DZ1, KFM08C)		1						
Gently dipping fractures								
ZFMWNW0001 (498-630 m in DZ1, KFM11A)				1			2 (dextral)	1 (normal)
ZFMWNW0004 (DZ1, KFM12A)	1	1		1				
ZFMWNW0004 (DZ2, KFM12A)		1		1			2 (in part dextral)	1
ZFMWNW0123 (DZ1, KFM10A)						1		1 (reverse)
ZFMWNW2225 (DZ3, KFM08C)	1							
ZFMNNW0100 (920-999 m in DZ4, KFM07A)	1		2				1	3 (in part reverse)
ZFMNNW0100/ZFMENE0159A (DZ3, KFM09A)							1 (dextral)	
ZFMNNW1205 (DZ2, KFM08B)				1				
ZFMENE0060A/ZFMB7 (DZ4, KFM06A)						1		
ZFMENE0060A/ZFMENE0060C (DZ3, KFM01C)				1				
ZFMENE0060B (DZ3, KFM06B)					1			

Zone ID code (DZ in SHI, borehole)	Strike-slip			Dip-slip			Oblique-slip	
	Dextral	Sinistral	Not specified	Reverse	Normal	Not specified	Strike-slip dominant	Dip-slip dominant
ZFMENE1061A (DZ1, KFM08A)	1			1				
ZFMENE2320 (DZ2, KFM07C)						1	1	
ZFMENE2320 (DZ3, KFM09B)							1 (dextral)	
ZFMNE1188 (DZ4, KFM04A)			1					
ZFMNNE0725 (DZ7, KFM06A)						1		
ZFMNNE2263 (DZ3, KFM06C)				1				
ZFMNNE2280 (DZ11, KFM06A)			1				2 (dextral)	
ZFMNNE2300 (DZ12, KFM08D)				1				1 (reverse)
ZFMNNE2312 (DZ2, KFM08C)								1 (reverse)
ZFMA2/ZFMENE1192 (DZ1, KFM01C)				1				1
ZFMA2 (DZ2, KFM01C)			2			3		
ZFMA2/ZFMF1 (DZ6, KFM02A)	1	1	4	1		1		3 (in part reverse)
ZFMF1 (DZ5, KFM02B)						1		1 (reverse)
ZFMA2 (DZ2, KFM04A)			1					
ZFMA2 (DZ3, KFM04A)							1	
ZFMA2 (DZ2, KFM10A)							2 (sinistral)	
ZFMA2 (DZ3, KFM10A)						1		
ZFMA3 (DZ3, KFM02A)	1		1	3	1	1	2 (in part sinistral)	3 (both reverse and normal)
ZFMA3 (DZ2, KFM02B)						2		
ZFMA4 (DZ1, KFM03A)						1		
ZFMA8 (DZ1, KFM06B)				1				
ZFMB4 (DZ8, KFM02A)				1		2		1
Zone possibly related to ZFMB4 (DZ9, KFM02A)				1		3		
ZFMB7 (DZ2, KFM06C)						1		1 (reverse)
ZFM866 (DZ2, KFM02A)				1			1 (dextral)	3 (reverse and normal)
ZFM1203/ZFMNNW0404 (DZ1, KFM07A)				2			4 (in part sinistral)	
PDZ (DZ1, KFM07B)						1		
PDZ (DZ4, KFM08A)			1	2	1			